UC Berkeley
UC Berkeley Electronic Theses and Dissertations

Title
Electrospun Direct-write Multi-functional Nanofibers

Permalink
https://escholarship.org/uc/item/9n1306k1

Author
Chang, Jiyoung

Publication Date
2012

Peer reviewed|Thesis/dissertation

Electrospun Direct-write Multi-functional Nanofibers

by

Jiyoung Chang

A dissertation submitted in partial satisfaction of the
requirements for the degree of
Doctor of Philosophy

in

Engineering – Mechanical Engineering

in the

Graduate division

of the

University of California, Berkeley

Committee in charge:

Professor Liwei Lin, Chair
Professor Albert P. Pisano
Professor Seung-wuk Lee

Spring 2012

Electrospun Direct-write Multi-functional Nanofibers

Copyright 2012

by

Jiyoung Chang

Abstract

Electrospun Direct-write Multi-functional Nanofibers

by

Jiyoung Chang

Doctor of Philosophy in Engineering – Mechanical Engineering

University of California, Berkeley

Professor Liwei Lin, Chair

Multi-functional fibers by means of direct-write near-field electrospinning process have been developed for versatile applications on a wide variety of substrates, including flexible ones. Several mask-less lithographoy techniques have been established by using the direct-write fibers in dry etching, wet etching and lift-off processes. By selecting the proper functional materials, electrospun direct-write fibers have been demonstrated in prototype working devices, such as large array piezoelectric nanogenerators made of polymeric PVDF (Polyvinylidene fluoride) and direct-write micro heaters made of metallic copper nanoparticles.

In the first example, continuous yet uniform PVDF fibers have been electrospun on a flexible substrate. A post, electrical poling process has been introduced on electrodes with PDMS (Polydimethylsiloxane) as the filling media to achieve an electrical potential of 2×10^7 V/m. In the prototype device, 500 energy harvesting points formed by 50 pairs of fibers and 10 pairs of comb-shape electrodes have generated about 30nA of electrical current on a flexible substrate under an estimated strain of 0.1%. Both FTIR (Fourier Transform Infrared Spectroscopy) and XRD (X-Ray Diffraction) have been utilized to characterize the electrospun fibers and good beta-phase formation, an essential property for piezoelectricity, has been confirmed.

For the next example, electrospun direct-write fibers have been employed to show three mask-less lithography techniques; lift-off, wet-etching and dry-etching. These include the demonstration of sub-micrometer wide gaps between a thin metallic gold film using the lift-off process; 20μm-wide, 20mm-long lineshape micro heaters made of 30nm-thick copper film by a wet-etching process; and a 2μm-wide, 10μm-long graphene channel FET (Field Effect Transistor) via a dry-etching process. Electrospun PEO (Polyethylene oxide) fibers

have been utilized in the aformentioned processes which has shown strong adhesion to the Kapton substrate, robust chemical resistance to wet copper etchant and good resistance to oxygen plasma for the related lift-off, wet etching and dry etching processes, respectively. Experimentally, a fabricated copper micro heater has reached 92°C under an input power of 37mWatt. The graphene-based channel FET on 285nm-thick gate dioxide has 30μA of current under 1V of applied bias voltage while the gate voltage sweep has shown Dirac point at +21V.

In the final demonstration example, electropun direct-write conductive copper wire has been constructed on top of a glass substrate. Copper dinitrate and PVP have been tested as the best polymer mixture for the electrospinning process. A two-step post annealing process has been developed to decompose the polymer and reduce copper oxide to copper for good conductively. The prototype copper wires are 20~100μm in length and 500nm in height with an average measrued resistivity of 5.6×10^{-6}Ohm·m from tested 25 samples. As such, electrospun direct-write fibers could find potential applications in various fields, including low-cost electronics.

Acknowledgment

First, I would like to thank Prof. Byung-Kwon Min and Prof. Sang-jo Lee in Yonsei University. I had a life-changing opportunity to learn and study about "NANO" for the first time in the manufacturing lab in Yonsei University during my master degree. Prof. Jongbaeg Kim in Yonsei University was not only a considerate research advisor but he showed invaluable mentorship during my master degree and encouraged me to realize my dream.

It is impossible to describe my doctoral study without mentioning Prof. Liwei Lin's advice and support. He was always approachable and willing to help me in terms of research advising and personal matter as well. I cannot thank enough about the consideration I was gifted for my whole graduate year in Berkeley.

The Linlab members were always supportive and friendly. I would like to thank Kedar, Brian, Qin, Yingqi, Jong-yoon, Koo-hyun, Sanghoon, Kisik, Alina, Guoqing, Kosuke, Ryan, Kevin, Adrienne, Armon, Casey, Roseanne, Heather, Minsong and all others in Linlab. In addition to that, I will not forget the sincere efforts and contribution that Michael and Simon showed to the project that we worked together.

I would like to express my sincere appreciation to my parents, Moon-sam Chang and Songae Kim, who always supported my decision and believed me. I cannot think of an appropriate word to express my sincere love and appreciation to them. I want to thank my nephews, Sunwoo and Sunjae, for being brave and bright despite the hard time they had to suffer.

During the long journey, I could laugh and cheer up because of my wife, Pilsoon Lee, and my baby Ellen Eunje. They were the energy of my life and they made me overcome all the barriers I had to confront. Without them, I could not be writing this page. Pilsoon! You are the navigator in my life!

Lastly, I want to thank my sister, Soyoung, who passed away last year. As I know how she sincerely did care about me and felt proud of me, I feel the deepest sadness that I cannot share this moment with her. I dedicate this dissertation to my sister remembering all the memories we shared.

Lift of Figures

Lift of Tables

Contents

1. Introduction

1.1. The making of fibers

The history of fiber production could date back when human being first started making clothes to warm up or protect their body from surroundings. The primitive fiber producing method, so called 'hand-spinning' is known as the origin of spinning of fiber. Inherently, the hand-spinning had low productivity and efficiency. In about early 10th century, invention of spinning wheel brought dramatic change in the history of fiber productions. The method of rotating wheel speeded up the fiber production such that clothes made from fiber became much more popular at lower price. Furthermore, various types of fibers have been used as the fiber materials. Fiber spinning process by electricity has first developed around early 20th century. The invention is called electrospinning to generate polymeric fibers with very fine diameters continuously. In the electrospinning process, the polymer jet formed at the end of a syringe needle is pulled to the bottom substrate due to the strong electrostatic force. The typical positive high voltage applied at the tip of the needle is more than 10kV and the bottom substrate is grounded. Fibers are randomly deposited on the substrate due to the chaotic, whipping process and it is difficult to have orderly deposition. As a result, electrospun fibers have been utilized in industry that do not require the controllable deposition in terms of fiber locations such as air filters [1] or tissue scaffold for *in-vitro* tests [2]. The near-field electrospinning (NFES) was developed recently to enable fiber deposition in orderly manner with the possibility to generate arbitrary patterns. The key is to move the electrode very close (less than 1mm) to the bottom substrate for a more stable deposition [3]. The transition from far-field to near-field in spinning process enables possible other engineering and scientific applications with the direct-writing ability and various selections of polymers by using the near-field electrospinning process.

Several possible engineering applications are presented by using the direct-write multi-functional fibers process using near-field electrospinning. Specifically, electrospun fibers have been utilized to make large array energy harvesters, direct-write lithography processes including lift-off and wet/dry etching processes. Key background information in these applications and the far and near-field electrospinning processes are introduced here.

1.1.1. Piezoelectric energy harvesters by direct-write fibers

Portable and self-charging energy harvesters are attractive renewable energy sources for practical applications. Specifically, low power systems such as wireless devices could use energy harvesters instead of traditional batteries. There are many different kinds of possible candidates for energy harvesters and generators, such as micro fuel cells, [4] and micro turbines [5]. However, energy generators rely on chemical reactions need constant supply of energy sources. On the other hand, energy sources that can be scavenged from the environment in the form of light, heat and vibration could be attractive alternatives to power low energy consumption systems such as remote sensors and small electronics. Another potential advantage of these renewable energy devices is that they generally do not produce by-product to harm the environment. Some of these energy systems have been heavily studied such as the solar cells, which generate power by converting sunlight to electricity. Ambient thermal energy can also be transformed into electrical energy by means of Seebeck effect [6]. This approach would be directly applicable to places that have constant heat generations. Another energy harvesting scheme utilizes kinetic or vibratory movements for energy scavenge from common household sources such as refrigerator, dishwashing machine, and microwave to large scale systems such as industrial equipment, automobiles and air planes. There are several ways to collect the energy such as electromagnetic, electrostatic and piezoelectric. This work utilizes direct-write piezoelectric nanofibers as energy harvesters to be described in chapter 2.

In general, piezoelectric ceramics such as lead zirconate titanate (PZT) have been used for energy harvesting based on vibrational energy for many years based the piezoelectric effect discovered in 1880 by Curie. The principle found is that when certain crystalline material is mechanically strained, the electrical dipoles are formed and the amount of electrical potential is proportional to the applied strain. Interestingly, vice versa test also applies in which certain amount of electrical field is applied which results in corresponding mechanical deformation. Such crystalline materials are easily accessible such as quartz, PZT [7], zinc oxide and polymers such as Polyvinylidene fluoride (PVDF) [8,9]. In general, piezoelectric material shows un-symmetric characteristics in which the overall response depends on the direction the force and the orientation of dipoles inside the materials. Therefore, the notation of axes is important to characterize the piezoelectric strain constant, d , [10]

$$d = \frac{strain\ applied}{field\ applied}\left(m/V\right) = \frac{short\ circuit\ charge\ density}{stress\ applied}\left(C/N\right) \qquad (1\text{-}1)$$

Following the above equation, two different notations are commonly encountered in piezoelectric materials, d_{33} and d_{31}. The piezoelectric coefficient d_{33} is the coefficient of the piezoelectric material that experiences strain in a direction parallel to the voltage generation direction, while d_{31} is that of the piezoelectric material which experiences strain in a direction perpendicular to the voltage generation direction. In general, the outputs from the piezoelectric responses increase by having multi-layers of piezoelectric material layers. In most cases, piezoelectric energy harvester utilizes vibrational energy in both d_{31} and d_{33} modes and coupling designs are necessary for higher outputs.

Another constant, electro-mechanical coupling coefficient, k, is needed to describe the efficiency of energy that is converted between electrical and mechanical.

$$k^2{}_{ij} = \frac{W_i^e}{W_j^m} \tag{1-2}$$

Where W_i^e is the electrical energy stored in the i axis and W_j^m denotes the mechanical input energy in the j axis. The mechanical input energy in PVDF nanogenerator can be assumed as stored strain energy and is calculated as

$$W_j^m = \frac{1}{2} nAE\varepsilon^2 L_o \tag{1-3}$$

Where n is the total number of fibers in the array, A is the cross sectional area of the fiber, E is Young's modulus of the PVDF material, ε is mechanical strain and L_o is the total length of the fiber between electrodes. PVDF is a polymer known for its high piezoelectric property compared to other types of polymers. Using such unique physical property, single-fiber nanogenerator operated by mechanical strain has been demonstrated using the PVDF polymer solution in 2010 [11] with superior piezoelectric energy conversion efficiency. In this dissertation, expansion from single fiber to multiple fiber array structure is presented to amplify energy harvesting capability.

1.1.2.   Mask-less lithography by direct-write fibers

Near-field electrospinning can deposit fibers at desired positions with sub-micrometer size and low-cost for applications in many research fields. One example is micro/nano lithography processes in which multiple steps could be eliminated. Lithography process typically requires the usage of a conventional mask aligner or a wafer stepper with low design flexibility. Several new approaches have been introduced such as nano imprinting [12] and direct-write femto-second laser mask printing method [13] which can produce small features not available in the conventional lithography processes. However, most of these aforementioned processes are limited to high process cost. Another important method, e-beam lithography has been widely used in various fields such as microelectronics circuits [14] and optical fields such as photonic crystal [15,16]. However, e-beam lithography has issues in high-cost and low yield. Furthermore, AFM has been used to generate sub-100nm scale features to fabricate electronics [17] and NEMS devices [18]. However, AFM lithography requires expensive equipment and is difficult for wafer-scale processing.

In this dissertation, direct-write, near-field electrospun polymer fibers have been utilized for mask-less lithography with corresponding experimental results. As a proof-of-concept, simple yet complete processes for wet-etching, lift-off and dry-etching schemes using direct-write nanofibers have been tested for working device demonstrations. For example, electrospun fibers can be used as the sacrificial layer in micro fabrication process or backbone structures for culturing of living cells. In the usage as sacrificial structures such as the lift-off process, electrospun fibers function like the photoresist. When the metal layer is deposited, metal on top of the fibers will be removed when the fibers are etched away. Compared to the conventional lithography process, photo mask, aligner and the exposure processes are no longer needed. In the usage for wet- or dry-etching processes, electrospun fibers function as typical photoresist to protect materials underneath the fibers during the etching processes.

1.2. Electrospinning

In this section, the electrospinning process is briefly introduced which is the primary tool to generate fibers in this work. Electrospinning can make fibers from polymer solutions or melt to provide the foundation for electrospun fibers. The diameters of electrospun fibers range from tens of nanometers to micrometers and a large number of different materials have been produced by electrospinning, including synthetic/natural polymers, polymer alloys, polymer composites as well as metals and ceramics [19]. The versatile possibilities in the selections of materials and easy process setup of electrospinning could provide unique pathways to enhance the performance of various devices. Furthermore, the electrospinning process has high throughputs for mass production in various applications such as filtration, wound dressing, bio-scaffolds and medical implants, to name a few [20–22]. In recent years, electrospinning has also been applied in the making of micro/nano devices such as field effect transistors [23], sensors [24], actuators and so on [25]. In the following, far-field and near-field electrospinning processes are discussed in details.

1.2.1. Far-field electrospinning

The typical setup for conventional electrospinning includes four major components [26,27], a syringe pump to maintain a constant flow rate of the polymer solution, a dispense needle that is connected to the a high voltage supply as a cathode, a high voltage power supply unit, and a collector electrode which collects electrospun nanofibers. When a high voltage is applied, a strong electrostatic field is established between the needle tip and the collector electrode. The electrostatic force attracts the polymer melt out of the needle and is balanced by the surface tension force of the polymer melt. This results in a conical shape droplet, a so-called Taylor cone. When the electrostatic force surpasses the surface tension force, a thin liquid/melt jet is ejected from the droplet toward the collector electrode. For a short distance immediately below the droplet, the polymer jets is stable and can be utilized in the near-field electrospinning process [3]. If the collector electrode is placed far away (tens of centimeters) from the needle tip, the jet will undergo a whipping and chaotic process to deposit nanofibers randomly on the collector electrode which is the conventional far-field electrospinning process. The solvent evaporates and the polymer stream solidifies to form thin solid polymer fibers on the collector electrode. For far-field electrospinning, the typical inner diameter of the dispense needle is in the order of a few hundred μm and the applied voltage is in the range of several tens of kilovolts and the needle-to-collector distance is tens of centimeters. The formation of thin fibers is based on the uniaxial stretching of the viscoelastic solution by the electrostatic force for materials with suitable properties, such as conductivity which can be influenced by salt solutions, and surface tension which can be changed by adding surfactants. One key characteristics of the far-

field electrospinning is the random and chaotic distribution of nanofibers on the collector electrode.

1.2.2.   Modified far-field electrospinning

For applications such as nanofiber nanogenerators, good fiber alignment could be necessary to improve the energy generation efficiencies.   Research groups have demonstrated methods for aligned depositions of nanofibers with modified conventional electrospinning process. For example, Boland et al. used a rotating collector to control the alignment of deposited nanofibers [28].   In their experiments, poly (glycolic acid) and collagen were electrospun on a cylinder collector rotating at a speed of 1000 rpm and 4500 rpm, respectively. The use of fast-spinning collectors in the form of drums [29], wheel like disks [30], and wire drums [31] have all shown various levels of success in controlling the deposition positions of nanofibers. These methods could be the potential manufacturing approaches to make continuous aligned nanofibers for nanogenerator applications.

Instead of using mechanical means to improve the conventional electrospinning process for better controlled deposition positions, researchers have also exploited electric fields to guide the deposition locations of nanofibers, including the usage of two parallel electrodes on the collector [32] as shown in and the designs of one or several charged rings as auxiliary electrodes [33].
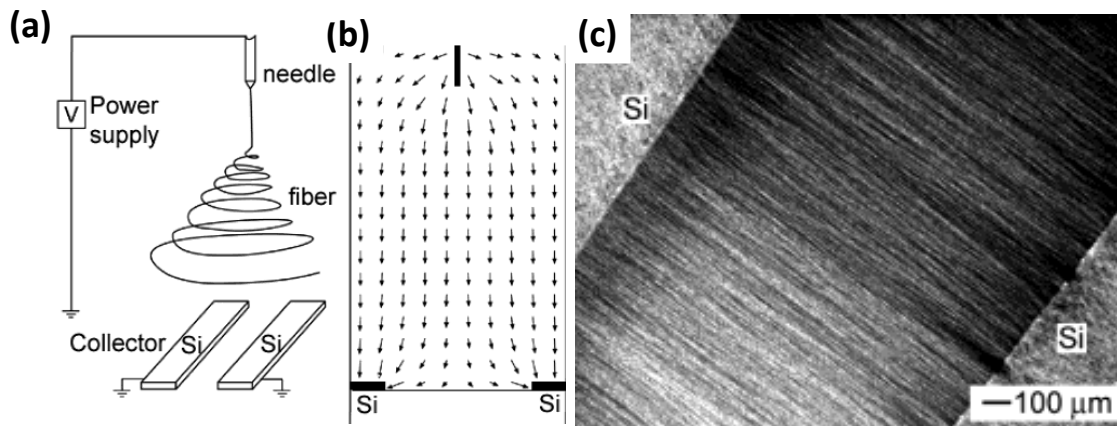
Figure 1.1 (a) Schematic diagram of a modified far-field electrospinning process using two parallel electrodes on the collector substrate to control the alignment of nanofibers with electrostatic field similation in (b) where arrows are the direction of the field lines [32]. (c) Deposition results showing aligned poly(vinyl pyrrolidone) fibers [32].

1.2.3. Near-field electrospinning

Another method to have controlled deposition of nanofibers is the so called near-field electrospinning (NFES) [3], where the needle-to-collector distance is reduced to enhance the controllability of the fiber deposition positions as illustrated in figure 1.2(a). The needle-to-collector distance is reduced to less than millimeter range and the applied voltage is reduced to the order of 1kV. The reduction in distance and the increased electric field (as the result of much shorter distance) make possible the controlled nanofiber deposition on the collector by utilizing the stable liquid jet region. In the earlier stage of the near-field electrospinning process, a dip-pen type approach was adopted as shown in Figure 1.2(b). In this case, repeated dipping into that polymer solution was necessary to obtain more polymer sources which interrupted the deposition process. Continuous near-field electrospinning was later developed [34] by using a syringe instead of a probe as shown in figure 1.2(c) such that polymer solution can be supplied continuously to deposit continuous nanofibers. These innovative modifications make NFES to maintain the continuous deposition characteristics similar to the conventional FFES with a superior controllability on the deposition locations. These and other similar approaches on NFES [35,36] can be the foundations to construct devices made by nanofiber previously unachievable by FFES such as parallel arrays of nanofibers for nanogenerators [19].
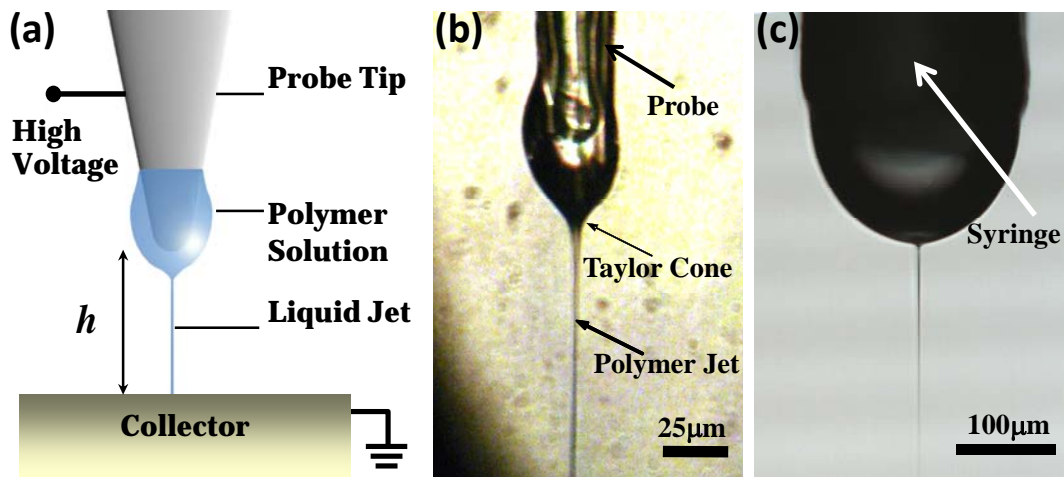
Figure 1.2 (a) Schematic diagram of the setup of near-field electrospinning (NFES) process where the probe-to-collector distance, h, is reduced to mm range to utilize the stable polymer jet region for better controllability of the deposition locations [11]. The polymer is attached to the top of the tungsten electrode in a manner analogous to that of dip pen. (b) An optical image photo showing the NFES with the dip-pen approach in operation [3]. (c) An optical image photo showing the continuous NFES in operation by using a syringe to supply the polymer solution continuously [34].

1.3. Dissertation goal and organization

The goal of this thesis work is to present diverse potential applications by using direct-write multi-functional fibers based on the near-field electrospinning process. In the first chapter, historical backgrounds on the making of fibers and various methods of the electrospinning processes were described. Two key applications demonstrated in this work by the direct-write electrospun fibers are detailed as illustrated in Figure 1.3: (1) large array PVDF nanogenerators on flexible substrate, and (2) direct-write mask-less lithography.
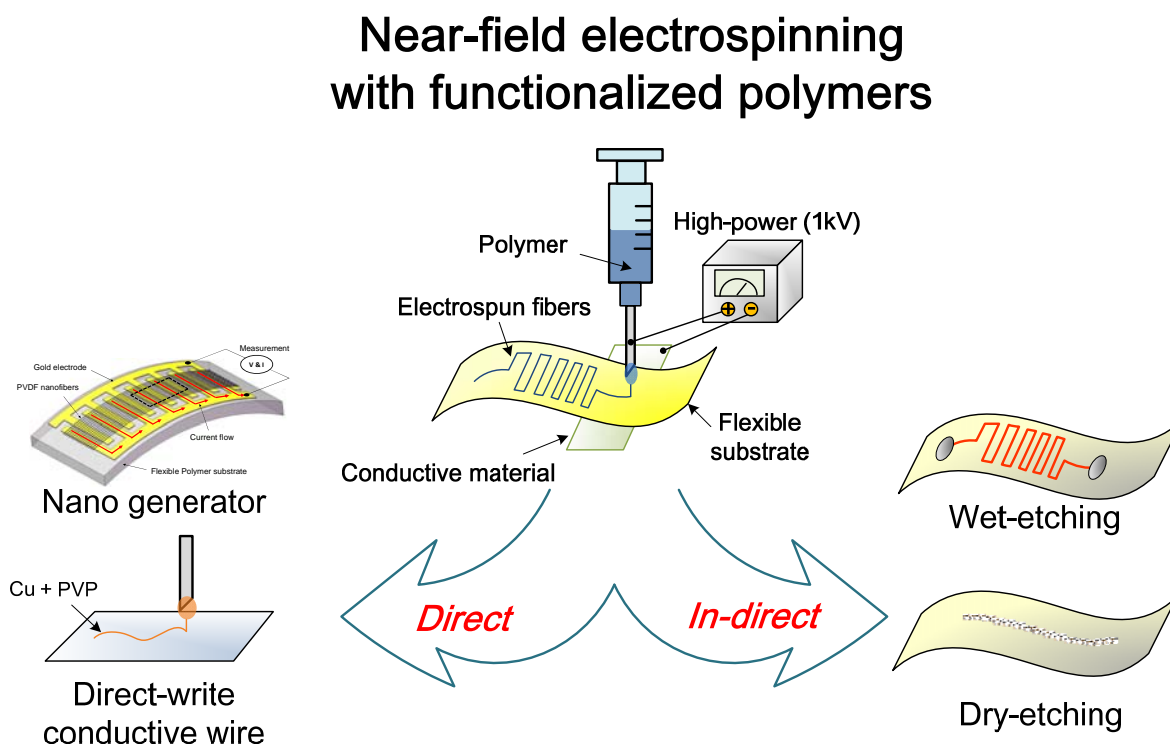
Figure 1.3 Near-field electrospinning process can produce fibers with specific functionality. Direct-write fiber utilized property of polymer itself where in-direct use of fiber utilizes fiber as sacrificial layer in subsequent processes. A typical example of direct use is PVDF nanogenerator and that of in-direct use is shadow mask in lithography and live cell scaffold backbone structure.

Chapter 2 details the development of utilizing large array of electrospun PVDF fibers for nanogenerator applications. This work continues the previous efforts on nanogenerators based on a single fiber [11]. Array of fibers have been constructed to increase total outputs. Material property characterization tools such as XRD (X-ray Diffraction), PFM (Piezoelectric force microscopy), FTIR (Fourier Transform Infrared) have been adopted to have better characterizations of basic piezoelectric properties of fibers made from different processes. Moreover, common experimental artifacts are discusses and possible schemes to verify the measurement results are discussed.

Chapter 3 presents several possible approaches utilizing direct-write fibers for mask-less lithography processes. These include the usage of fibers in wet- and dry-etching process as well as in the lift-off process. These fibers could be deposited on flexible substrates with diameter from sub-micrometer to several micrometers without using the masks in conventional photo lithography. Prototype devices have been fabricated and tested as the proof of concept demonstrations, including sub-micrometer metal gaps, micro heaters and definition of graphene structures on flexible substrates. .

Chapter 4 summarizes the work and proposes future direction of the research. Some of concepts and preliminary results are also presented for various future research topics based on electrospun direct-write fibers, such as in-situ doping for graphene based CMOS, 3-D micro-fluidic mixing channels, and cell migration platforms.

2. Large array PVDF fibers for energy harvesting applications

2.1. Introduction

After decades of developments in the miniaturization of portable and wireless devices, new power sources beyond rechargeable batteries have become important topics for the current and future stand-alone devices and systems. Specifically, ideal power sources should be scalable for power demands of various portable devices without the necessity of a recharging process or replacement. Recent works in the field of nanomaterials have shown good progresses toward self-powered energy sources by scavenging energy from ambient environments (solar, thermal, mechanical vibration, etc.). In particular, the use of piezoelectric generators by nanomaterials as a robust and simple solution for mechanical energy harvesting has attracted lots of attentions. One of the earliest nanogenerators for possible energy scavenging applications from mechanical strain utilized piezoelectric zinc oxide (ZnO) nanowires [38]. By coupling their semiconducting and piezoelectric properties, mechanical strains can be converted into electricity. In recent years, numerous research groups have demonstrated results in the field of mechanical energy scavenging using nanomaterials with different architectures, including: film-based, nanowire-based and fiber-based nanogenerators. Film-based nanogenerators are often made by the spin-on or thin-film deposition methods [39][19]. Mechanical strains due to the bending or compression of the thin-film structure can be the source of the energy generation. Nanowire-based nanogenerators [40] are typically made of semiconducting materials such as ZnO [1][41][42], ZnS [43], GaN [44,45] or CdS [46,47]. These piezoelectric nanowires have been demonstrated to build up an electrical potential when mechanically strained by an AFM tip [38], zig-zag electrodes [48] or a compliant substrate [49] to convert mechanical strains into electricity. The third group of nanogenerators is based on fibers often constructed by the electrospinning process. For example, structures made of PZT (Lead zirconate titanate), a ceramic material that exhibits exceptionally good piezoelectric properties, are often utilized [50–52]. Organic fibers made of polymeric PVDF have also been studied as nanogenerators [11,53,54]. Compared with those aforementioned nanomaterials, PVDF fibers have the unique good combination of material properties in flexibility, lightweight, biocompatibility and availability in ultra-long lengths, various thicknesses and shapes, making them an interesting candidate for energy harvesting applications in wearable and/or implantable devices.

There are many forms of ambient energy generation ranging from human scale to massive scale such as ocean waves and waterfalls. Energy harvesting devices based on one-dimensional nanostructures have been proposed and demonstrated only in recent years while great progresses toward potential practical applications have been the key research targets. Since nanostructures are very small in nature, it will require a significant amount of nanostructures to generate enough power for practical usages. For example, nanogenerators using large amounts (1400~1500 nanowires/mm^2) of ZnO nanowires have been shown to generate decent values of energy outputs to power LED light with up to 1V of voltage being generated [38,40,55]. However, these nanowires also have some drawbacks including short structural length (a few μm) which limits overall energy harvesting capacity, high processing temperature and difficulty of controlling the orientation of individual wires. Another possibility is using polymer based piezoelectric material. Our group has demonstrated single PVDF nanogenerator using near-field electrospinning [11] with good control over the deposition location. Theoretically, infinite length of fibers can be constructed for possible applications such as electric clothing [3,56]. This chapter describes efforts in making parallel PVDF fibers to advance the current state-of-the-art technologies based on single PVDF fiber. Parallel connections of multiple fibers are used to enhance the current outputs and the energy harvesting device is fabricated on flexible substrate through conventional lithography process to have easy integration processes.

2.1.1. Piezoelectric Nano Materials

2.1.1.1 PZT Nanowires and Fibers

In the area of energy harvesting by using PZT nanowires, Wang et al. have successfully demonstrated a series of nanogenerators using epitaxially grown PZT nanowires as shown in Figure 2.1(a) with outstanding performances [38][57–59]. These PZT nanowires have limited length as constrained by the fabrication method similar to ZnO nanowire-based nanogenerators. PZT microfibers have also been machined either by using a computer controlled dicing saw to cut fabricated PZT thin films by using mixed oxide powders with extrusion/suspension spinning, or by wet-chemical sol-gel process via VPP (viscous plastic processing) [60]. These fibers can have rectangular or circular with diameters from 50-500μm as shown in Figure 2.1(b).

A nanogenerator has been constructed in a similar fashion by using lithography process to define PZT ribbons (5μm in width and 500nm in thickness) and a dry transfer process using a PDMS substrate as illustrated in Figure 2.1(c) [61]. Two recent reports, on the other hand, by Chen et al. [50] and Zhang et al.[52] have applied far-field electrospinning to produce long PZT fibers for nanogenerator applications. In the device

demonstrated by Chen et al., PDMS was used to cover electrospun PZT fibers on top of the comb-shape platinum electrodes as shown in (d) [50]. A post electric poling process was conducted at 140°C for 24 hours at 4V/µm between two adjacent platinum electrodes for enhanced piezoelectricity. When a pressure is applied using a Teflon stack/human finger, the device was able to generate an output voltage up to 1420mV. Zhang et al. have also demonstrated a PZT nanowire-based nanogenerator using electrospun PZT fibers without any post poling process [52]. These PZT fibers were contacted on either end using silver paste. A three point bending test with applied strain of 0.5% was used to the creation of an output voltage of 170mV which can be attributed to the strain-induced charge of the PZT fibers.
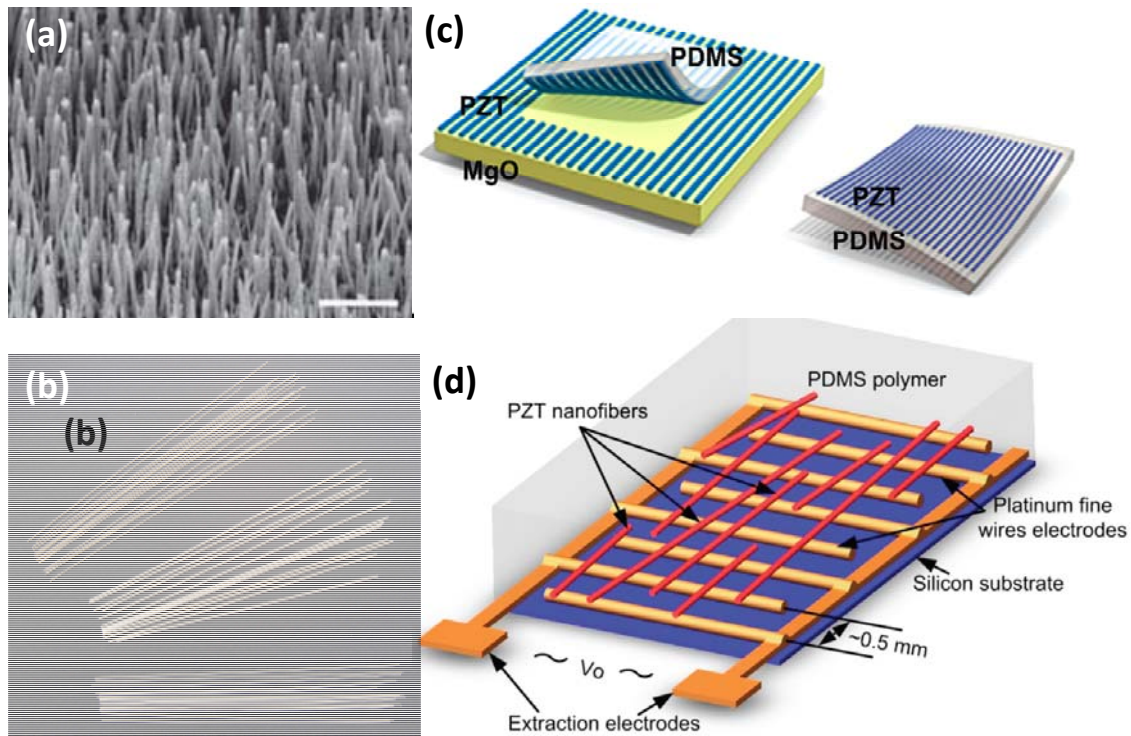
Figure 2.1 (a) Scanning electron microscopy image of the epitaxially grown PZT nanowire arrays by hydrothermal decomposition [58]. Scale bar, 5 µm. (b) PZT microfibers with rectangular or circular and different diameters [62]. (c) A transfer process using lithography to define PZT ribbons and PDMS substrate to transfer the PZT fibers [61]. PDMS was used to cover electrospun PZT fibers on top of the comb-shape platinum electrodes (d) [50].

2.1.1.2 Electrospun PZT and PVDF Fibers

Ceramic PZT and polymeric PVDF are two piezoelectric materials which have been previously demonstrated as viable fiber nanogenerator materials. In these efforts, either near-field electrospinning (NFES) [3] or the conventional far-field electrospinning (FFES) process has been the key manufacturing tool to produce fibers [63]. For the NFES process, a continuous single fiber can be deposited in a controllable manner, while the FFES process can produce dense fibers networks on large areas for the nanogenerator demonstrations. In general, a poling process, consisting of both electrical poling and mechanical stretching, is required in the fabrication of materials with piezoelectric properties at moderate temperature. Given the high electrostatic field and polymer jet characteristics of the electrospinning process, electrospinning is ideally suited for producing piezoelectric fibers through in-situ electric poling and mechanical stretching. Here, key achievements in fiber nanogenerators made of PVDF and PZT are described and discussed.

PVDF has superior piezoelectric properties as compared with other types of polymeric materials due to its polar crystalline structure. In nature, PVDF polymer consists of at least five different structural forms depending on the chain conformation of trans (T) and gauche (G) linkages. Figure 2.2(a) shows the crystalline structure of the α and β–phase, respectively. While the α-phase is known as the most abundant form in nature, β–phase is responsible for most of PVDF's piezoelectric response due to its polar structure with oriented hydrogen and fluoride (CH_2-CF_2) unit cells along with the carbon backbone. In order to obtain the β-phase PVDF, electrical poling and mechanical stretching processes are required during the manufacturing process to align the dipoles in the crystalline PVDF structures as illustrated in Figure 2.2.

PZT is another good piezoelectric material with its crystalline structure illustrated in Figure 2.2(b). An electric polarization of PZT can shift up/down of Zr/Ti atom and remain their positions after applying and removing an external electric field for the piezoelectric property. In their bulk or thin film format, PZT can generate higher voltage as compared with other piezoelectric materials for sensing [64], and actuation [65] and energy harvesting applications . As a ceramic material, bulk PZT is more fragile in comparison to organic PVDF, but has demonstrated very good mechanical strength in nanowire form [51].
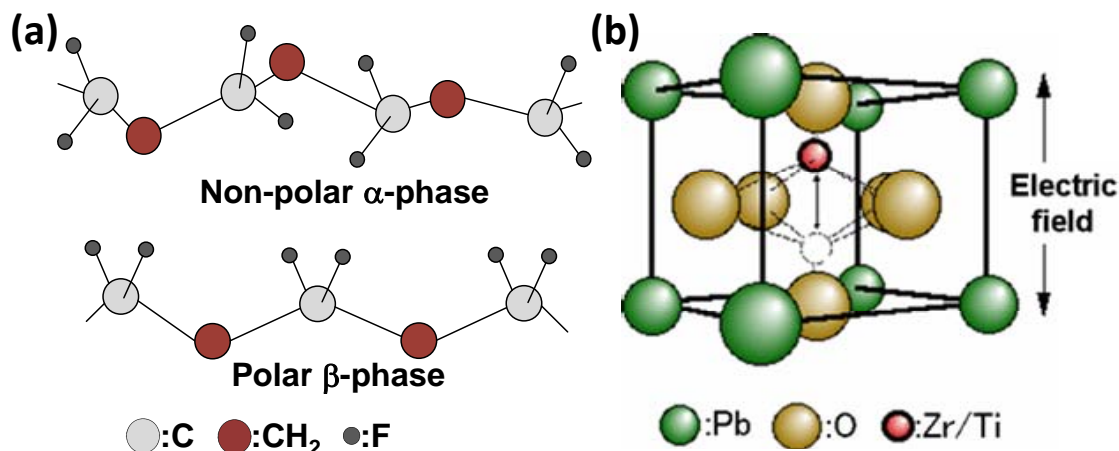
Figure 2.2 (a) Schematic diagrams showing crystalline structures of PVDF: (top) non-polar α-phase, and (bottom) polar β-phase. The dipoles in the non-polar, α-phase PVDF could be stretched and oriented by an electrical field to become the polar, β-phase structure under electrical poling and mechanical stretching. (b) Schematic diagrams showing crystalline structures of PZT. An electric polarization of PZT can shift up/down of Zr/Ti atom and remain their positions after applying and removing an external electric field for the piezoelectric property.

2.1.2 State-of-Art Electrospun Nanogenerators

Table 2.1 summarizes key characteristics of nanofiber nanogenerators from aforementioned works. Clearly, electrospinning has been used in all demonstrations to make continuous, long nanofibers either in orderly fashion (NFES) or as randomly distributed networks (FFES). Nanogenerators using a single nanofiber nanogenerators are marked as "S" those using multiple nanofibers are marked "M". The diameters of these fibers range from 60nm to a few micrometers. While some reports did not provide information on the applied strain or strain rate or record the peak current values, all have measured the peak voltage values over a wide range of less than 1mV to 2.21V (large number of nanofibers). In order to provide better prospects for the future directions stemming from the current results, manufacturing methodologies, material properties and experimental procedures/characterizations are to be discussed in the following sections.

Table 2.1 Summary of Nanofiber Nanogenerators

Material	Synthesis Method	Diameter (nm)	Strain/ Strain Rate	Peak current	Peak voltage	Ref.
	FFES (M)	60	12%	N/A	1.63V	[50]
PZT	FFES (S)	100	N/A	N/A	0.4mV	[51]
	FFES (M)	50–150	0.5%	N/A	0.17V	[52]
	FFES (M)	187	34mm/s (at 5Hz)	4μA/2cm^2	2.21V	[53]
	NFES (S)	500-6500	0.085%	0.5-3nA	5-30mV	[11]
PVDF	NFES (M)	1000-2000	N/A	30nA	0.2mV	[54]
	FFES (M)	600	0.05%, 1.67%/s	0.3nA	20mV	[66]
P(VDF-TrFE)	FFES (M)	60–120	N/A	N/A	400mV	[67]

FFES: Far-field electrospinning, NFES: Near-field electrospinning,
(S): single fiber, (M): Multiple fibers

It is Important to generate continuous and reliable fibers to have strong piezoelectric effect. Uniform mixing of PVDF polymers in solutions enhances dipole alignment during electrospinning process such that high electrical output could be available. Starting point of such good solution is to optimize fiber producing setups such as molecular weight of PVDF, solvent, tip to substrate distance and bias voltage. There are various different recipes from many research groups to optimize the process to meet their own application needs. Those parameters are summarized in Table 2.2. Typical solvent used in PVDF polymer is DMSO and DMF. The most popular one is DMF as it shows good adhesion to substrate than DMSO. However, DMF is known to be not a good material to create continuous polymers and it is toxic to the environment. Also, high molecular weight of PVDF has long chain length such that good dipole alignment could be challenging.

Table 2.2 Fabrication parameters of PVDF-based nanofibers

Material	Molecular weight	Solvent	Method	Typical Bias	Tip-to-substrate	Mean Field Strength	Piezo-electricity?	Ref
PVDF	172,000 (16% wt)	DMF	FFES	15kV	15cm	10^5 V/m	Yes	[53]
PVDF	534,000 (20% wt)	DMSO (50%) + Acetone (50%)	NFES	1kV	1mm	10^6V/m	Yes	[11]
PVDF	534,000 (20% wt)	DMF (60%) + Acetone (40%)	FFES	12kV	10cm	1.2×10^5V/m	No	[68]
PVDF	534 000 (12% wt)	DMF (40%) + Acetone (60%)	FFES	12kV	15cm	0.8×10^5V/m	Yes	[69]
PVDF	275 000 (various)	DMF + Acetone various ratios	FFES	13kV	15cm	0.87×10^5V/m	Yes	[70]
PVDF	Solef 1100 (20% wt)	DMF (60%) + Acetone (40%)	FFES	15kV	15cm	0.75×10^5V/m	Yes	[71]
P(VDF-TrFE)	(77:23 mol%)	Butan-2-one	FFES	20kV	10cm	2×10^5V/m	Yes	[67]
PVDF	687,000 (10-20% wt)	DMF	FFES	20kV	15cm	1.3×10^5V/m	Yes	[72]
PVDF+ CNT	115 000 (20%)	DMF (60%) + Acetone (40%)	FFES	15kV	N/A	N/A	Yes	[73]
PVDF	Foraflon® 4000HD (various)	DMF + Acetone various ratios	FFES	10kV	3cm	3.3×10^5V/m	Yes	[74]
PVDF	268,000	DMF (60%) + Acetone (40%)	FFES	15kV	20cm	0.75×10^5V/m	Yes	[75]

2.2. Working principle

Piezoelectric material has great potential for micro to nano scale energy harvesting devices for its low material cost and high piezoelectricity. Among the piezoelectric polymers, PVDF powders can be dissolved in solvents and electrospun onto various substrates with high piezoelectric constant, superior mechanical properties and biocompatibility [76,77]. However, PVDF in its natural form does not exhibit piezoelectric property and electrical/mechanical poling processes are critical to transform alpha-phase to beta-phase. Once the beta-phase is obtained, mechanical strains can create local potential difference to generate electrical voltages as nanogenerators.

Figure 2.3 shows the working principle of the nanogenerator device on top of a flexible polymer substrate. A total of 10 pairs of gold electrodes were designed in the prototype system in the shape of comb fingers. The narrow, 100μm-wide gaps were used as the working distance and the 1mm-wide gaps were used as the separation distance between each pair of working electrodes. A total of 50 parallel fibers were electrospun on top of the electrodes as illustrated such that there were 500 active working contact points to collect charges generated from these PVDF fibers. The device experienced axial strains by bending the plastic substrate to generate electrical potential. As the connections are in parallel, the total output current was amplified.
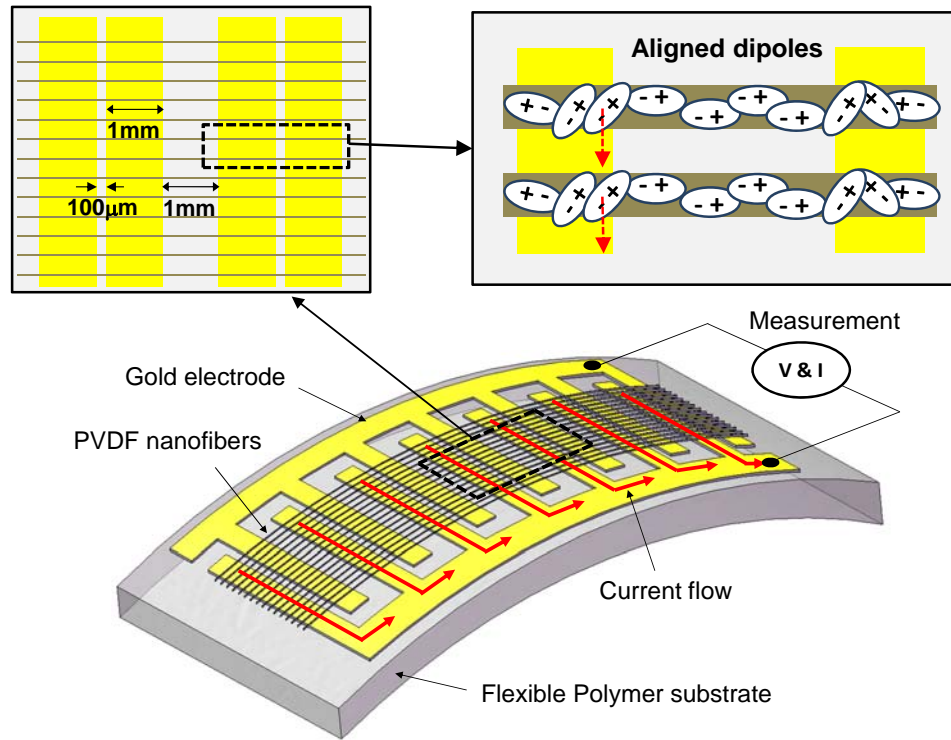
Figure 2.3 Working principle of the large array energy harvesting device by electrospun fibers. A total of 50 fibers and 10 electrode pairs have been designed in the prototype device on top of a flexible substrate.

2.2.1. Measurement artifacts

In order to test the performance of the nanogenerators, electrical outputs generated by mechanical inputs are conducted for fibers. These signals are often very small and are difficult to measure due to the nature of the small size of the fibers. The background noise or artifacts can easily overshadow the true signals. It is especially problematic when dealing with single fiber structures. For example, the capacitance changes between the wires and the electrodes and possible electrical coupling of the measurement instruments could surpass the real fiber signals. Therefore, it is important to filter out or reject noises generated from the surrounding experimental environment. Some of these experimental validation conditions have been previously proposed for semiconductor-based or ceramic-based nanogenerators such as ZnO nanowires, while PVDF nanogenerators do not apply to some of the requirements such as the Schottky behavior test.

2.2.1.1. Switching polarity criterion

The polarity of the generated potential from the nanogenerator should be the same after the device fabrication process under the same direction of mechanical deformation. This leads to the electron flow direction to be independent to the connection wires to the instrument such that switching the polarity of the measurement instrument should lead to a reversed in output signals. Therefore, to confirm the validity of the recorded piezoelectric responses, different combinations of probe connections with experiments on both stretching and compressive operations of the nanogenerators should be characterized. In the forward connection, the positive and negative probes were connected to the positive and negative potential of the nanogenerator, respectively. In this case, a single PVDF fiber nanogenerator with known polarities as shown is used as the illustration example [11]. In the backward connection, this connection is reversed. Since the polarity of the nanogenerator is fixed, this switching polarity test should generate electrical outputs with reversed responses.

2.2.1.2. Linear superposition criterion

When two nanogenerators are connected in series, the voltage response should be the sum of the two nanogenerators, while the current response should be sum of the two when connected in parallel. Similarly connecting two identical devices in series with opposite polarity should result in nearly a zero voltage response.

2.2.1.3. Artifacts due to contact electrodes

In order to measure the electrical outputs from the nanogenerators, it is necessary to have at least two electrical contact pads (or multiple electrodes) typically placed on top of a substrate with fibers as illustrated in Figure 2.4(a). Large mechanical actuation of the substrate nanogenerator could result in a capacitance change due to the varying distance of adjacent contact electrodes as artifacts. Specifically, the total capacitance of the device due to contact pads is the sum of the capacitance of the gap between adjacent electrodes and that of the overlapping area as illustrated in figure 2.4(a).

$$C_{contact\_pad} = C_{gap} + C_{overlap} \qquad (2\text{-}1)$$

Since the magnitude of capacitance is proportional to the area and inversely proportional to the gap distance, small contact electrode area and large gap distance are preferable to reduce the impact of artifact due to the contact pads. Under small actuation as shown in the left side of Figure 2.4(a), $C_{overlap}$ could be insignificant while under large actuation as shown in the right side of Figure 2.4(a), $C_{overlap}$ could dominate the total responses. By switching the actuation direction upward or downward, the output responses due to the electrode gap will have opposite effects as C_{gap} between two electrodes decreases or increases, respectively. On the other hand, $C_{overlap}$ should always increase due to the increased overlapping area under either direction of upward or downward actuation. Figure 2.4(b) are experimental results based on upward actuation and release to the original flat position under small actuation (left) and large actuation (right), respectively. Figure 2.4(c) shows the measurement results from the same tests based on downward actuation and release to the original flat position. The specimen used in these tests has an electrode area of 20mm×20mm and cross-sectional area in the 100μm wide gap of 50nm×20mm in cross sectional area without depositing any fibers. The output signals from small actuation (left side of Figure 2.4((b) and (c)) are smaller than 1mV which can be considered as noise when compared with the typical voltage outputs of a single fiber at tens of mV [11] while the clear change in the polarities of the output signals suggests the outputs come from the changes in C_{gap}. On the other hand, under large actuation, the contribution of C_{gap} is small and the changes of $C_{overlap}$ dominate the output signals while either upward or downward actuation should increase $C_{overlap}$. As expected in the right side of Figure 2.4(b) and (c), larger outputs up to 10mV were observed while the polarity changes are the same in both figures under either upward or downward actuation. Nevertheless, these effects could be easily filtered out if the "switching polarity criterion" is checked.
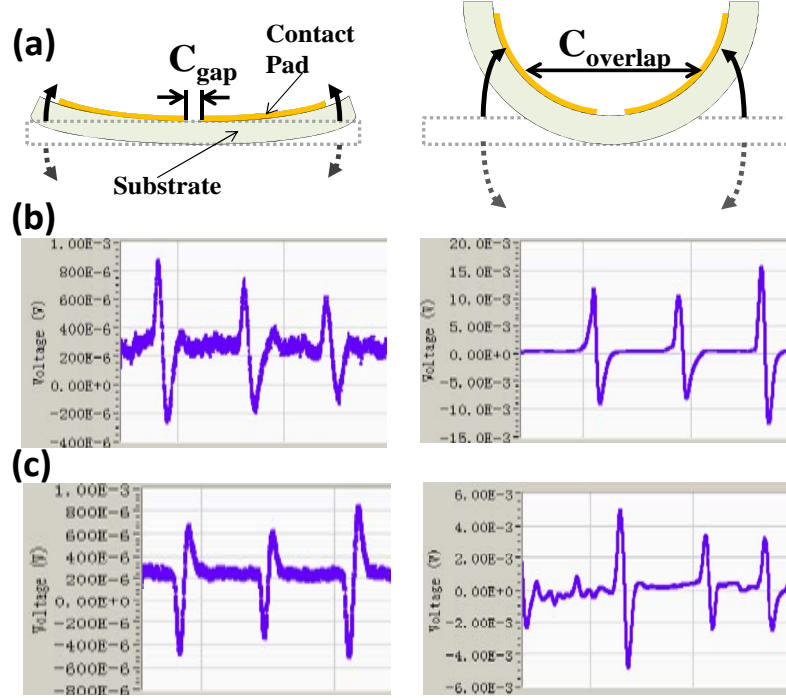
Figure 2.4 (a) Schematic diagram showing the possible artifacts of nanogenerator outputs due to the contact electrodes from the sources of C_{gap} and $C_{overlap}$ under small (left) and large (right) substrate actuation tests. (b), (c) Experimental voltage outputs from upward and downward actuation tests, respectively, with small (left figures) and large (right figures) substrate actuation. Under small actuation, C_{gap} could be the dominating factor to change the polarity of the output signals of upward and downward actuation as shown. Under large actuation, $C_{overlap}$ could be the dominating factor and no polarity change is found due to upward or downward actuation as $C_{overlap}$ increases in both actuation directions.

2.3. Device fabrication and experimental results

Device fabrication process is based on the combination of both the conventional lithography and near-field electrospinning processes as shown in figure 2.5. First, the flexible substrate (Thermanox®) is cleaned by IPA and dried with nitrogen prior to the lithography process. A 2μm-thick G-line photo resist is spun on the polymer substrate followed by patterning the photoresist for a lift-off process. Afterwards, a layer of 15nm-thick silicon dioxide is deposited by e-beam evaporation to provide better electrical insulation and promote adhesion. A 10nm-thick chromium layer is evaporated as the adhesion layer and followed by the 150nm-thick gold deposition process. After these steps, Figure 2.5(a) applies. The electrode areas are then defined by the lift-off process as shown in figure 2.5(b). The near-field electrospinning process is performed to deposit PVDF fiber as illustrated in figure 2.5(c). The fibers are deposited continuously to the collector by a designed circular pattern as controlled by an x-y stage. The direction of fibers is therefore controlled to be the same on top of the electrode structure to assure same polarity. A high potential is applied to between electrodes with 100μm-wide gaps for the alignment of dipoles. The breakdown voltage of air is only ~30kV/cm which is low for the poling process. A 2mm-thick PDMS (breakdown voltage: ~250kV/cm) is deposited and cured at 70°C for 30minutes to increase the possible breakdown voltage. As shown in figure 2.5(d), an electrical poling process with field strength of 200kV/cm is then applied for 30mins [66] while the substrate is sitting on top of a 70°C hot plate to activate the piezoelectricity of PVDF fibers. Higher temperature could further help the active movement of dipoles inside the polymer.
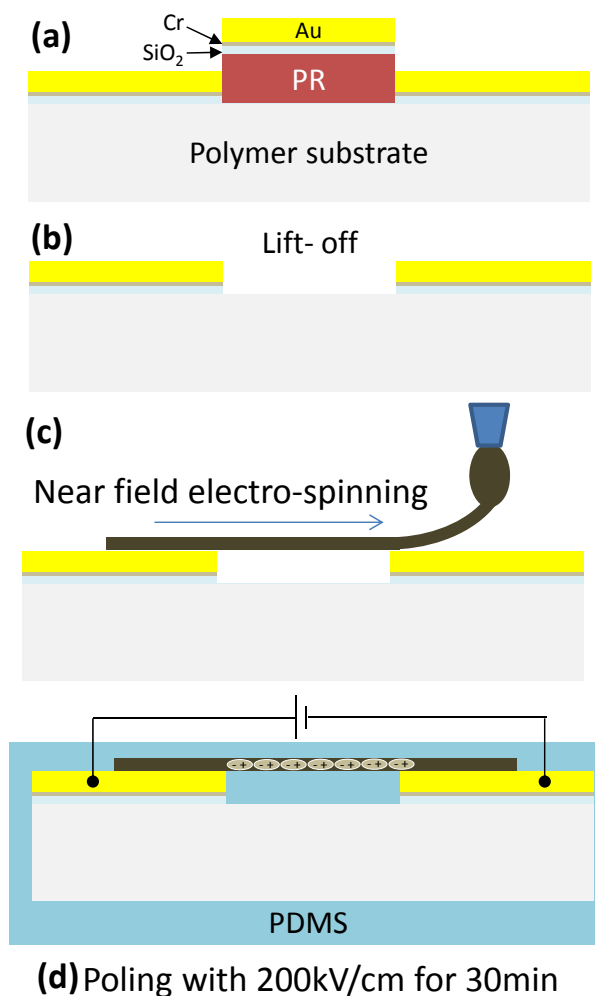
Figure 2.5 Device fabrication flow chart by using a chemically inert flexible polymer substrate (Thermanox™). (a) Photolithography followed by silicon dioxide (15nm), Chromium (10nm) and Gold (150nm) deposition. (b) Lift-off of the photoresist. (c) Deposition of PVDF fibers using near-field electrospinning. (d) PDMS shielding and electric poling under estimated electrical field strength of 200kV/cm for 30mins.

2.3.1. Experimental setup

The fabricated device is shown in Figure 2.6. In the left image, continuous fibers could be seen on transparent plastic substrate. The magnified image on right shows aligned fibers on the surface of gold electrodes. These fibers are deposited with the continuous near-field electrospinning process with diameter of 1-2μm. The diameter of the fibers can be controlled via the magnitude of applied electrical field (voltage and electrode-to-collector

distance) as well as the property of polymer solution. In general, smaller electrical field strength will result in thinner diameter of fibers. On the other hand, the gap between two adjacent fibers is designed as 100μm with a total number of 50 fibers as shown.
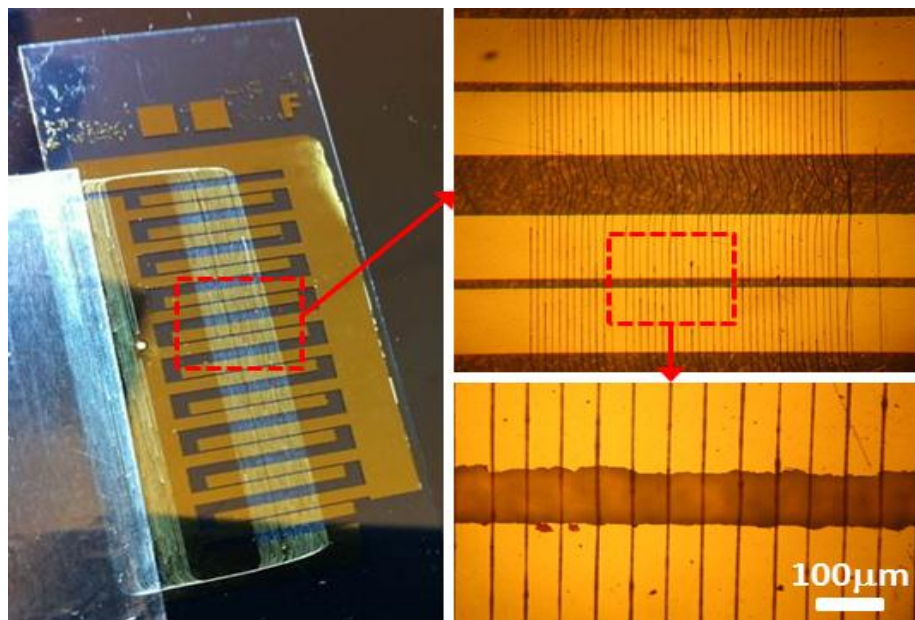
Figure 2.6. Optical images of fabricated nanogenerator device with aligned fibers. The working gap between two electrodes is 100μm. Fibers are electrospun continuously and these fibers have the same polarity (same electrospun direction).

Figure 2.7 shows COMSOL® simulation results of the electrical field during the electric poling process. The simulation is to analyze the strength of electrical fields in the 100μm- and 1mm-wide gaps. The electrical potential streamlines are simulation results when one side of the electrode is applied with 0V and its neighboring electrode is applied with 2kV. Due to the design of the comb-shape electrode, the same electrical voltages of 0 and 2kV are naturally applied sequentially between electrodes with 1mm-wide gap. The preferred situation is that the electrical field is strong enough for electric poling process between the 100μm-wide gaps and is weak without causing electric poling between the 100mm-wide gaps. Otherwise, the total piezoelectric effect can be canceled on the fiber due to opposite electric poling effects in different segments (100μm-wide and 100mm-wide gaps) of the fiber. Simulation results show that the electric fields in the 100μm- and 1mm-wide gap are 200kV/cm and 20kV/cm respectively. As a result, the much stronger field between the 100μm-wide gap is designed to provide effective electric poling for the fiber while the weak field in between the 1mm-wide gap is not expected to cause electric poling.
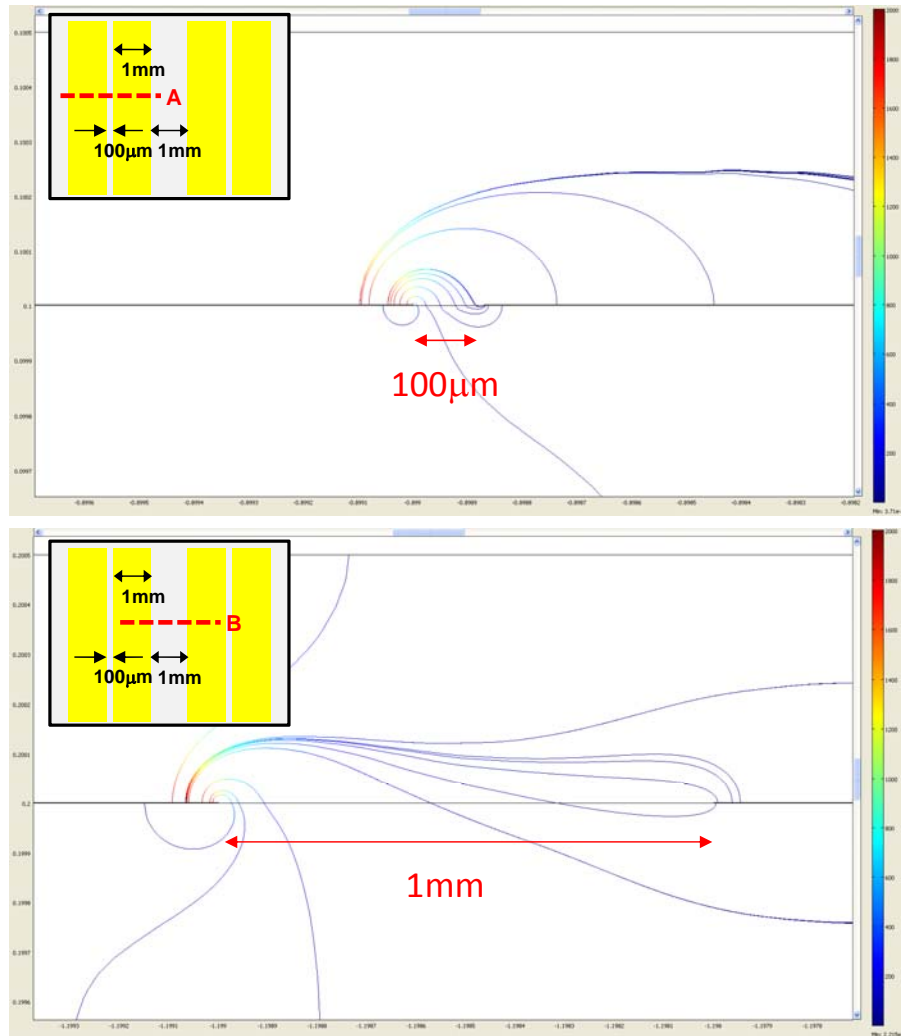
Figure 2.7   Electrical fields between the100μm-wide gap and 1mm-wide gap are simulated. Strong electrical field of 200kV/cm is simulated in the 100μm-wide gap (cross section A) while weak field of 20kV/cm is simulated in the 1mm-wide gap (cross section B) when 2 kV of voltage is applied.

2.3.2. Measurement results

The fabricated device goes under repeated strain generated by a DC motor at 1Hz frequency. The bending deformation given by the motor provides a strain of $0.1 \pm 0.05\%$. Current and voltage generated from the device are measured inside a Faraday cage to block outside noise.

Figure 2.8 shows the current measurement results for the forward and reverse connections, respectively. The reason for the two way connections is to validate that the measured results are true piezoelectric responses instead of artifacts. If the signal is coming from the noise instead of piezoelectric responses, the shape of the response should not change. True piezoelectric responses will have polarity effects such that simply switching the measurement polarity will flip the response as shown in the figure 2.8. The bottom plots show magnified pattern from a single bending and releasing process. The peak current in the forward connection measurement was about 30nA while in the reverse connection measured was only about 2nA. The reduced response observed after the change of polarity change requires further investigations. However, it is possible that inherent current flowing inside the measurement equipment has contributed the responses. If this is the case, the real current generated from the device is the average of the two responses in which the inherent current should be subtracted from measured data with forward connection and data with reverse connection.
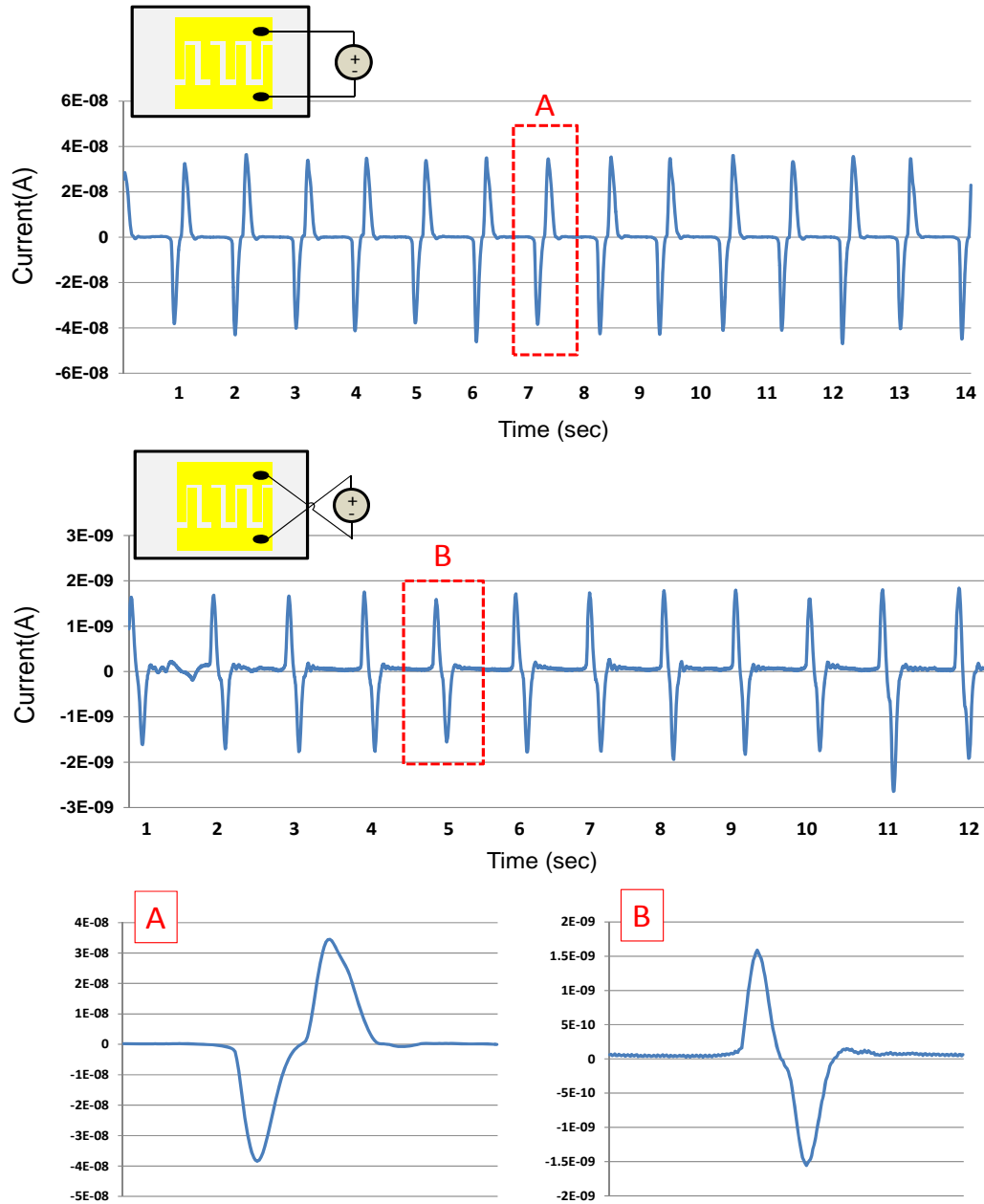
Figure 2.8 Current generated from device is monitored under repeated application of strains. The response shape is flipped when the measurement polarity is switched.
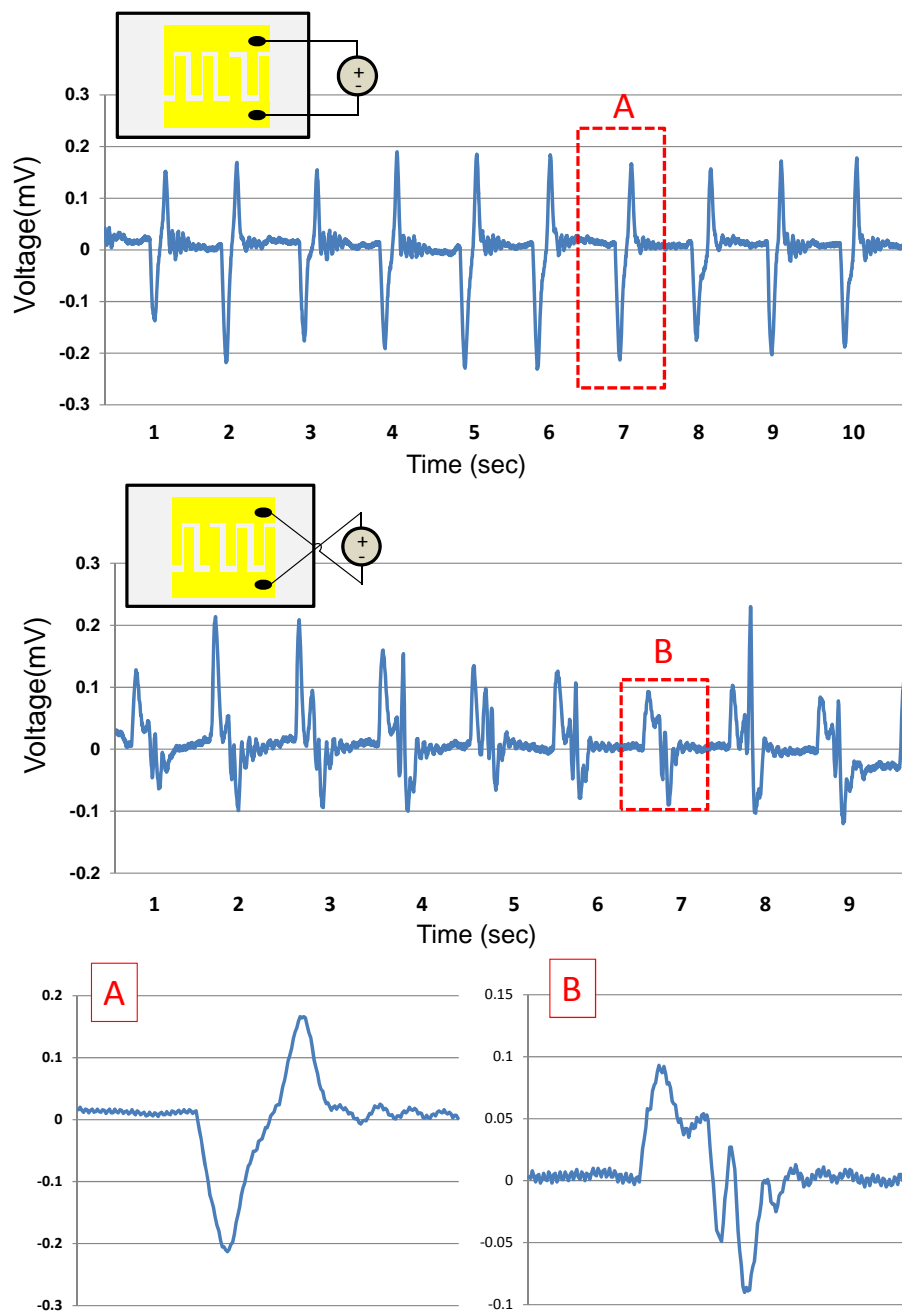
Figure 2.9. Voltage generated from the device is measured in both forward and reverse connections. The response shape is flipped when the measurement polarity is switched. Peak voltage is about 0.2mV and no significant reduction of signal is monitored in the reverse connection measurement. The output is small under the parallel connection of nanogenerators.

The voltage measurement result is plotted in Figure 2.9. Similar to the results from current measurements, the shape of voltage responses was flipped as expected. The bottom plots in Figure 2.9 show voltage measurements from a single bending and releasing test. The peak voltage was about 0.2mV in both forward and reversed connections. Interestingly, the significant decrease in current measurement results under reversed connection was not observed in the voltage measurements.

It is noted that both current and voltage outputs of these PVDF nanogenerators are about at least one order of magnitude less than the previous report on a single PVDF fiber [6]. Possible explanations are: (1) the *in-situ* poling process could be more effective to induce stronger piezoelectric effects as compared with the post poling process in this work; (2) partial reverse energy generation effects from the opposite neighboring electrodes which generate counter voltages and currents in the current work; and (3) encapsulation of the fiber in the current work could increase the loss of charges to the package material. These will be further investigated.

2.4. Material property characterization

Four different methods are commonly applied for fundamental piezoelectric property analysis of PVDF fibers: FTIR (Fourier transform infrared spectroscopy), XRD (X-ray diffraction), PFM (Piezoelectric force microscopy) and Second Harmonic Generation analysis. In collaboration with laboratories in the chemistry and physics departments of UC Berkeley, the first three methods have been used to analyze PVDF fibers manufactured by the NFES process. Both FTIR and XRD analyses provide general information on the content of beta-phase in PVDF fibers. The PFM analysis provides the capability to investigate a tiny local area (by using the AFM tip) for the piezoelectricity of fibers.

Experimentally, three types of polymer solutions have been chosen for the analysis: PVDF by using DMSO as solvent, PVDF by using Dimethylformamide (DMF) as solvent and P(VDF-TrFE) by using DMSO as solvent. The first two samples were selected in order to study the impact of solvent to the piezoelectricity of PVDF fibers. Commercial PVDF thin films with good piezoelectricity have been using DMF as the solvent. However, PVDF is toxic such that the material handling process has to be very careful under a fume hood. PVDF fibers fabricated by using DMSO could lead to different piezoelectric properties as compared with PVDF thin films with DMF as the solvent and should be investigated. On the other hand, P(VDF-TrFE) has also been analyzed in this work. In general, P(VDF-TrFE) has preferential beta-phase form even without electric poling in bulk materials. However, it will be interested in studying the material properties in the form of fibers by means of electrospinning processes.

In addition to different materials, different fabrication methods have also been applied and the material properties from different manufacturing processes have been analyzed. For example, results from fibers fabricated with syringes with sharp and flat tips could provide information on the influence of the syringe shape to the beta-phase content of the fibers. The properties of hand-drawn (fabricated by pulling fibers without the application of an electric field) fibers are also compared with samples made by FFES and NFES processes. These studies aim to provide guidelines to produce high quality fibers for applications such as PVDF nanogenerators.

2.4.1. XRD (X-ray diffraction)

X-ray diffraction (XRD) has been commonly used for the analysis of the crystalline structure of materials. Baji et al. have analyzed PVDF fibers fabricated by far field electrospinning using XRD. It was found that the β-phase is most abundant in electrospun PVDF fibers while other crystalline forms did also exist. Electrospun fibers with smaller diameters were found to have higher contents of β-phase probably due to the strong stretching effect. Other groups have also utilized XRD to analyze the structures of electrospun Polar β-Glycine Fibers [78] and polycrystalline barium titanate fibers [79]. For PZT fiber based nanogenerators XRD is interesting because it can be used to confirm the presence of the pervoskite phase of the material. This phase is crucial for piezoelectric PZT. Using metallo-organics decomposition (MOD) method for PZT fiber fabrication the pervoskite phase is formed during the fiber annealing process between 600 to 850°C [80]. Yu Wang et al. used XRD analysis during the annealing process. They observe that above 600°C the pervoskite phase starts appearing while coexisting with the pyrochlore phase. Only above 850°C the pyrochlore phase is completely replaced by the pervoskite phase. Xi Chen et al. conduct a similar experiment using a PZT sol-gel, poly vinyl pyrrolidone and alcohol mixture [50]. The XRD results can confirm the pure pervoskite phase of the fibers for an annealing temperature of 650°C.

XRD tests have been performed on the PVDF materials of various forms, including bulk film, hand-drawn fibers, FFES fibers and NFES fibers, fabricated in this work. These film/fibers were made by PVDF/Acetone (10% v/v) polymer solutions with DMSO (10% v/v) as surfactant. The thin film samples were made by a spining process (2000 rpm) to have about ~5μm in thickness. HS fibers are made by putting a needle tip into the polymer solution and pulling some fiber solutions out to connect two points. Multiple connections had to be made to cover the samples with large number of fibers (more than 100 times) and those fibers are collected to make a cotton ball shape as shown in figure 2-10. Other samples are also prepared to have the similar shape to be tested in XRD and FTIR machine.
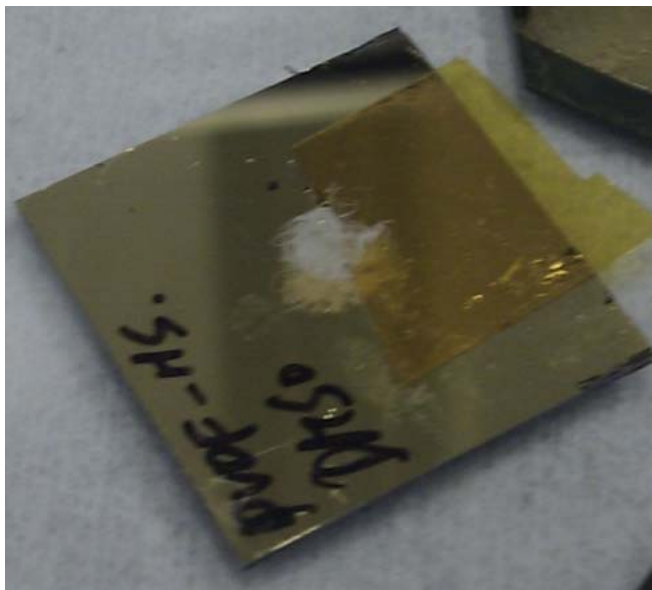
Figure 2.10 The white color fibers at the center of the specimen were prepared with hand-spun method. Large number (more than 100 times) of fibers was drawn manually by using a tungsten probe to dip-in and -out of the solution to make individual fibers.

FFES process is conducted with 15cm gap between syringe and conductive substrate by applying 15kV of potential. The fibers are collected during spinning process with a size of 3mm in diameter. NFES process is performed with 1kV of potential applied between 1mm-wide gap. The substrates used for all samples are silicon chips which have very different crystalline structure than PVDF. The most apparent peak at 24º is the alpha-phase peak. Interestingly, bulk film and hand-spun samples show similar peaks at 24º while fibers made by FFES and NFES do not have clearly identifiable peaks. Materials with strong beta-phase contents should have peaks at 20.4º in the XRD tests. However, it is very difficult to prepare large and dense fibers by the electrospinning process in our current setup such that there were no clear signs for the beta-phase content in the XRD tests as shown in Figure 2.11. Another characterization method, FTIR, is utilized as discussed in the next section.
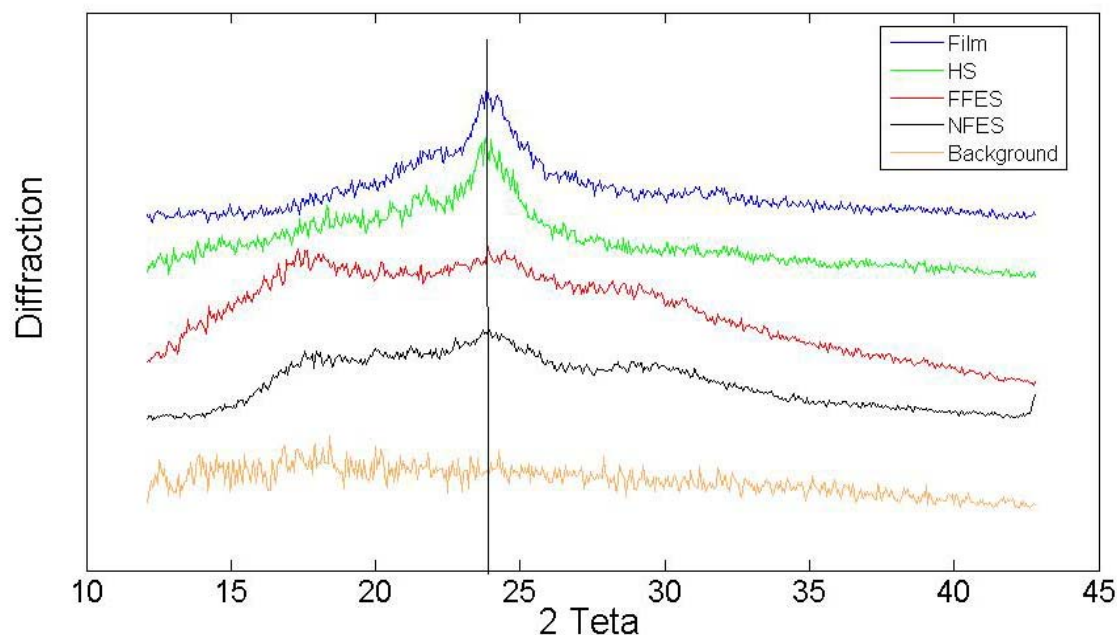
Figure 2.11 XRD spectrum for thin film (blue), hand-drawn (green), FFES (red) and NFES (black) samples.

2.4.2. FTIR (Fourier transform infrared spectroscopy)

Fourier transform infrared spectroscopy (FTIR) can be used to characterize both the dipole orientation and crystallographic structure of fibers based on the sensitivity of CF_2 orientation changes. For example, Dipankar et al. have used FTIR to examine the dipole orientation of electrospun P(VDF-TrFE) fibers [67]. They have shown that the dipoles were aligned in the direction of the electrical field during the electrospinning process [67]. A comparison between the FTIR spectra of an as-spun fiber and a heat-treated fiber (heated above the Curie temperature in order to cause random dipole alignments) has resulted a difference in absorbance of perpendicularly polarized light for the CF_2 sensitive wavelengths. Baji et al. have also confirmed the presence of the crystal β-phase using FTIR in good correspondence to the results obtained using XRD [36]. Yu Wang et al. use FTIR in order to examine the PZT fiber annealing process. The decomposition temperature of organic groups as well as the appearance of the pervoskite phase can be determined.

The FTIR tests performed on handspun, bulk film, far-field electrospinning and near-field electrospinning samples are summarized in Figures 2.12 and 2.13 by using DMF and

DMSO as solvents, respectively. Results from Figure 2.12 show that peaks at 610/cm representing the alpha-phase are visible in the bulk-film and hand-drawn samples. On the other hand, the peaks at 1280/cm representing the beta-phase is a bit stronger in FFES and NFES samples. For both DMS and DMSO samples, no clear difference was detected and both of them show differentiable results between alpha- and beta-peaks. Figure 2.14 shows FTIR of the PVDF-T(rFE) polymer which is known to form much stronger crystalline structure due to more Fluoride atoms in the molecular chain. Results of the FTIR test data show beta-peak on most of the samples regardless of fiber producing methods.
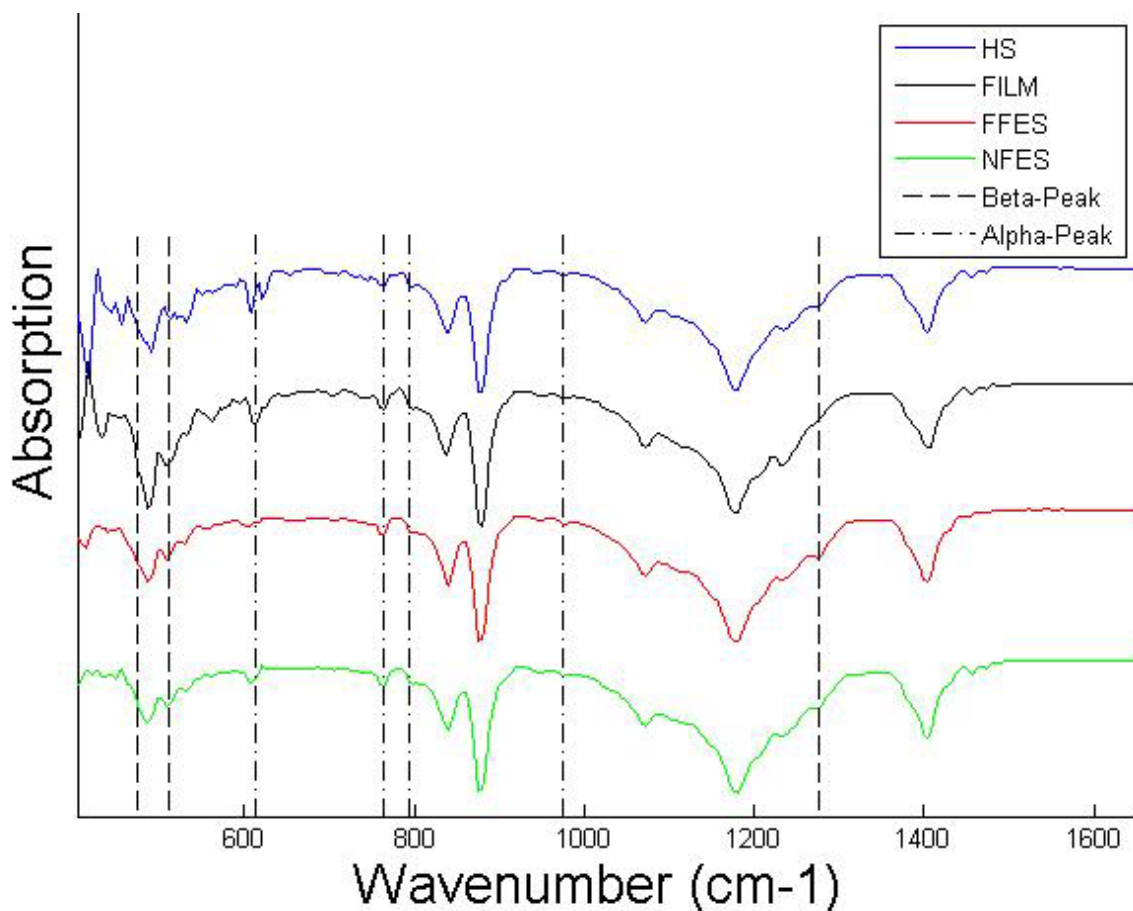
Figure 2.12 FTIR absorption spectrum obtained for PVDF with DMF and acetone solvent. The theoretical absorption peaks are indicated by the dashed lines.
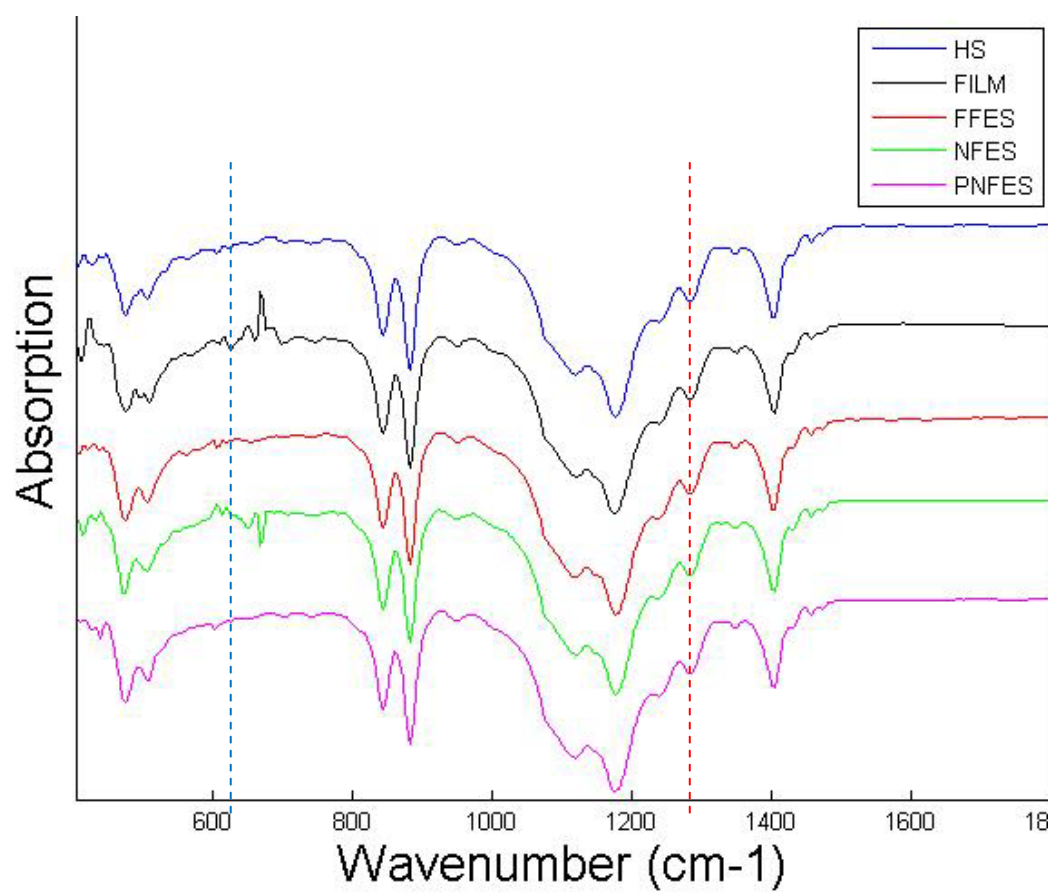
Figure 2.13 Absorption spectrum obtained for PVDF with DMSO and acetone solvent. The characteristics of the five curves from fibers manufactured by different methods are very similar.
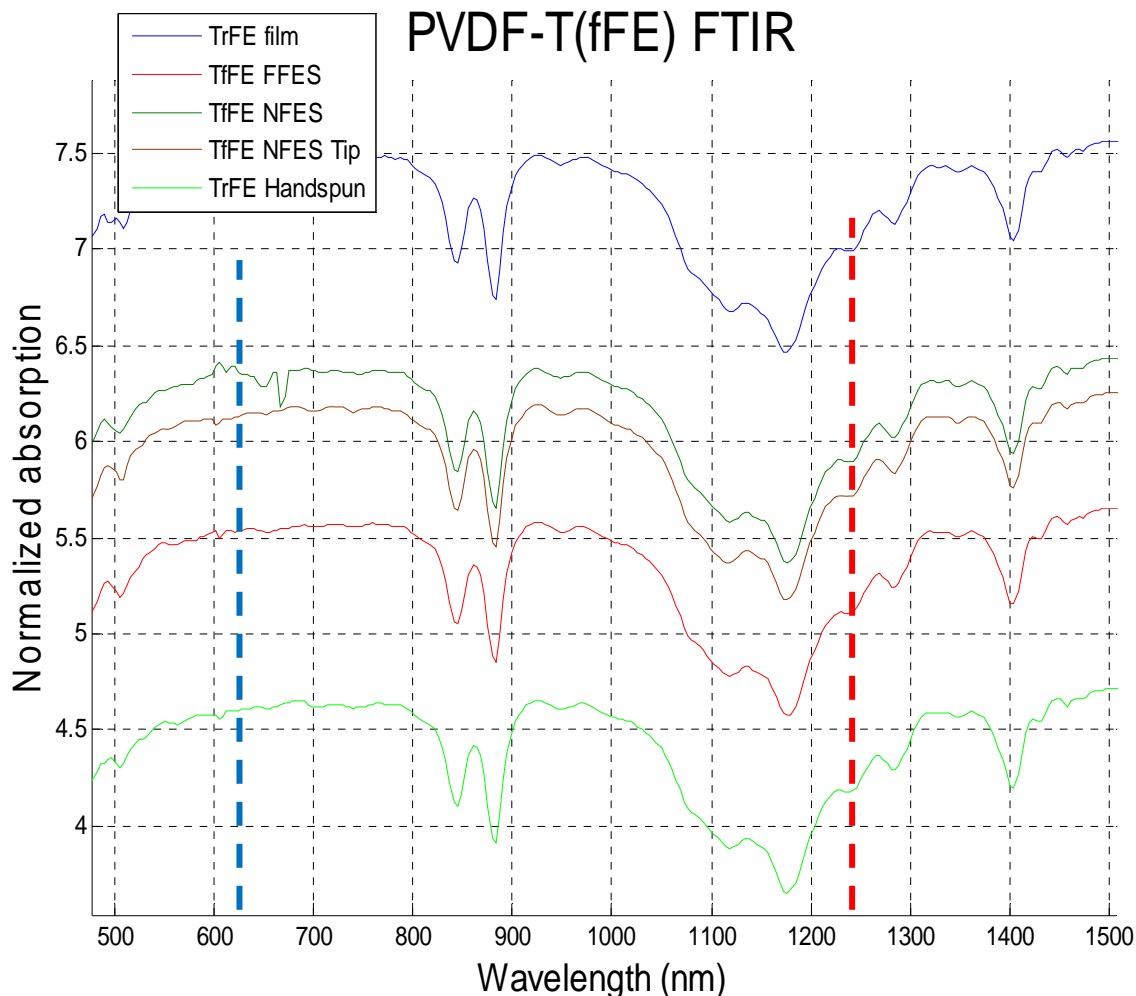
Figure 2.14 Absorption spectrum obtained for P(VDF-TrFE) with DMSO and acetone solvent. Regardless of the spinning method, strong beta-phase was formed.

2.4.3. PFM (Piezoelectric force microscopy)

Piezoelectric force microscopy (PFM) measurements are based on the detection of a voltage induced deformation of the piezoelectric material. Measured data can quantify the degree of the polarization as well as the polarization direction of the tested sample [81]. The PFM setup is comparable to Atomic Force Microscopy (AFM) by using a micro tip to be in contact with the surface while applying a sinusoidal voltage. In the case of a piezoelectric material with a poling direction in parallel to the direction of the PFM bias voltage, this leads to a detectable deformation of the material due to the piezoelectric response which is considered as the "in phase" response. For an opposite poling direction at

the contact area, the observed phase should shift by 180 degrees as the "out of phase" response. Lateral deformations can also be sensed by the detection of the torsional responses of this same tip.

PFM is particularly well suited for the analysis of individual fibers in contrast to other characterization tools because it allows local piezoelectric measurements. For example, in the work to study triglycine sulfate (TGS) nanocrystals embedded poly(ethylene) oxide (PEO) fibers, the morphology of the fiber mat was first characterized by the AFM scan. For the vertical, out-of-plane PFM measurements, the image contrast is used to roughly characterize the effective longitudinal piezoelectric coefficient, d_{33eff}. The response in the lateral mode PFM reflects the effective shear piezoelectric coefficient, d_{15eff}. Similar experiments were conducted by Baji et al. for electrospun PVDF fibers [36].

Figure 2.15 (top) shows the AFM image taken on a PVDF near-field electrospun fiber with a scanning area of 20μm × 5.5μm. The background is a silicon substrate coated with a thin-gold layer. The scanning image from the profile shows the shape of electrospun fiber by the near-field electrospinning process. Due to the short distance between the needle and the collector, the solvent inside these fibers did not complete evaporate in the electrospinning process such that their cross sectional shape is hemi-circular instead of circular. The amplitude response is illustrated in Figure 2.15 (center). It is much less noisy with small amplitude on the gold surface and the responses from the fiber seem to be random but much higher values than other areas. This implies that the near-field electrospinning process may not have aligned the dipoles perfectly along the longitudinal direction. Similarly, the phase response in Figure 2.15 (bottom) shows the directions of the dipoles are random on the fibers and the responses are much lower but uniform on gold surface. Further tests are required to characterize the piezoelectricity of these electrospun PVDF fibers as the direction of measurements is vertical to the axial direction and noisy responses from the edge of the fiber can affect the measurement results. Particular, it is found that AFM tip can easily slip around the edges of the fiber during the scanning process. In the next session, scanning on the cross-section of the fiber is designed and conducted to provide better characterizations of piezoelectric response.
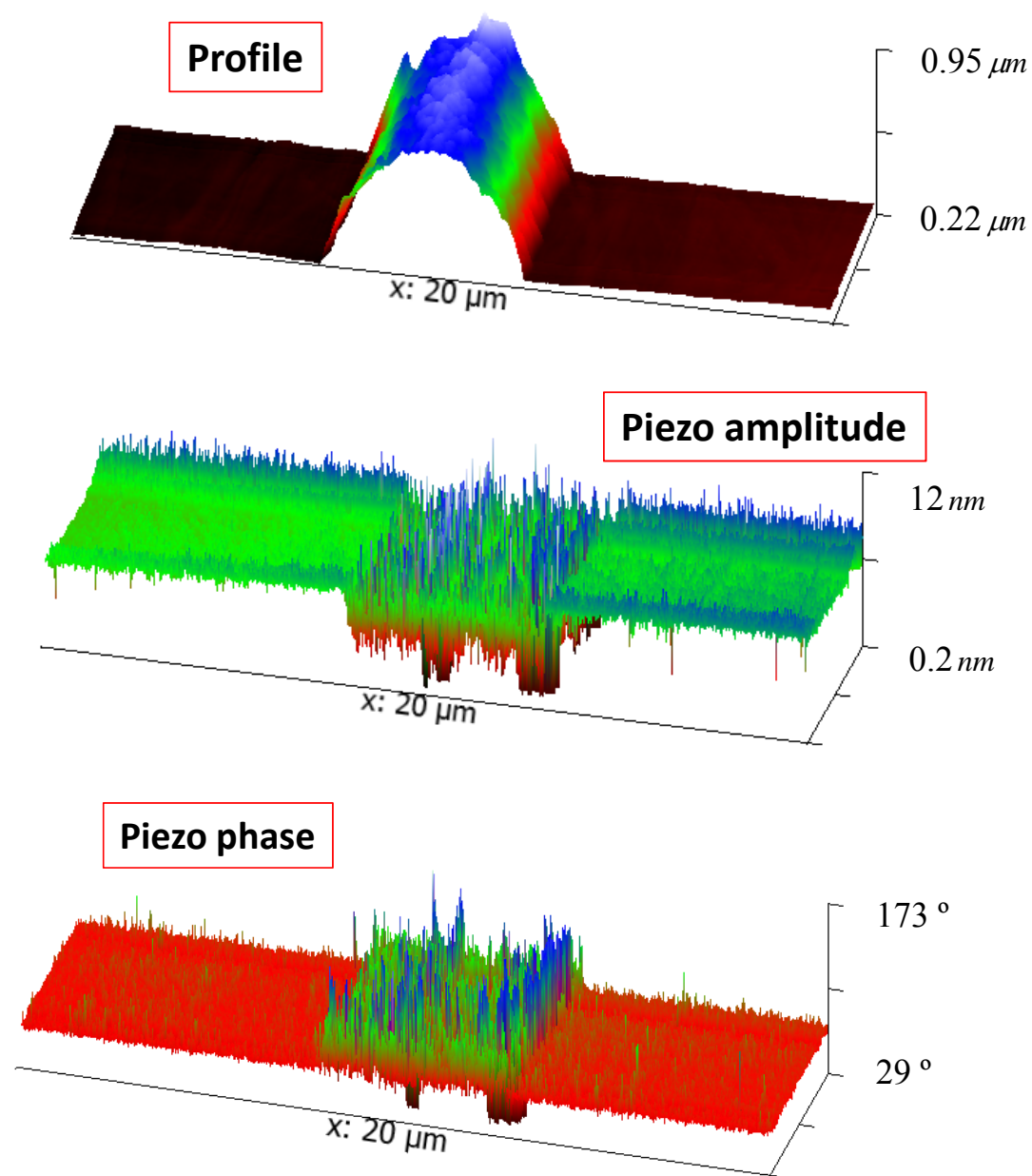
Figure 2.15 PFM scanning results of an electrospun PVDF fiber from the near-field electrospinning process with, (top) topography, (center) amplitude, and (bottom) phase.

2.5. Circuit demonstration

Nanogenerators have been integrated with a circuitry board to demonstrate their possible responses from applied strain/deformation. As these prototype nanogenerators have poor piezoelectric responses and low outputs, the generated power will not be high enough for practical electrical demonstrations. Alternatively, a circuit layout was designed to show the possible power accumulation and nanogenerator operations. In this case, the main power of the circuitry is provided by a battery with accumulating capacitors, and nanogenerator is used as a sensor to trigger the responses to light up the LED. The circuit is consisted of low current detector with amplification logic and once the incoming current from nanogenerator exceeds a small threshold current, the signal triggers the circuitry to power the LED. The capacitor in the circuit is charged with battery power and the LED signal is used to indicate that energy in capacitor is discharged. Afterwards, a recharge process is followed to charge up the capacitor again from the battery. Figure 2.16 shows the nanogenerator with a total of 600 PVDF nanogenerators connected in parallel, and the circuitry built on the breadboard. The operation sequence is summarized as follows:

1. The input current from the nanogenerator is detected and sent to the comparator. The comparator checks if there is true signal (5V) or the output is 0V.

2. The counting circuit counts the number of signals from the comparator. When it reaches designated number (for example 3), it sends out a signal of 5V (otherwise 0V) to the switch. This is to confirm that the signal generated by the nanogenerator is not a noise but from reliable actuation.

3. Once the signal is sent to the switch, the switch connects the capacitor to the LED to light it up using energy stored in the capacitor. After the dissipation process, the circuit is closed and the capacitor is charged with a commercial battery.
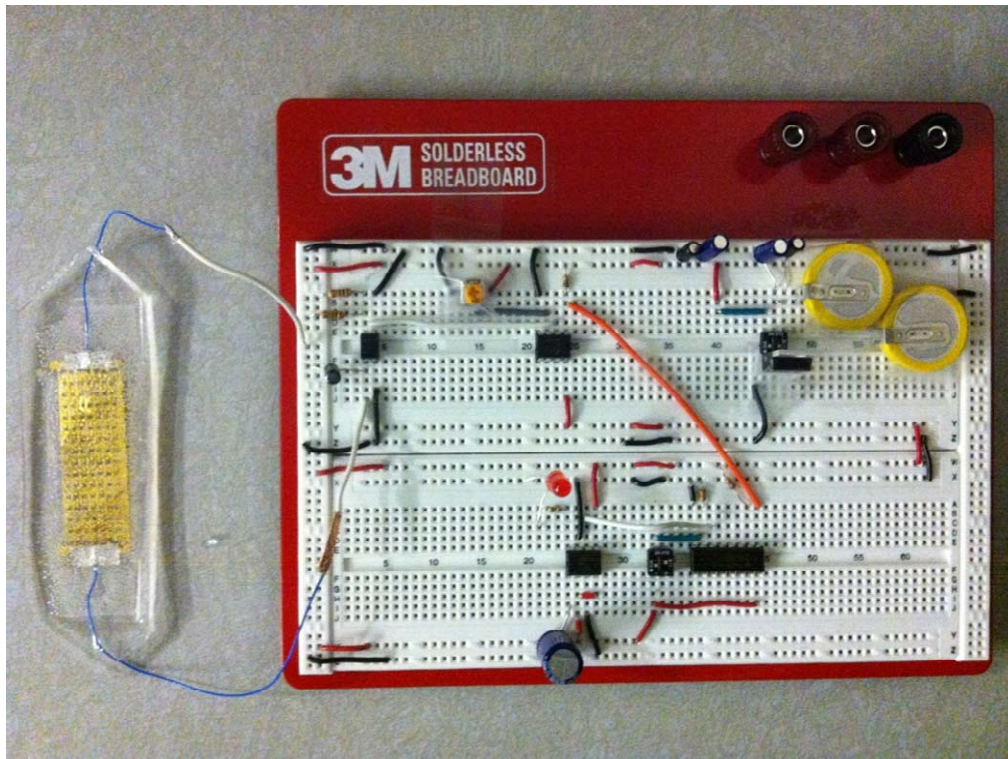
Figure 2.16 An example of electrical circuit connection for the PVDF nanogenerator (left). The nanogenerator is designed to have parallel connections to increase the output while the piezoelectric responses are too weak to provide enough power. Alternatively, a commercial battery is used to power an LED light and the signal from the nanogenerator is used to trigger the on-off operation of the LED.

Figure 2.17 show captured images of the electrical circuit in off and on stage, respectively. The on stage is triggered by bending of the nanogenerator for at least 3 times.
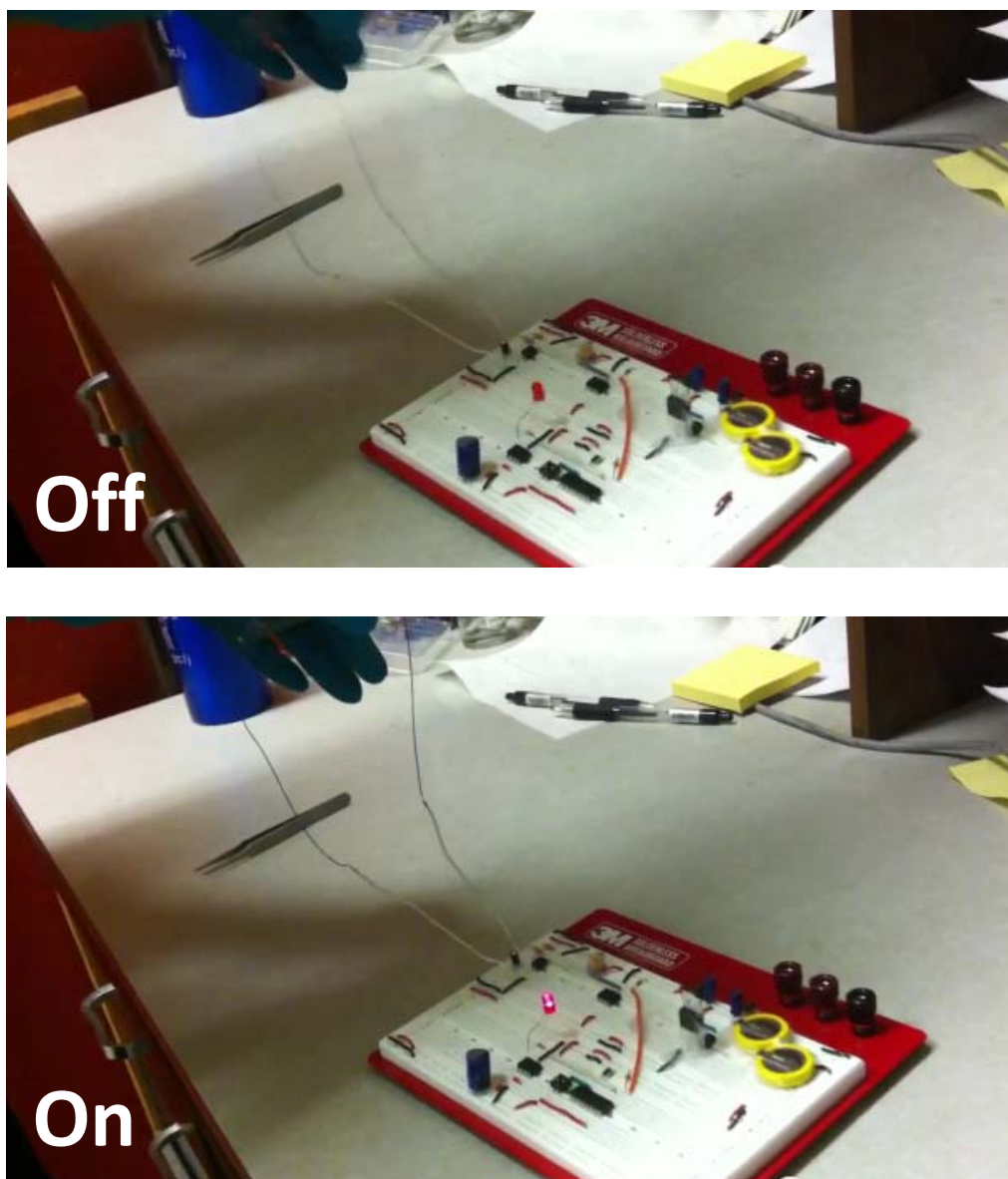
Figure 2.17 The optical image of operation of LED connected to nanogenerator. The nanogenerator performs as a trigger and the input current has to be above the threshold level to turn on the circuit. Once the LED is on, the energy charged in the capacitor releases and the commercial battery recharges the capacitor.

2.6. Conclusion

Piezoelectric energy harvesting device with current amplifying design was successfully implanted on flexible substrate. Total of 500 active parallel connecting points were made between gold electrodes and PVDF nano fibers. Maximum strain of 0.1% was applied with DC motor for repeated actuation on PDMS covered substrate. Peak current of 30nA and peak voltage of 0.2mV were measured. Switching in measurement direction showed that the response flipped such that the output was coming from piezoelectric response. Various electrodes design to boost either current or voltage harvest is available by simply modifying electrodes design and number of contact points. Piezoelectric property in nanofiber was investigated and analyzed in material aspect as well. FTIR, XRD and PFM tests were performed to characterize fibers fabricated with bulk-film, hand-spun, far-field and near-field electrospinning. It was clear that the beta-phase was formed during electrospinning process, however, the direction and amplitude of piezoelectric response has to be verified with further tests ahead.

3. Direct-write fibers for mask-less lithography

3.1. Introduction

Lithography process is one of the most important and widely used processes in the fabrication of IC (Integrated Circuitry) and MEMS (Microelectromechanical Systems). Large area patterns are generated using photoresist and mask via the conventional optical aligner at moderate cost. Some limitations in the typical lithography processes include low design flexibility and difficulty in processing flexible substrates such as roll-to-roll fabrications. Furthermore, for sub-micrometer features, several advanced lithography solutions have been introduced such as nano imprinting [12], and direct-write femto-second laser mask [13] to realize small features which are not available in conventional lithography processes. On the other hand, e-beam lithography has also been used in areas such as electronic circuitry [14] and photonic crystal patterning [15,16]. AFM (Atomic Force Microscopy) has been used to generate sub-100nm scale features for nanoelectronics [17] and NEMS (Nanoelectromechanical Systems) devices [18]. All of these aforementioned processes are excellent tools in creating ultra-small features in nanolithography processes but they are limited to either very expensive equipment or small area operations.

In this chapter, direct-write fibers are introduced for mask-less lithography on flexible substrates for processes such as lift-off, wet-etching and dry-etching. A direct-write process for conductive polymer wires is also presented. Typically, conductive material is not adequate for the near-field electrospinning process as breakdown could occur to cause short circuit. An alternative methodology via post-annealing is used to achieve the electrospinning of conductive polymer material [82,83].

Direct-write electrospun fibers could provide some advantages for mask-less lithography processes. First, the process does not require photoresist as the hard mask as polymeric fibers are deposited to the substrate by controlling the movement of an x-y stage for designated patterns via the near-field electrospinning technique [3]. Second, the process is simple and low-cost without any expensive equipment. The basic setup includes a high voltage power supply and x-y stage to generate continuous fibers with well-controlled deposition precision. Third, the process can deposit fibers on flexible and dielectric substrates for possible applications in new emerging areas such as flexible electronics. Fourth, the diameter of fibers is adjustable with a range from sub-micrometer to 10μm.

These features make the technology an excellent candidate for mask-less lithography processes. Several proof-of-concept prototype demonstrations have been conducted and characterized in this work with details on the experimental setups.

The efforts on the electrospinning of conductive material aims to address possible applications for transparent electrodes in touch screens, solar cells and transparent electronics. Currently, Indium tin oxide (ITO) is the key material for transparent electrodes. However, its fabrication process requires high vacuum and expensive materials leading to brittle films such that it is not suitable for applications in flexible electronics. Materials such as graphene or carbon nanotubes have been suggested for the use of such electronics, but the high price and difficulties in material handling make them too expensive for commercial applications. NFES process has been applied in this work to make copper wires for possible a cheap alternative as transparent electrodes on flexible substrates.

3.2. Process setup

3.2.1. Polymer solution preparations

All kinds of different polymer materials can be applied in the electrospinning processes as long as the solution has adequate viscosity. For example, the high electrical potential during the near-field electrospinning process can pull the polymer solution from the tip of a syringe toward the bottom collector substrate. Several polymer materials have been characterized in this work, including PVDF (Polyvinylidene fluoride), PEO (Polyethylene oxide) and PEI (Polyethylene imine). These polymer materials have different viscosity, adhesion property to specific substrate, and spinning characteristics, such that proper selections of polymer and solvent mixtures require detailed experimental characterizations. Table 3.1 lists three tested polymer solutions by using the NFES process with specific mixing ratios of solvents and comments on their spinning test results.

Table 3.1 Three tested polymer solutions by NFES

Polymer	solvent	Mixture	Spinning result
PEO (Polyethylene oxide)	DI water	10% v/v	Moderate spinning, low adhesion to substrate
PEI (Polyethylenimine)	DI water	50% v/v	Very uniform fiber width 1-3µm
PVDF (Polyvinylidene fluoride)	Acetone	20% v/v	High viscosity → reliable and continuous yet solvent evaporates fast

In preparing polymer solutions for conductive fibers, several extra things are needed. First, precursor is needed as it becomes the conducting material in the fiber. For example, high percentage of copper precursor leads to fibers with higher conductivity but it makes electrospinning process more challenging. Second, polymer has to be mixed with the precursor and the best mixing ratio typically requires trial and errors by real experiments. Last, solvents to dissolve polymer and precursor are required which further complicate the electrospinning process. Table 3.2 lists several experimental combinations of polymer, precursor and solvent for the copper fiber deposition conducted in this work and it is found that copper dinitrate and PVP (Polyvinylpyrrolidone) polymer dissolved in ethanol gives best results for both electrospinning and fiber conductivity. All these results are obtained by the NFES process.

Table 3.2 Experiments on conductive polymer for electrospun copper fibers by NFES

Precursor	Polymer	Mixture	Result
Copper acetate	PVDF	41 wt.% Acetone 41 wt.% DMSO 4 wt.% Zonyl 16 wt.% PVDF 8-24 wt.% (of above wt.) Copper acetate Various other mixtures tried.	The mixing ratio of large amounts of copper acetate into the PVDF solution is critical. PVDF loses its excellent spinning properties.
Copper acetate	PEO	44 wt.% Ethanol 22 wt.% Water 12 wt.% PEO 22 wt.% Copper acetate Various other mixtures tried.	Adequate for electrospinning but the material shows clear accumulations of copper acetate. Copper acetate dissolution problem.
Copper acetate	PVA	56 wt.% Acetone 22 wt.% PVA 22 wt.% Copper Various other mixtures tried.	PVA is not soluble in water. PVA is soluble in acetone. The different obtained mixtures are not useful for NFES.
Copper acetate	PVP	Various other mixtures tried.	Adequate for electrospinning. The amount of copper and its dissolution is a problem. No continuous Cu-Fibers are obtained after the thermal treatment.
Copper dinitrate	PVDF	N/A	Cu(NO3)2·3H2O reacts with PVDF since it contains water. Not suitable for electrospinning
Copper dinitrate	PVB	75 wt.% Isopropanol 15 wt.% Copper dinitrate 10 wt.% PVB Various other mixtures tried	Challenging but possible for NFES. Some conductive Cu-Fibers are obtained.
Copper dinitrate	PVP	33 wt.% Ethanol 63 wt.% Copper dinitrate 4 wt.% PVP	Good mixture between Copper dinitrate and ethanol. The solution can be electrospun and conductive fibers can be obtained.

Polyvinyl butyral (PVB), Polyethylene glycol (PEO),
Polyvinyl acetate (PVA), Polyvinylpyrrolidone (PVP)

3.2.2. Near-field electrospinning setup on dielectric substrate

Previously, the well-controlled NFES process has been conducted on hard and conductive substrate [8] as a strong electrical field between the syringe and substrate is required to generate and control the deposition location of fibers. Here, a modified setup is utilized to enable direct-write of fibers on flexible and dielectric substrates. Figure 3.1 shows the schematic diagram of the near-field electrospinning process used for flexible and dielectric substrates. In the prototype experiments, a doped silicon wafer or metal coated hard substrate is placed underneath the flexible or dielectric substrate. The conductive substrate is grounded by connecting itself to the negative side while the metal syringe tip is connected to the positive side of the power supply, respectively. In contrast to the far-field electrospinning process, a small gap of less than 1mm is used in near-field electrospinning process and about 1kV of voltage is strong enough to generate continuous fibers. The target flexible substrate such as Kapton film is placed on top of the conductive substrate. As illustrated in the electrical field simulation results in the right image of figure 3.1, the electrical field between syringe and conductive material can still be established with the existence of the dielectric substrate. Therefore, electrospun fibers can be pulled from the tip of the syringe onto the dielectric substrate.
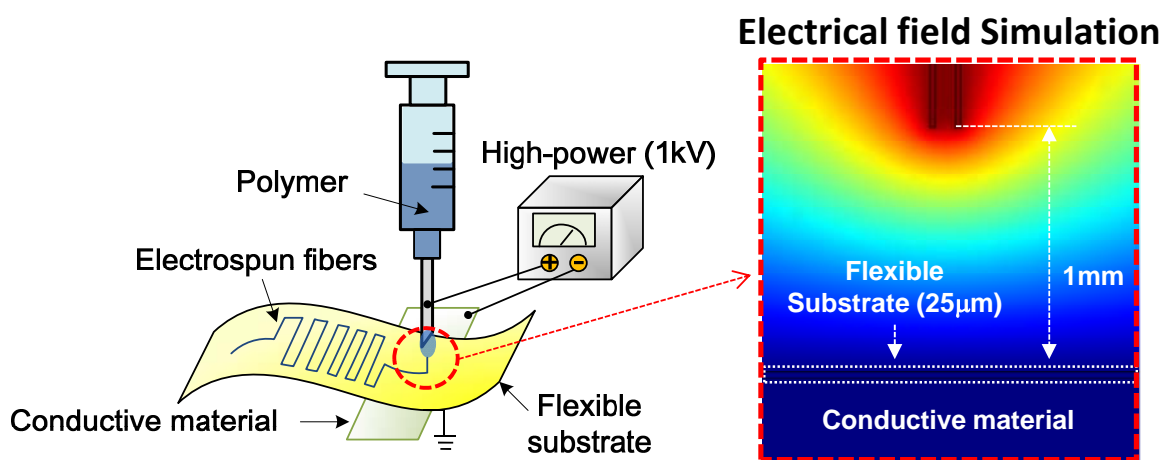
Figure 3.1 Schematic diagram of the direct-write nanolithography process on a non-conductive flexible substrate. The near-field electrospinning process utilizes high electrical field formed between the metal syringe tip and conductive substrate lying underneath the target dielectric flexible substrate. COMSOL® simulation shows electric field can be established within the flexible dielectric substrate on top of grounded conductive substrate.

3.3. Structural patterning by electrospun fibers

Based on the proposed direct-write lithography process as shown in Figure 3.1, three lithography-based microfabrication patterning processes including lift-off, wet-etching and dry-etching, are chosen as the demonstration examples in this work to be described in details in chapters 3.3.1, 3.3.2 and 3.3.3. In all experiments, the flexible dielectric film, Kapton, were chosen as the substrate and PEO (Polyethylene Oxide) was selected as the electrospun fiber material. Figure 3.2 illustrates process flows for lift-off, wet-etching and dry-etching processes, respectively, using the direct-write mask-less lithography technique. A fourth patterning example is presented in chapter 3.3.4 for direct-write conductive wires.

(a) Lift- off	**(b) Wet-etching**	**(c) Dry-etching**
Kapton film	Kapton film	SiO$_2$ on Kapton film
NF electrospinning	Metal deposition	Graphene transfer
Gold deposition	NF-electrospinning	NF-electrospinning
Lift off	Wet-etching	O$_2$ plasma etching
Sub-1μm electrode gap	Micro heater on flexible substrate	Graphene patterning
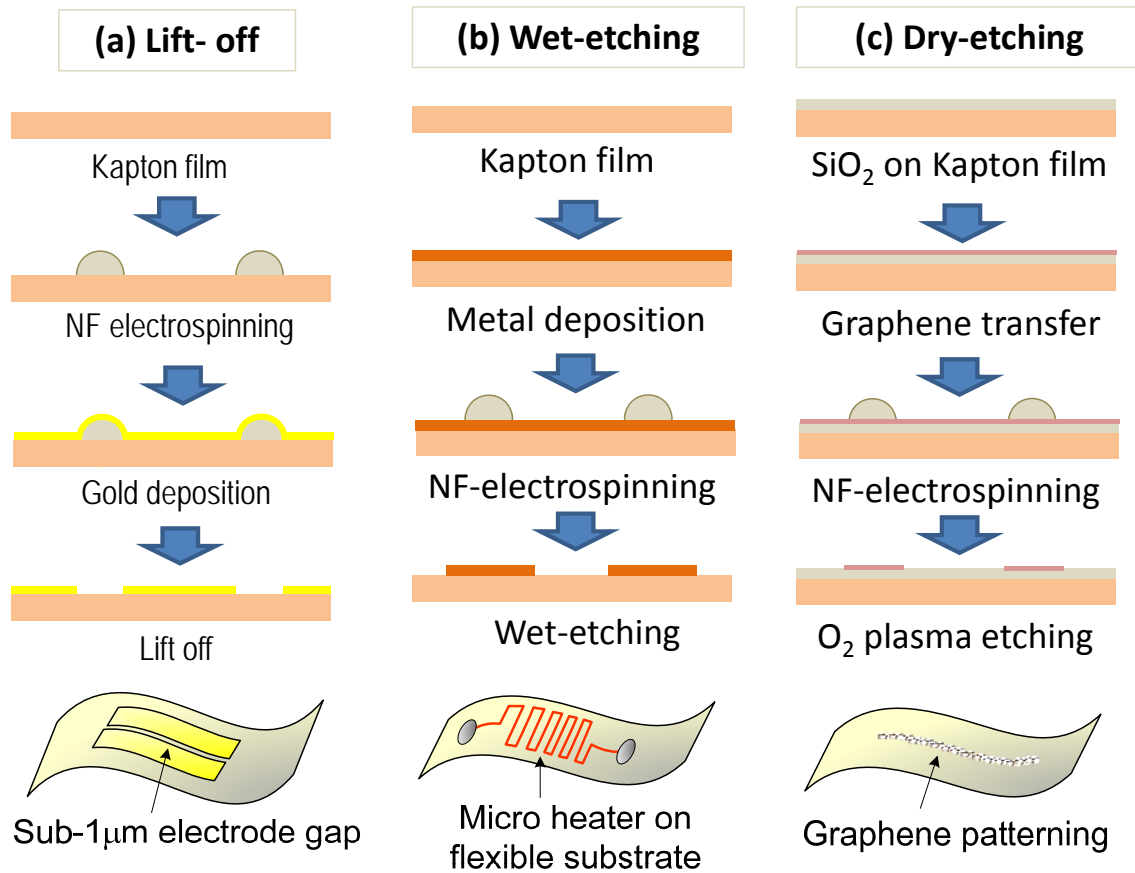
Figure 3.2 Three basic mask-less lithography and etching processes via the direct-write nanolithography technique: (a) lift-off, (b) wet-etching, and (c) dry-etching to demonstrate (a) sub-micrometer gap, (b) micro heater, and (c) graphene etching processes.

3.3.1. Lift-off

In the lift-off process as shown in figure 3.2(a), a gap of narrower than 1μm is the target demonstration. First, a 25μm-thick Kapton film is placed in the near-field electrospinning setup. Thin PEO fibers are directly deposited on top of Kapton film to form the gap. A 50nm-thick gold layer is deposited using e-beam evaporation and the lift-off process is performed by dipping the sample into DI (Deionized) water for 5 minutes. The unnecessary area other than electrodes on the Kapton film could be manually blocked from metal deposition by Kapton film as the deposition masking layer. As the PEO fiber is dissolved in DI water, the sub-micro meter metal gap is defined by the diameter of the electrospun fiber. Figure 3.3 shows the optical image of a fabricated sub-micrometer gap at the top and a SEM image at the bottom.
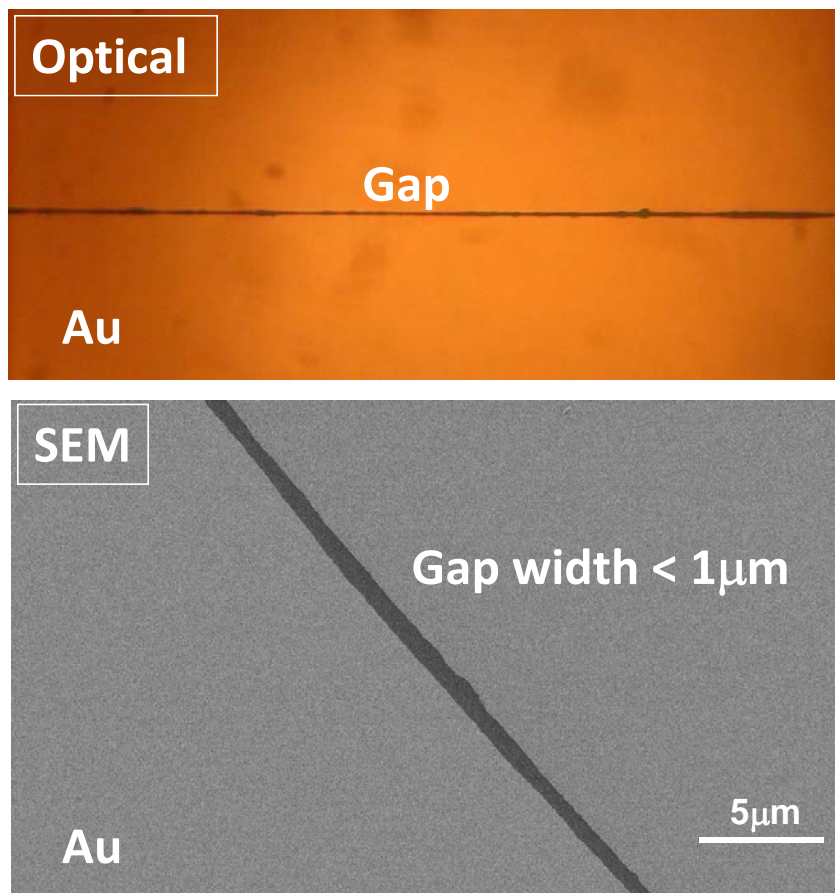
Figure 3.3 A sub-micrometer gap was formed by using electrospun PEO fiber as the lift-off shadow mask, (a) optical and (b) SEM images.

3.3.2. Wet-etching

For the wet-etching process as shown in figure 3.2(b), two requirements should be fulfilled for the electrospun fibers to be effectively used as masks. First, the fibers must have good adhesion to the substrate to prevent possible leakage of etchant underneath the fiber during the etching process. The adhesion strength between the fiber and the substrate is generally determined by the choice of polymers and solvent used in the electrospinning process. Solvents such as acetone evaporate fast and result in weak adhesion force. Polymers which use DI water as solvent typically have better adhesion strength with the Kapton substrate. Experimentally, PEO polymer with 20% v/v mixing ratio with DI water has shown good adhesion strength on Kapton and copper substrate in the prototype tests.

The second requirement for the electrospun fiber as the etching mask in the wet-etching process is its chemical resistance to the etchant as the physical dimension of masking fibers should be maintained throughout the whole wet-etching process. It turns out that the PEO polymer used in the prototype experiments is robust during entire copper wet-etching process. In the process as shown in figure 3.2(b), a 30nm-thick copper is via the sputtering process on top of the Kapton substrate. The designed device pattern, a micro heater, is then written on to the copper thin film via the near-field electrospinning process. After the wet-etching process, figure 3.4(a) shows the optical image of a fabricated substrate being deformed under the force between two fingers. Figure 3.4(b) is the image of the fabricated micro heater under an optical microscope. The width of the heater could be adjustable during the timed etching process. However, as the copper film has many grain boundaries which result in uncontrolled etching in the boundary areas, the overall wet-etching process is challenging with poor pattern accuracy compared with the lift-off and dry-etching process to be discussed in the next session.

(a)

Copper

Kapton film →

200um
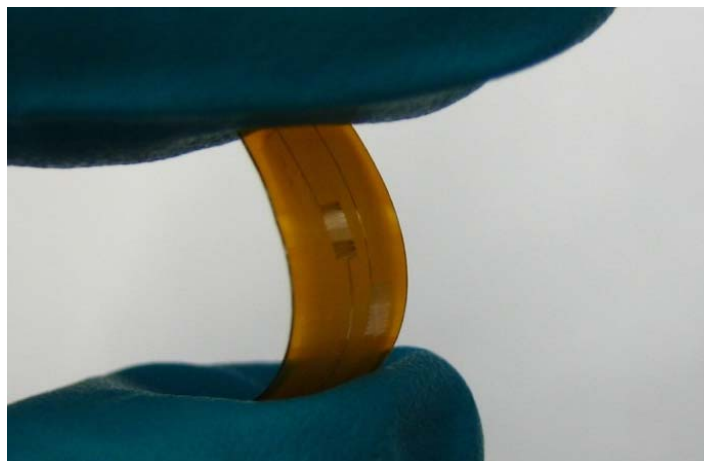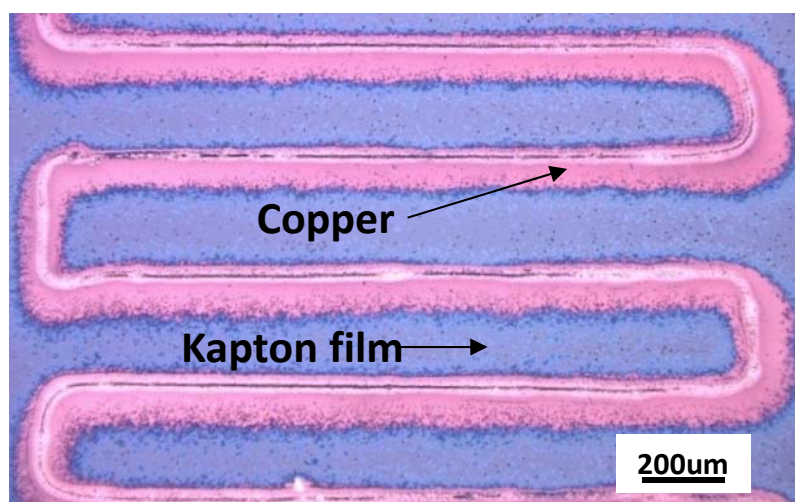
(b)

Figure 3.4 Optical image of micro-heater fabricated on flexible Kapton film. The PEO fiber is written on copper layer on Kapton film and wet-etching is performed to form heater pattern. The width of heater can be adjusted by time-etching.

3.3.3. Dry-etching

Figure 3.2(c) shows the dry-etching process using direct-write electrospun fibers. Similar to the wet-etching process, good adhesion of fiber to substrate is desirable. Moreover, dry-etching is generally used to generate patterns with smaller line width such that even small amount of gas/plasma leak under the fiber can severely impact the process. Multiple tests have been conducted and the conclusions from the prototype experiments indicate that PEO fibers have good adhesion to Kapton substrate and their gas barrier property against oxygen plasma is very good. Therefore, graphene patterning by means of oxygen plasma has been chosen as the demonstration example for the dry-etching process. A CVD grown, single-layer graphene is transferred on the substrate via the scoop and dry method [84]. Figure 3.5 shows the process flow where graphene has been grown on both sides of a copper foil by CVD (purchased from graphene supermarket®). PMMA A5 photo resist is spun on one side of the foil and baked for 1min at 120°C as shown in Figure 3.5. The foil is then put into copper etchant for 1 hour to etch the copper by floating the film on top of the solution as shown. The floating PMMA film with graphene underneath is cleaned with DI water several times by scoop and float on new solution. Finally, the film is scooped by the target device and dried in vacuum chamber. The top PMMA layer is removed by acetone. This transfer process involves very delicate procedures during which the graphene is easily detached from PMMA or cracked during the handling process.
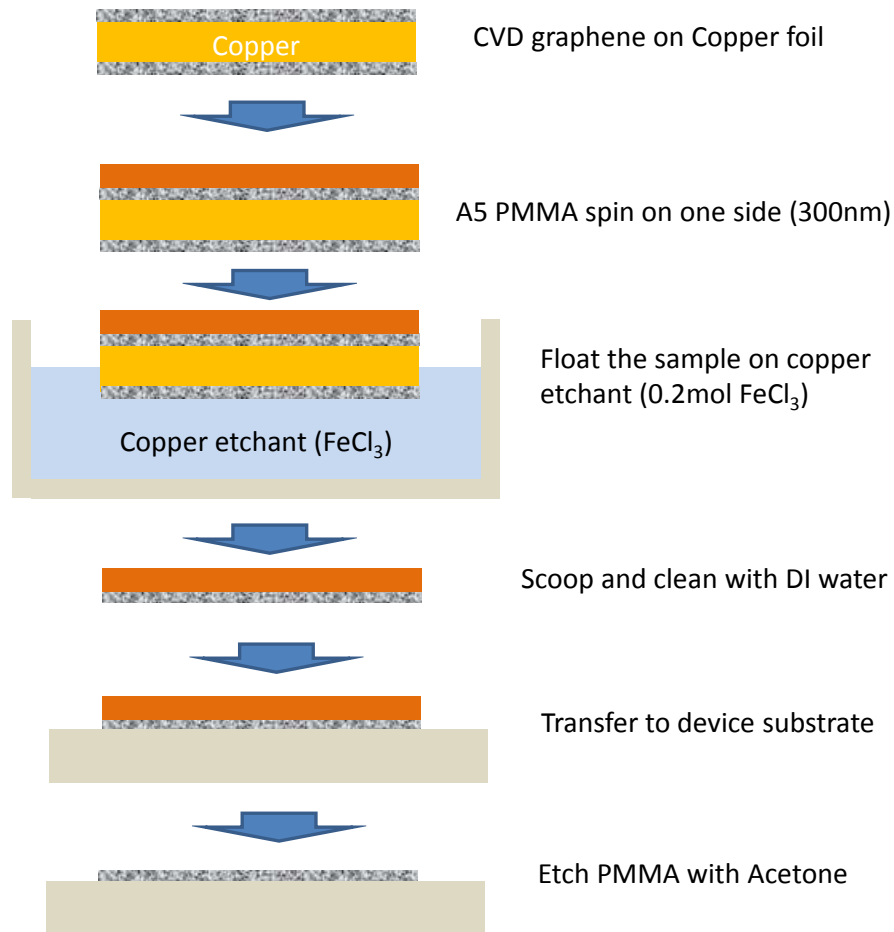
Figure 3.5 A Process flow chart for the graphene transfer process. The single-layer graphene is grown on both sides of copper foil with CVD (purchased from graphene supermarket®). PMMA A5 photo resist is spun on the foil and baked for 1min at 120°C. The foil is then floated on the copper etchant for 1 hour to etch away the copper layer. The floating PMMA film with graphene underneath is then cleaned with DI water several times by scooping on new solution. Finally, the film is scooped by the target device and dried in vacuum chamber. The top PMMA layer is removed by acetone.

The graphene transfer process is examined by two different methods. First, visual examination is conducted under an optical microscope. After being transferred onto a silicon dioxide surface, the graphene layer shows slightly different light reflection patterns as compared to the bare silicon dioxide surface as shown in Figure 3.6(a). This difference can be easily missed. However, the boundary of the graphene layer can be easily identified as illustrated. The second examination uses I-V sweeping under a probe station as shown

in Figure 3.6(b). Since the graphene exhibits metallic property, the I-V sweep on two adjacent points should be ohmic. The slight curved response as shown in the I-V measurements is due to the work function difference between graphene and the tungsten probe. If palladium is used as the contact material, an I-V response with better linearity is expected and this will be presented in a later section. In this prototype example, the current level of about 50μA at 1V shows good electrical property after the graphene transfer.

(a)

(b)
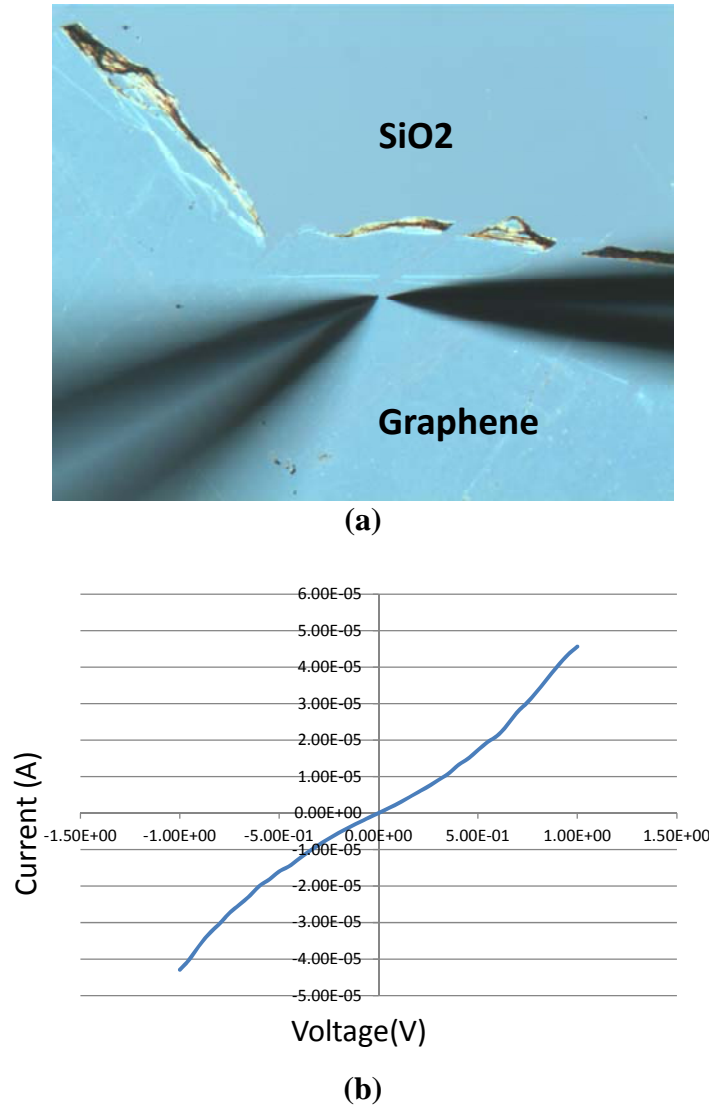
Figure 3.6 (a) Optical photo after the graphene transfer process on top of a silicon dioxide surface. (b) I-V measurement of as-transferred graphene layer showing linear response with around 50μA at 1V.

After the confirmation of the transfer process, the graphene layer is patterned using an electrospun fiber as the mask. In the prototype experiment, an electrospun PEO fiber is directly-written. An oxygen plasma etching process is followed for 5 seconds at 50Watt to define a 2μm-wide line-pattern of graphene as shown in Figure 3.7. The fiber is then removed by dipping into DI water with sonication for 5minutes. Figure 3.7(a) shows the Raman spectroscopy results on the left and corresponding optical images by examining the graphene area as illustrated in the optical photo on the right side. The typical responses of single-layer graphene can be observed. Figure 3.7(b) shows the Raman spectroscopy results performed at the adjacent area on the left side and the corresponding optical image on the right side and only background noises are observed.
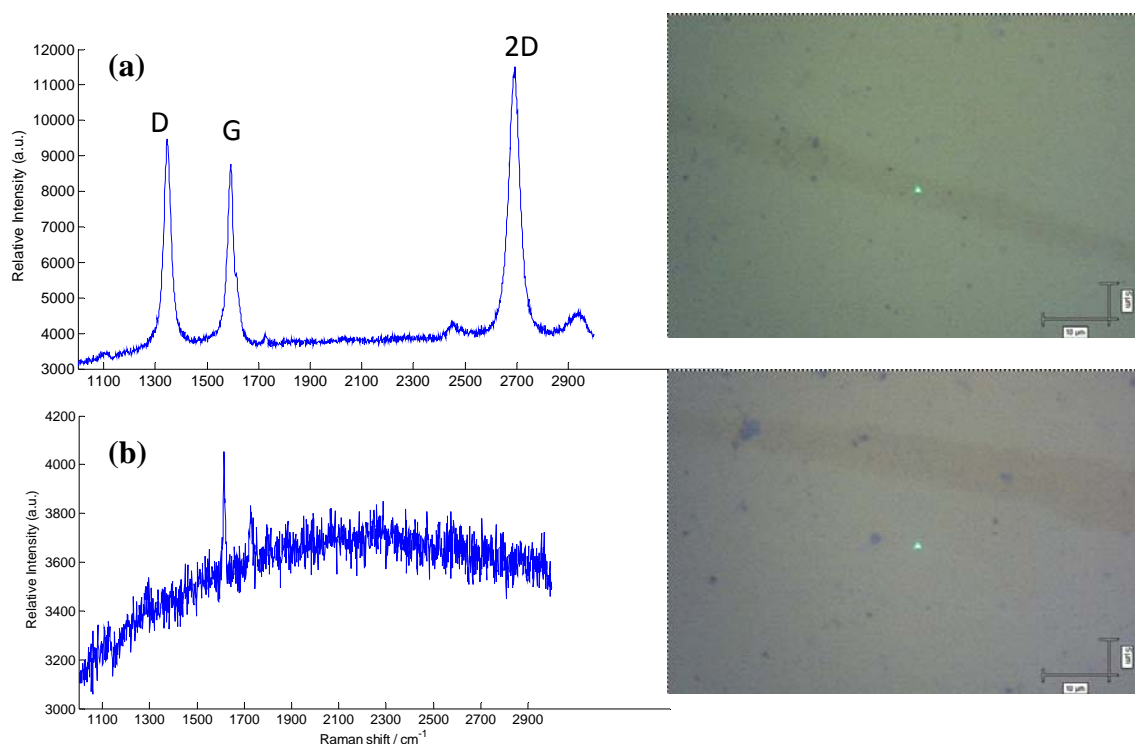
Figure 3.7 (a) Raman spectroscopy taken on the patterned 2μm-wide graphene structure using a direct-write PEO fiber as the mask and O_2 dry plasma etching at 50Watt for 5 seconds. (b) Raman spectroscopy taken on the adjacent oxide surface showing only background noises.

Figure 3.8 shows the capability of using electrospun fibers to construct an array of graphene lines. Specifically, Figure 3.8(a) is four 2μm-wide electrospun fibers on top of a graphene layer with an equal separation of 50μm and Figure 3.8(b) shows the etching result of the patterned graphene. As clearly seen, the graphene film was successfully patterned by using the PEO fibers as the dry-etching mask and the fibers were successfully removed afterwards.

(a)

(b)
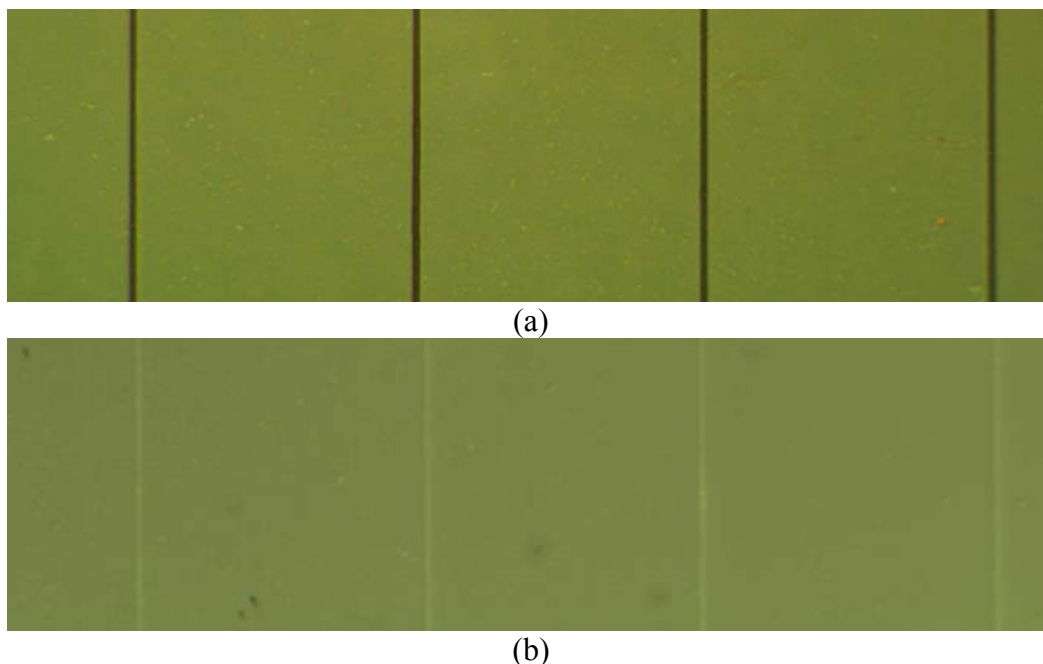
Figure 3.8 (a) The 2μm-wide PEO fiber array with 50μm spacing is used as a dry-etching mask to pattern graphene. (b) After the oxygen plasma etching and removal of fibers, and the graphene array is patterned.

3.3.4. Direct-write conductive wires

The near-field electrospinning process is also applied for direct-write conductive wires. In this case, copper dinitrate solution is used and the substrate material is glass as the wafer has to go through high temperature annealing process. The 1mm-thick glass chip is placed on a doped silicon wafer which functions as the conductive collector substrate. The voltage required to initiate the electrospinning process is increased to 3kV compared to 1kV for 25μm-thick Kapton films used in the previous sections. Furthermore, it is found that the copper dinitrate based polymer solution can easily clogged which leads to the formation of

droplets instead of fibers and disrupts the continue deposition of electrospun fibers. As discussed in chapter 3.2.1, copper dinitrate with PVP polymer generates most reliable and uniform fibers with sufficient level of conductivity after the post annealing process among tested solutions. The prototype direct-write conductive wires are mostly based on this combination of solutions. After the electrospinning process, a thermal treatment process is necessary to enhance the conductivity of the wires. These processes are described in details in the following sessions.

3.3.4.1.   Annealing Profiles

The annealing process for the as-spun fibers is conducted in two steps. The first step is to decompose the polymer material at high temperature to remove unnecessary compounds for enhanced conductivity [85]. The process is performed in the nitrogen environment to prevent possible undesired chemical reactions with a thermal treatment curve depicted in Figure 3.9. Two heating periods are used in the heat treatment process as shown. The first one is responsible for the decomposition of polymer while the second one is dedicated to the reduction of copper oxide. During the first heating period, the copper dinitrate is transformed to copper oxide as the copper forms copper oxide from the residual oxygen in the fiber at a temperature above 150° [86]. Therefore, hydrogen is flowed into the tube with 200 sccm/min flow rate during the second heating period based on the chemical reaction as follows [87],

$$CuO + H_2 \rightarrow Cu + H_2O \hspace{4cm} (3\text{-}1)$$

Two types of heating profiles have been tested in this work. The fast heating profile at a speed of 250°C/hr (dotted line) did not provide good polymer decomposition results as cracked copper wires and clogged polymers have been observed. The slow heating profile at 100°C/hr has produced uniform and crack-less wires.
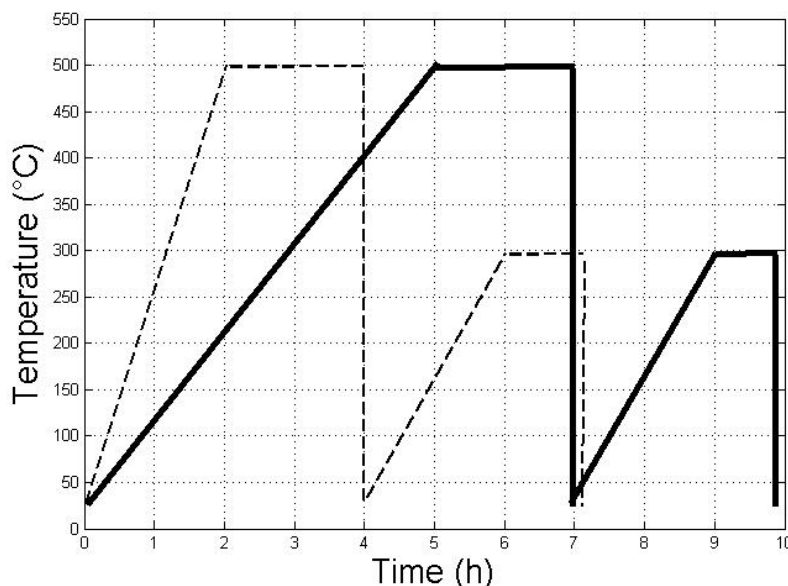
Figure 3.9 Two heating profiles to transform copper dinitrate & PVP mixture to conductive copper fiber. The fast-heating profile at 250°C/hr (dotted line) has resulted in poor quality of copper wires due to clogging. The slow-heating profile at 100°C/hr) (solid line) has resulted in good quality copper wires.

3.3.4.2.   Fabrication results

Figure 3.10 shows fabricated copper wires by near-filed electrospinning and subsequent thermal annealing process using the mixture of copper acetate and PVP. Copper acetate had low solubility even using ultrasonic agitation. As a result, frequent clogging of copper particles along the wire has been observed. Therefore, it is difficult to make continuous formation of wires. Either thin wire with big chunk of particles as shown in figure 3.10(a) or thick wire with spotted copper particles as shown in figure 3.10(b) has been observed.
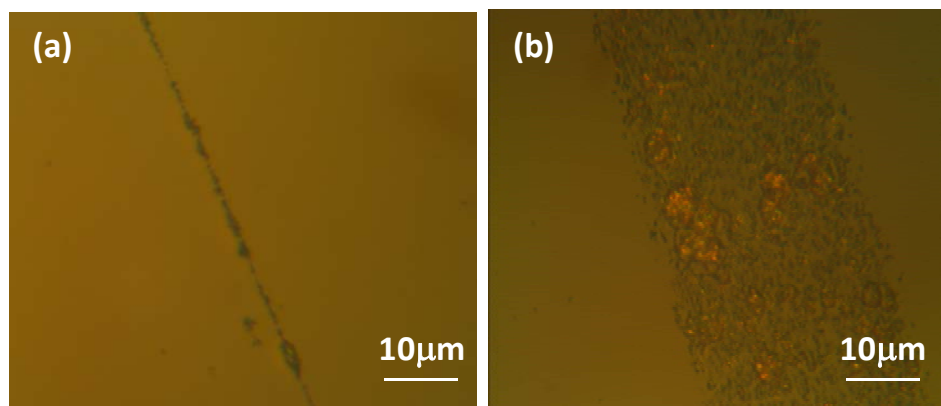
Figure 3.10 Electrospun copper wires obtained after the thermal treatment by using the mixture of copper acetate/PVP. (a) Clogging and (b) Non-continuous wires.

On the other hand, copper dinitrate and PVP mixture has resulted in electrospun wires with good quality. The solution was prepared with 65% wt.% of copper dinitrate (purchased from Sigma Aldrich), 1.5 wt.% PVP (purchased from Sigma Aldrich) and 33.5% wt.% of ethanol [88]. The copper dinitrate was dissolved in ethanol and stirred for 3 hours without heating. The PVP polymer power was then added into the mixture and stirred again for 5 hours after which the solution had adequate viscosity for electrospinning. Figures 3.11 are sequential images of the electrospun copper wires: (a) after electrospinning, (b) after copper decomposition process, and (c) after copper oxide reduction process. The polymer decomposition process was conducted at 500°C and it should remove PVP from the wire and copper oxide was formed during the process. The reduction of copper oxide occurred during the second annealing step to result in copper wires.
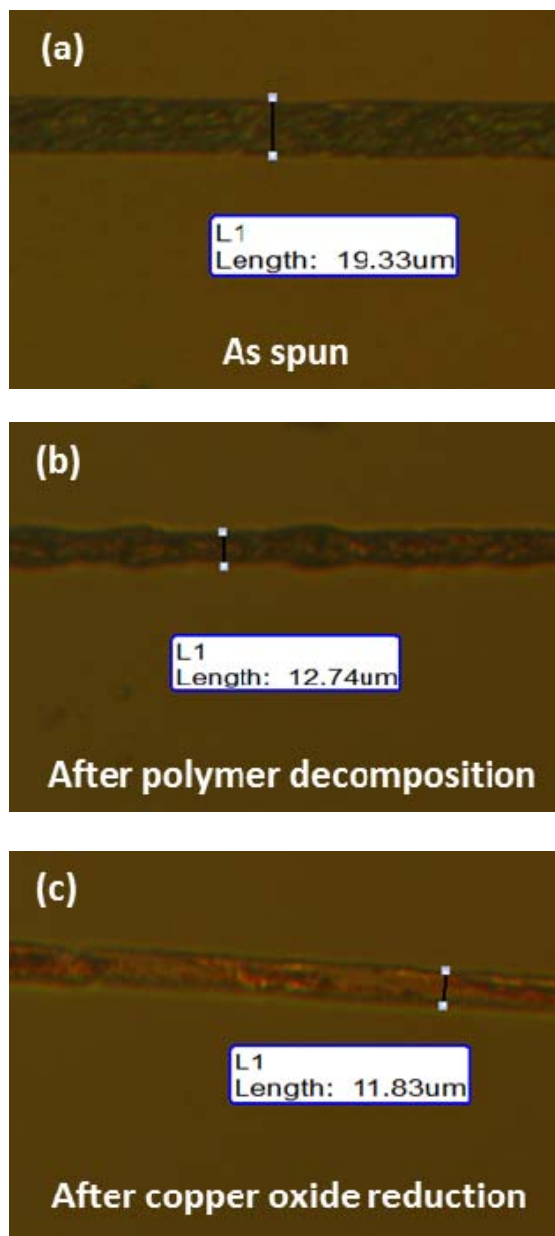
Figure 3.11 Sequential images of electrospun copper wires using copper dinitrate and PVP polymer solution: (a) after the electrospinning process, (b) after the polymer decomposition process at 500°C where darker color is the result of oxidation of copper, (c) after the copper oxide reduction process in hydrogen. These images are not taken from the same position.

3.3.4.3. Electrical measurements of electrospun copper wires

The resistivity of copper wire has been measured after the copper oxide reduction process. A total of 25 samples with different width from 20-100μm and average height of 500nm have been tested. The heights of these fibers are similar since the polymer wires were still wet instead of dry when they were deposited on the collector substrate from the near-field electrospinning process.   The short electrospinning syringe tip-to-collector distance was not enough for the evaporation of solvent in the polymer solution. As a result, the cross section of these fibers was semi-circular instead circular for fibers made of conventional electrospinning process as illustrated in the surface scan image in Figure 3.12(a).
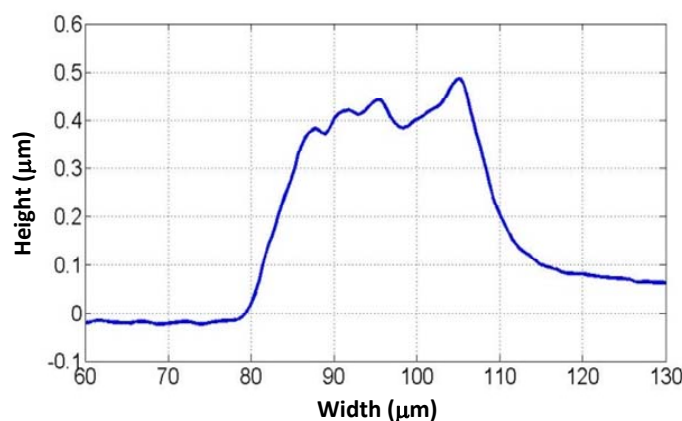
(a)
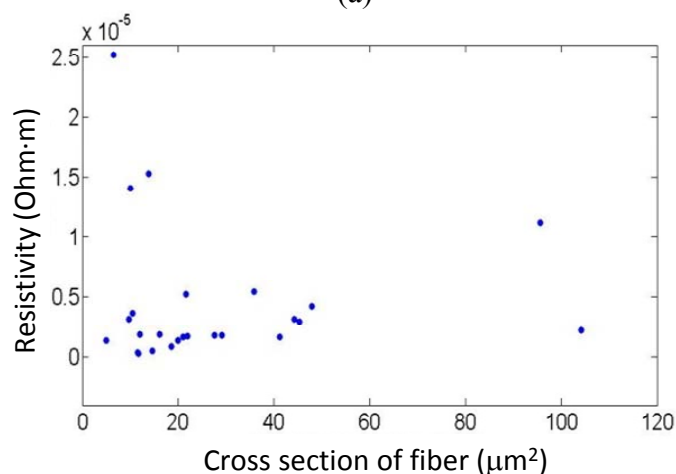
(b)

Figure 3.12 (a) Scanning profile showing the cross sectional of copper wire after the copper oxide reduction. The width of wires varied from 20μm to 100μm while the average height was about 500nm. (b) The resistivity of 25 electrospun copper wires.

The resistance of the fibers was measured under a probe station as shown in Figure 3.12(b). The average resistivity of the fibers was calculated to be 5.6×10^{-6} Ohm·m as compared with pure copper at 1.68×10^{-8} Ohm·m. The two orders higher resistivity could come from several possible factors: (1) gaps between copper particles in the electrospun wires, (2) non-uniformity of the copper wires in terms of the distribution of copper particles, and (3) residual polymer and contaminants in the wires. It is observed that some of the wires with small widths had higher resistivity. This could be explained as defects in these wires could have dominated their resistance. Furthermore, it is also observed that very thin wires (<5μm) had almost no conductivity.

3.4. Prototype device demonstrations

3.4.1. Micro-heater by electrospun fibers via wet etching

A micro heater by the electrospun fibers wet-etching process has been designed and fabricated as shown in Figure 3.13(a). It was made of 30nm-thick copper with width of 20μm and total length of 20mm. When an electrical current was applied, the heater heated up accordingly and an infrared camera was used to monitor the temperature and power generation during the experiments. Figure 3.13(b) is a sequence of IR photos showing the micro heater under different input power. It was observed that under an input power of 37mW, the substrate temperature reached 92ºC. Figures 3.13(c) show the measured power consumption versus input current and highest temperature versus power consumption, respectively. It is observed that the micro heater generated up to 92ºC under 37mW of power consumption. The linear response between temperature and power consumption indicated successful wet-etching process to construct the micro heater on flexible substrate. However, the control of wet-etching process is very difficult for line-width less than 10μm. The reason is partially due to the large grain boundary of the copper layer which causes irregular etching profile during the wet copper etching process. Different materials with small grain boundary could provide better controllability on the wet-etching process.
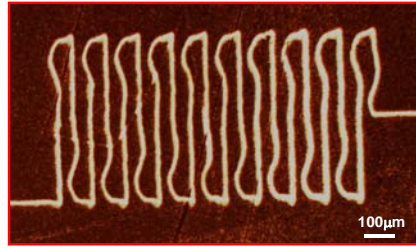
(a)
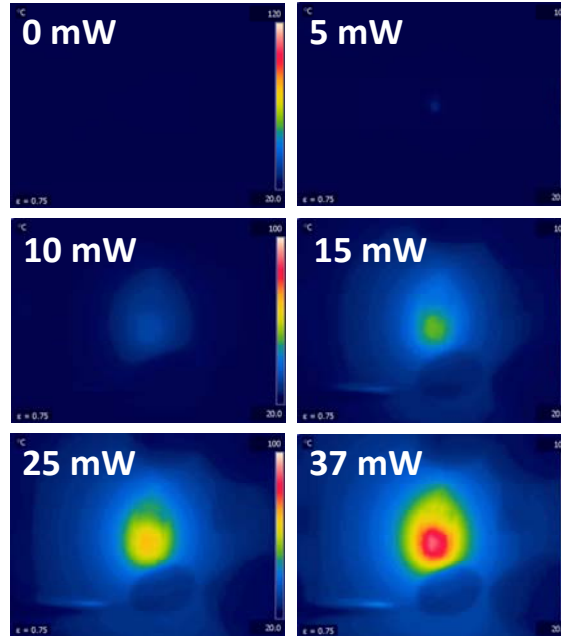
(b)
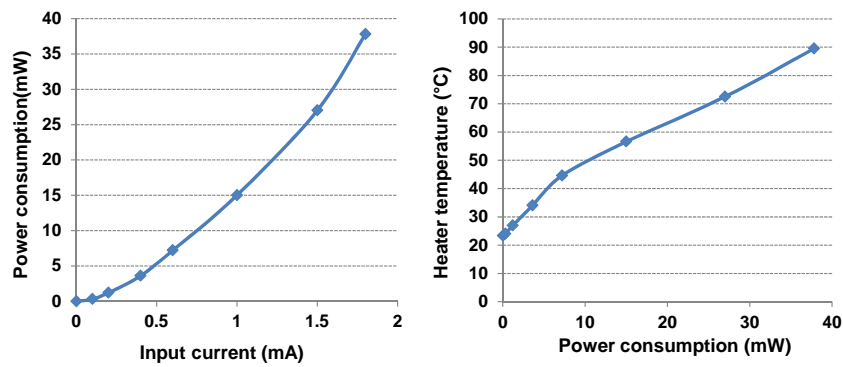
(c)

Figure 3.13 (a) The micro heater with 20μm in width and 20mm in total length was fabricated and tested as prototype device demonstration. (b) Infrared camera images provide temperature information of the heater in real time. The heater was tested to generate up to 92ºC of temperature at 37mW of power consumption.

3.4.2. Graphene channel FET by electrospun fibers via dry-etching

Graphene structures fabricated by the direct-write electrospun fibers using dry-etching have been constructed as channel field effect transistors (FET). In this case, the FET was fabricated on a p-type silicon wafer with 285nm of thermally grown silicon dioxide on top of it. The silicon dioxide layer worked as a gate oxide. First, a CVD grown single layer graphene film was transferred onto the silicon substrate and PEO polymer was electrospun to define the channel area. The width of the fiber was measured to be around 1-2μm. Afterwards, oxygen plasma at 50mW for 5 seconds was performed to etch graphene. Then the source and drain regions of the FET were patterned using the conventional lithography process in which OCG825 G-line photo resist is used. Photoresist was spun-on at 2200rpm for 30 seconds for a 2μm-thick photoresist layer. A lift-off process with 5nm-thick palladium and 100nm-thick gold layer deposition by e-beam evaporation was conducted and PR was removed to complete the device fabrication. Figure 3.14(a) shows the cross-sectional view of the graphene channel FET. The tow view optical image of the graphene channel FET shows the clearly visible graphene channel in figure 3.14(b).

(a)

(b)
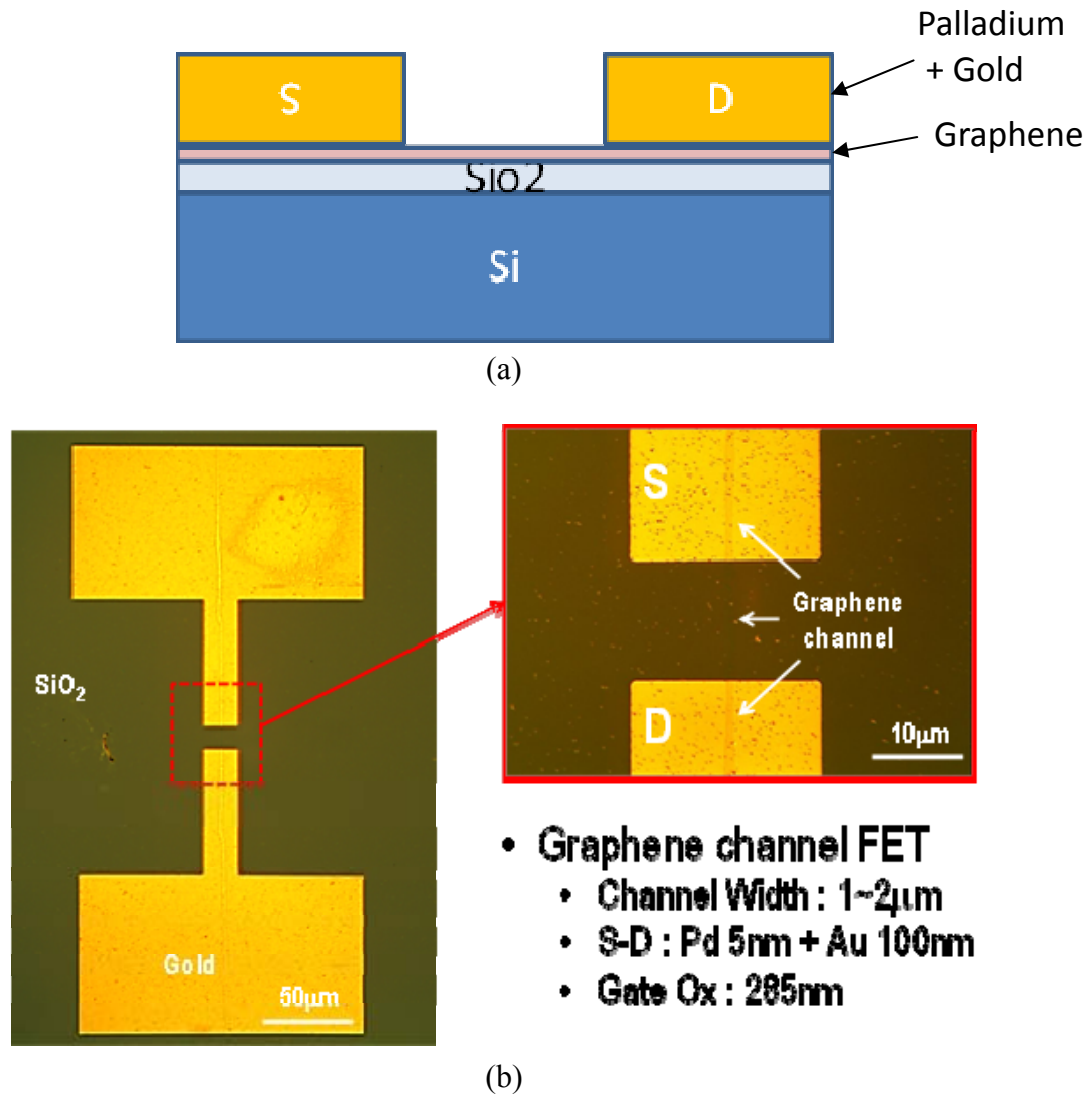
Figure 3.14 (a) The cross sectional schematic diagram and (b) optical image of graphene channel based FET. The FET was fabricated on a p-type silicon wafer which has 285nm thermally grown silicon dioxide to verify the quality of patterned graphene channel. The channel width and length were measured to be 2μm and 10μm, respectively.

Electrical measurement was conducted on Keithley semiconductor analyzer (Keithley SCS4200). As shown in figure 3.15(a), it is observed that graphene channel with 2μm in width and 10μm in length has good ohmic contact behavior. This is due to the fact that the graphene is metallic and palladium is used to promote adhesion between gold and graphene which has balanced work-function to graphene. For the characterization of the transistor, gate voltage was swept while keeping source and drain voltage. When the gate voltage is

swept from -35V to +35V with the SD voltage at 0.1V, the FET behaves like a p-type transistor where the Dirac point is observed around +21V as shown in figure 3.15(b). The Dirac point is where the carrier density is almost zero such that the current flow in graphene channel is minimal. These results show good FET characteristics and imply the patterned graphene of high quality without being damaged by the oxygen plasma process.

I-V sweep S-D

(a)

FET channel current

(b)
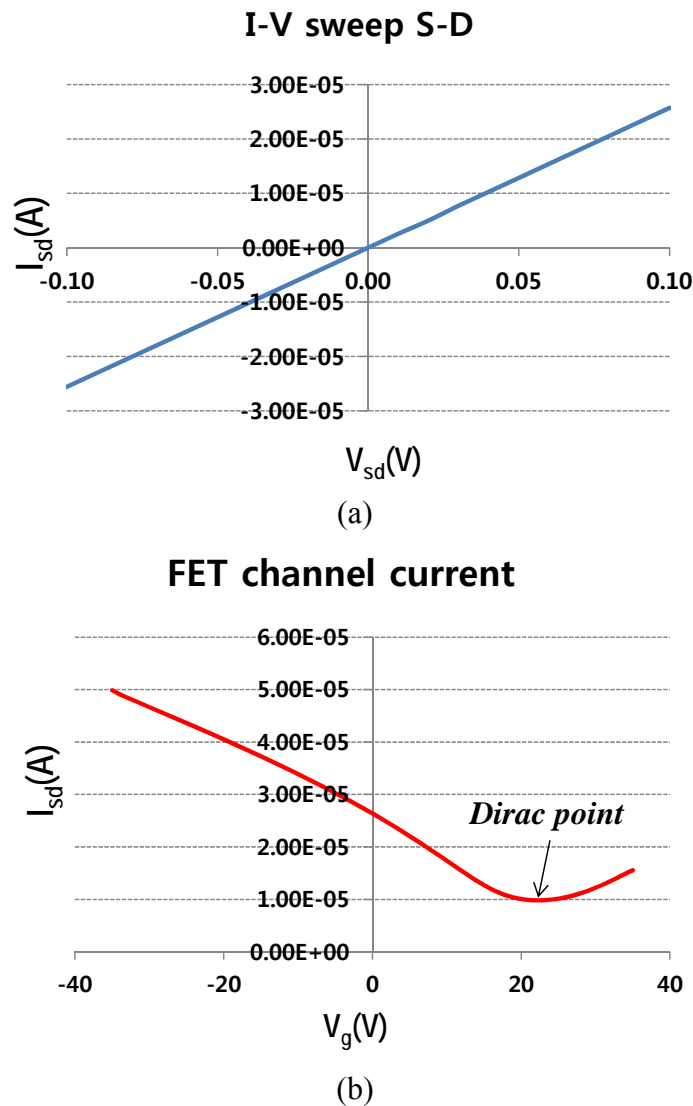
Figure 3.15 Graphene channel FET and its electrical characterization test results. The FET is fabricated on silicon wafer with 285nm of thermally grown silicon dioxide as gate oxide. (a) Graphene is metallic such that I-V sweep between source and drain shows good ohmic behavior. (b) Gate voltage sweep shows typical large area graphene channel FET characteristic.

In order to integrate more functionality into the device, doping of graphene has been conducted. The idea is to realize localized in-situ doping of graphene for electronic application. It is known that the PEI (polyethylene-imine) is a potential material in the doping process for CNT and graphene [89]. Dissolving the PEI into DI water with 50% v/v made adequate viscosity for electrospinning. The electrospun PEI fibers have been deposited on top of the graphene layer for 5 hours to enhance the doping effect. Then the device was processed with oxygen plasma at 50mWatt for 5 seconds to pattern the graphene. As the PEI is soluble in water, the whole device was dipped into DI water and sonication for 5 minutes to fully remove the PEO residue left on the graphene. Figure 3.16 shows the electrical measurement data for a graphene-based FET without doping and with doping with graphene channel width of 2μm and length of 10 μm. The red line is the testing result for the FET without doping by using PVDF fibers and p-type FET behavior is observed. The blue line is the testing result for FET with doping by using PEI as the masking layer. Based on the preliminary test, the doping effect was not satisfactory as the ideal n-doped graphene FET must show Dirac-point in the negative gate voltage region. The dotted line plotted on left could a possible n-type FET device response. The low doping effect could be attributed many factors. One possible issue is that the graphene layer was covered during the source and drain definition process with photoresist which could act as another doping process. In the future process run, doping and patterning process should be moved to the last step of the process such that no polymer or other chemical coverage is allowed on doped graphene.
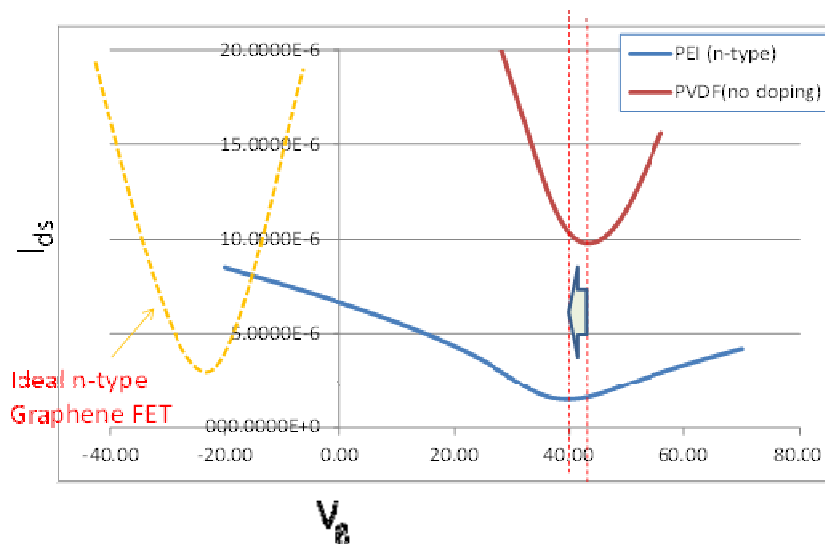
Figure 3.16 Characterizations of graphene channel FETs with (blue line) and without (red line) the n-type doping material and the ideal (yellow line) n-type graphene-based FET. The p-type and n-type FETs have been fabricated with PVDF and PEI fibers as the masking material, respectively. The ideal n-type FET should have Dirac point in the negative gate voltage region.

3.4.3. Direct-write copper wire micro-heater

In this session, a micro-heater was directly written using the near-field electrospinning process without additional etching processes as described in chapter 3.4.1 which may damage the adjacent electrical parts. However, the post thermal processing steps go up to about 500°C for polymer decomposition process and that could limit possible applications. Figure 3.17 shows a serpentine shape heating element created by the proposed method. The width of copper wire is about 50μm and the length of the heater is 20mm with better edge and shape control as compared with the micro-heater fabricated with wet-etching process in chapter 3.4.1. Figures 3.17 (a) to (d) are images from an IR camera showing the temperature of the heater increases as the input power increases. The heater heats up to 120°C under 1W of input power in Figure 3.17(d).
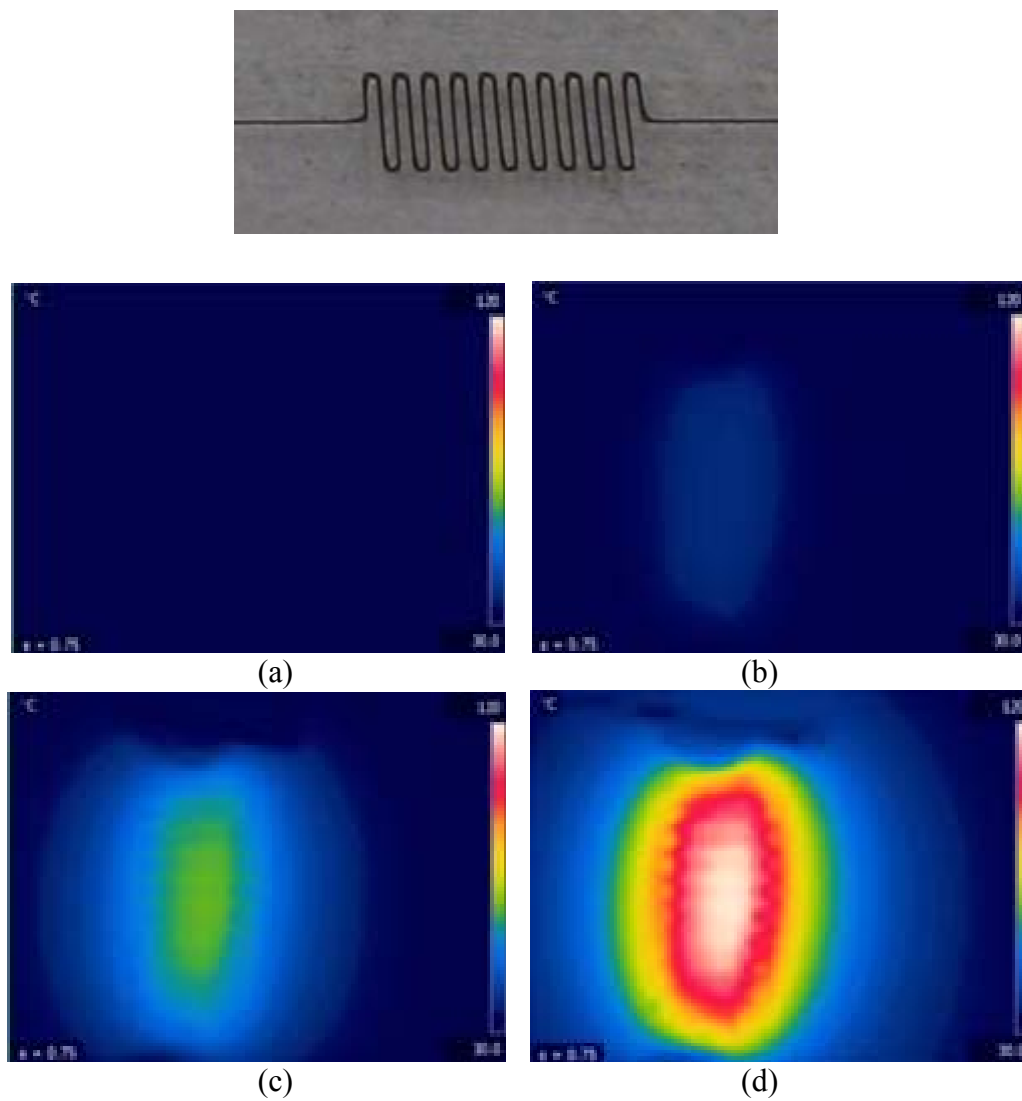
Figure 3.17. (top) Micro photo of a serpentine shape heater constructed by the direct-write copper wire technology. (a) to (d) IR images of micro heater with increased input power. Under an input power of 1W, the heater temperature reached 120°C.

3.5. Conclusion

Direct-write electrospun polymer fibers have been successfully utilized as the masking or structural materials in mask-less lithography processes. It has been found that PEO fibers have good adhesion strength on top of Kapton and copper substrates as well as good wet and dry-etching resistance to wet copper etchant and dry oxygen plasma, respectively. Four different structures have been manufactured using the direct-write fibers without any mask, including: (1) sub-micrometer gaps on a 30nm-thick gold layer in a lift-off process; (2) micro heaters made of copper in a wet-etching process; (3) graphene-based FET in a dry-etching process; and (4) direct-write copper wires as micro heaters. Testing results also confirms basic operations of micro heaters as well as graphene channel based FET. As such, the direct-write electrospun fiber lithography technique could have versatile application on flexible electronics and wearable electronics with possible simple, low-cost and large area processing capabilities.

4. Summary and Future works

4.1. Summary

Electrospun, direct-write micro/nano fibers via near-field electrospinning process have been utilized for different functionalities in various applications. Specifically, these new functionalities advance state-of-art technologies in the following areas: (1) flexible and dielectric substrate have been utilized as the collector substrate; (2) large array of PVDF fibers has been applied as nanogenerators; (3) mask-less lithography procedures have been developed for lift-off, wet-etching and dry-etching processes; and (4) direct-write metal wires have been used to build prototype micro heaters.

In the demonstration of large array nanogenerators, PVDF fibers have been constructed in parallel on a flexible substrate and integrated with comb-shape electrodes. A post electric poling process has been conducted within the PDMS shielding material which has helped to increase the breakdown voltage to achieve higher electric poling potential. An output current of 30nA has been recorded which is much smaller than the theoretical predication based on 0.5% of mechanical strain. Damages in fibers, low piezoelectricity and possible mechanical slips between fibers and contact gold pads could be the major sources of low energy conversion efficiency. FTIR and XRD methodologies have been used to characterize the formation of beta-phase polymer in the electrospun fibers. Further investigations will help to improve the performances of electrospun nanogenerators.

Fibers made of PEO, PVDF and PEI polymer have all been tested as effective masking layers in mask-less lithography processes using electrospun fibers. These fibers can resist either physical or chemical attacks during lift-off, wet-etching and dry-etching processes to perform similarly as photoresist by direct-write fibers with wide a variety of possible patterns on flexible substrates. For example, sub-micrometer metal gaps have been demonstrated using a three-step process: electrospinning, metal evaporation and lift-off. In the wet-etching process, copper etchant has been found to attack the grain boundary of thin copper films such that features smaller than 20μm have been challenging to define by using the direct-write fibers. In the area of dry etching process, CVD grown, single-layer graphene has been transferred from a copper foil to a flexible substrate and direct-write PEO/PEI fibers have been used to construct a graphene-channel FET. Electrical tests on the 1-2μm graphene channel FET have shown promising results while future development for n-type graphene channel FET is needed to make a fully functional, graphene-based CMOS on flexible substrate by direct-write fibers. These developments and future advancements are expected to drive various applications in low cost, flexible electronics.

4.2. Future works

4.2.1. Energy nanogenerators by electrospun direct-write fibers

Most of the current nanogenerators (including nanofiber nanogenerators) are limited to low power generation in laboratory environments. Some recent studies have advanced the records to higher power outputs [57] as well as using real mechanical actuation sources such as the human heartbeat [90] and mouse [91] to drive active devices like an LED [53]. Nevertheless, the electrical power generated by nanogenerators made of nanostructures is often too small to have practical applications for commercial hand-held systems such as an electrical watch which typically consumes electrical power in the range of a few μW. Therefore, commercial interests in nanofiber nanogenerators could be realized if and when the power generated by a single nanofiber nanogenerator in the recorded range of 10^{-11} Watt can be boosted up to the range of 10^{-6} Watt.

Furthermore, similar to all other electrical power generation devices, suitable energy storage/regulation systems will be required for nanofiber nanogenerators to store the generated energy and to release them at the right time. For example, repetitive deformation of piezoelectric nanostructure is essential to generate energy and the generated energy could be accumulated in an energy storage system such as a rechargeable battery or supercapacitor to be released at a later time. For example, a ZnO-nanowire nanogenerator has been connected to a capacitor and macro scale electrical circuitry for a system demonstration with discrete wires [59]. An integrated system that combines integrated nanowire nanogenerators, integrated circuitry, and integrated battery/supercapacitor on a single chip could be an important technology challenge for future developments.

As stated and discussed in this dissertation, fundamentals on the piezoelectricity of nanofibers have to be investigated systematically in all aspects to produce nanofibers with high piezoelectricity. These include optimizations in process parameters such as materials, solvents, concentrations, electrical bias, needle-to-electrode distance as well as electrospinning methodologies. Furthermore, detail analyses on the electrospun nanofibers have to be fully characterized with tools such as XRD, FTIR, PFM and SHG and Raman spectroscopy. As such, nanofiber nanogenerators with high energy conversion efficiency could be built in the future consistently.

4.2.2. Electrospun direct-write mask-less lithography

Future research directions on this topic can be divided in two ways; improvements in the processes and developments in various applications. The process improvement could focus on reliable and uniform fiber depositions. For example, continuous generation of fibers with uniform diameter of less than 1μm could be a challenging engineering problem. Currently, the average diameter of the fibers ranges from 1 to 3μm and the reduction of the fiber diameter to sub-micrometer requires better control on the overall electrospinning process. Different types of fibers have to be tested under the setup of near-field electrospinning before specific applications can be realized. Particularly, demonstration of large area deposition is needed to compete with conventional process at the whole wafer scale. Here, several ideas are proposed to further the presented experimental results in this work for future applications.

CMOS on flexible substrate via in-situ graphene doping

CMOS is the basic device architecture in integrated circuits. Graphene-based FET can form inherently p-type transistor and it has been an interesting topic to build both p-type and n-type graphene FET on a substrate to form a CMOS [92]. Doping of graphene to construct n-type FETs has been studied by means of chemical [89,93] and electrothermal [94] methods. Electrospun direct-write fibers bring one unique opportunity to locally dope graphene to make n-type FETs via near-field electrospinning with functional polymers for the doping process. For example, PEI has been known to provide n-type doping for CNT and graphene [89] while most of the other polymers such as PVDF can construct p-type FETs. In chapter 3 of this dissertation, n-type doping has been successful demonstrated with PEI in the setup of the n-type graphene FET. Both p-type and n-type transistors should be fabricated on a single device via a three-step process: electrospinning and plasma etching followed by polymer removal as illustrated in Figure 4.1. If the proposed process can be successfully demonstrated, it could open up a new class of research in low cost electronics on flexible substrates.
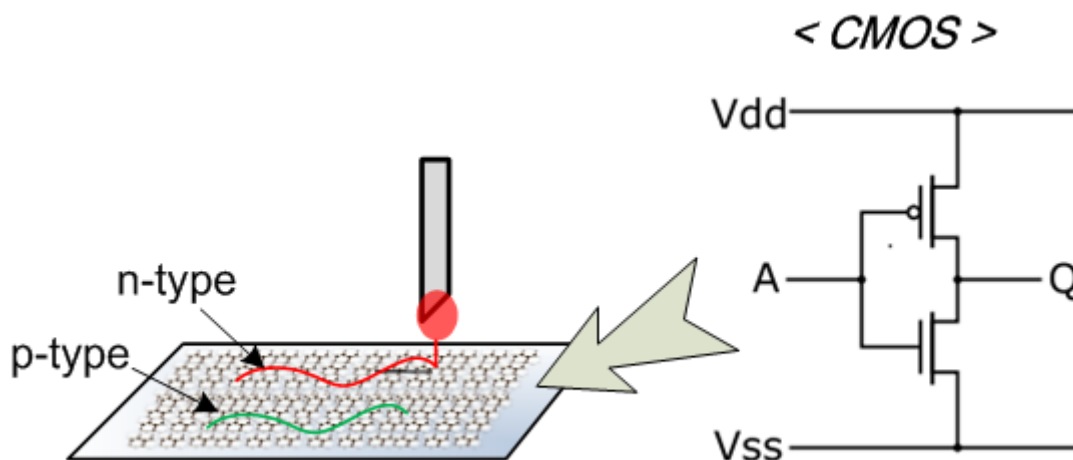
Figure 4.1 The CMOS structure could be constructed via in-situ doping of graphene using PEI polymer for n-type FETs and other types of polymers for p-type FETs locally via the in-situ doping process.

Multi-channel micromixer to mimic blood vessel

Micromixer is an important component in microfluidic and lab-on-a chip systems. Various types of micromixers have been developed previously by means of various driving forces such as pressure [95], dielectrophoretic [96], injection [97] and electro-wetting [98]. Regardless of the driving forces, the fabrication of mixing channels is required to make the micro/nano system. Typical channel width and height of a micromixer is in the range of tens of micrometers and fabricated using soft-lithography processes [99]. As a result, it is very challenging to make channels less than 5μm in diameter for ultra-low amount of flow and ultra-low Reynolds number micromixer [100]. For example, capillary blood vessels would demand small size channels [101]. One possible future direction for this work is to apply the electrospinning process to make fluidic channels from sub-micrometer to 10μm range. Furthermore, an overhanging micromixer constructed between two substrates could be transferred to other substrate via the possible scoop and place method to broaden the possible placements of fabricated micromixers. Figure 4.2 is the conceptual process flow to make overhanging, multi-channel micromixers. Two electrospun fibers with different polarity connections are used to make this micromixer. First, the syringe is connected to positive pin of electrical power supply such that the electrospun fiber has trapped positive charges as shown in Figure 4.2(a). Next, the syringe is connected to the negative pin of the power supply such that the second electrospun fiber has negative charges as illustrated in Figure 4.2(b). The attractive electrostatic force between the two fibers can pull the fibers together as shown in Figure 4.2(c) to form a micromixer as illustrated in Figure 4.2(d).
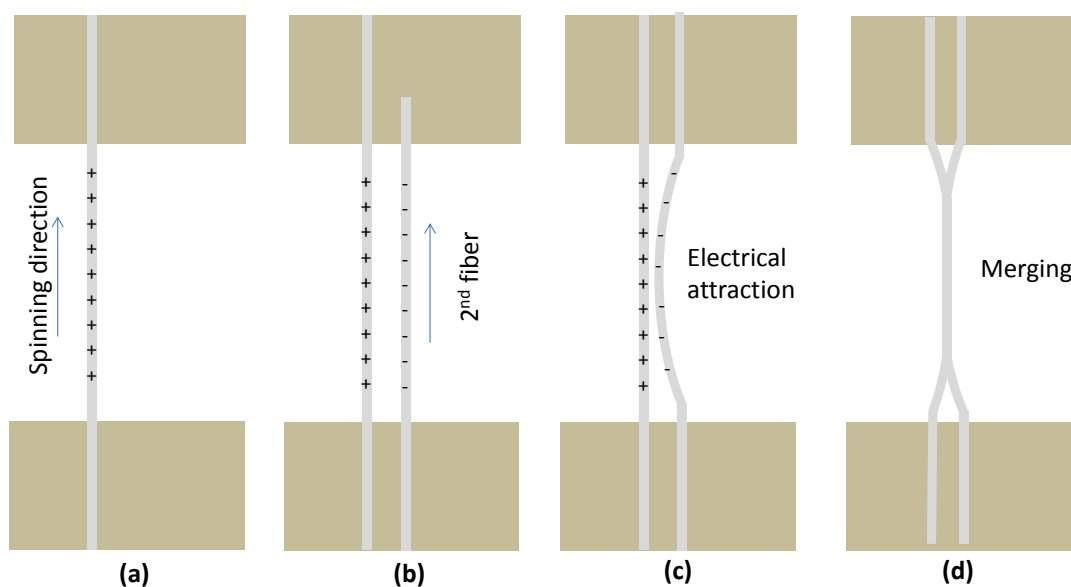
Figure 4.2 Conceptual diagram of mixing channel formation via electrical charge attraction. When syringe is connected to positive side of power, the as-spun fibers are charged with positive potential (a). Switching the polarity of syringe tip will charge the spinning fibers with negative potential (b). Two opposite sign of fibers attract each other (c) and eventually merge together to form single stream fiber.

Some preliminary tests have been conducted. First, fibers are electrospun over the open gap followed by a conformal coating process such as using parylene or a room-temperature CVD oxide to form the outside shells of microchannels. The polymer inside the microchannels has to be removed by either thermal decomposition or polymer etching after the construction of the shell such as the process demonstrated previously in the chip-to-chip fluidic connectors [102]. For the preliminary experiments, the micromixers have been fabricated using PVDF fibers between two aluminum blocks with two and three reservoirs as shown in Figure 4.3. By connecting additional fibers depositions with the first electrospun fiber, micromixers with multiple sources ports can be constructed. It is noted that the merging had to be done before the solvent was fully evaporated. In this prototype example, ITO has been used as the shell material. PVDF fibers have been decomposed by heating the whole system to 400°C for three hours [103].
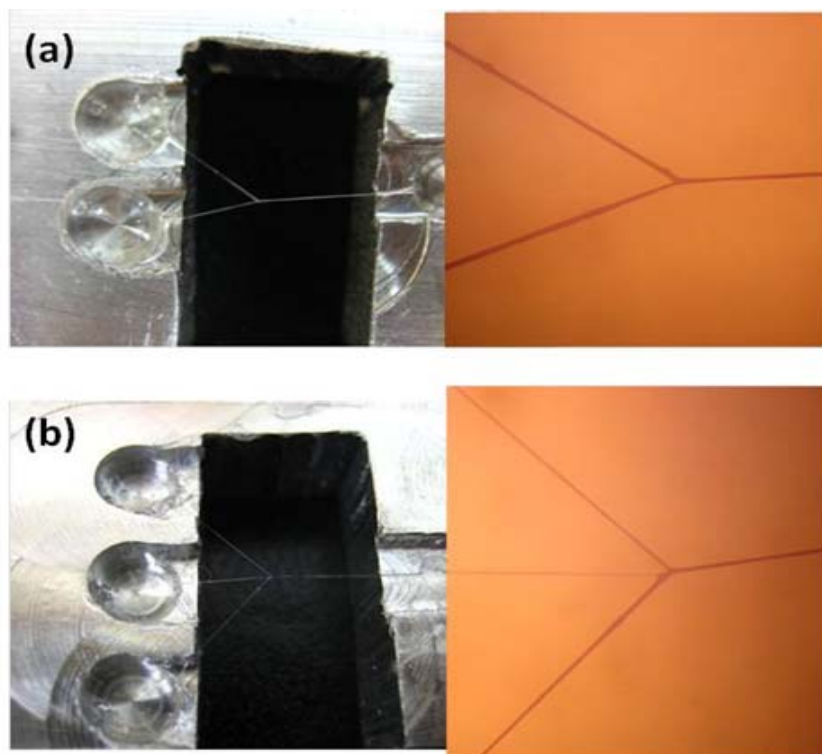
Figure 4.3 Prototype micromixer using electrospun direct-write fibers fabricated between two aluminum blocks. The micromixer was formed with (a) two and (b) three reservoirs as shown. In this prototype example, ITO has been used as the shell material.

Figure 4.4 shows preliminary testing results to verify the formation of fluidic channels. The ITO shell formation was verified with dyed IPA which has low surface tension force. When a drop of IPA was placed to the reservoir, IPA enters into the channel due to surface tension force. Several problems have been identified and further investigations are needed to solve these problem. These include collapsing of the ITO shells, residual polymer inside small channels and non-uniform thickness of the ITO layer which are due to non-conformal deposition. Nevertheless, these initial tests validate the basic concept to build multichannel micromixers to mimic blood vessels.
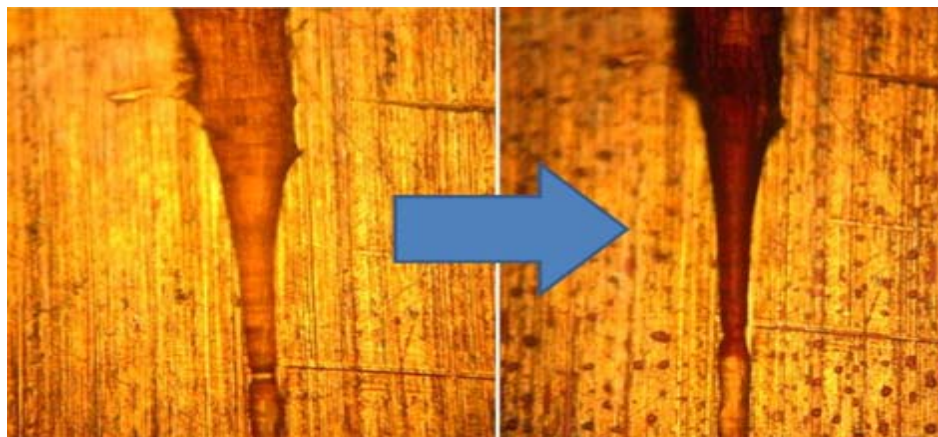
Figure 4.4 Dyed IPA has been used to verify the formation of micro-channels. (left) Before the infusion of IPA, clear microchannel can be observed. (right) After the infusion of IPA, the flow front can be clearly observed.

In summary, the concept of electrospun direct-write micromixer is validated with the preliminary tests. Some future investigations are needed. First, robust, flexible and biocompatible shell material should be used. Second, theoretical approach to analyze the merging phenomenon should be developed to help the design process. The long-term goal of this direction is to mimic mammalian blood vessels, especially targeting capillary vessels for *in-vitro* experiments at the beginning could bring important breakthrough in tissue engineering.

Reference

[1]   F. Dotti, A. Varesano, A. Montarsolo, A. Aluigi, C. Tonin, G. Mazzuchetti, Electrospun Porous Mats for High Efficiency Filtration, Journal of Industrial Textiles. 37 (2007) 151-162.

[2]   H. Yoshimoto, Y.M. Shin, H. Terai, J.P. Vacanti, A biodegradable nanofiber scaffold by electrospinning and its potential for bone tissue engineering, Biomaterials. 24 (2003) 2077-2082.

[3]   D. Sun, C. Chang, S. Li, L. Lin, Near-field electrospinning., Nano Letters. 6 (2006) 839-42.

[4]   B. Banazwski, R.K. Shah, The Role of Fuel Cells for Consumer Electronic Products and Toys, in: 1st International Fuel Cell Science, Engineering and Technology Conference, ASME, 2003: pp. 149-155.

[5]   A.H. Epstein, Millimeter-Scale, Micro-Electro-Mechanical Systems Gas Turbine Engines, Journal of Engineering for Gas Turbines and Power. 126 (2004) 205.

[6]   J.J. Kiely, D.V. Morgan, D.M. Rowe, J.M. Humphrey, Low cost miniature thermoelectric generator, Electronics Letters. 27 (1991) 2332.

[7]   N.M. White, J.D. Turner, Thick-film sensors: past, present and future, Measurement Science and Technology. 8 (1997) 1-20.

[8]   A.J. Lovinger, Ferroelectric polymers., Science (New York, N.Y.). 220 (1983) 1115-21.

[9]   S.-W. Hahm, D.-Y. Khang, Crystallization and microstructure-dependent elastic moduli of ferroelectric P(VDF–TrFE) thin films, Soft Matter. 6 (2010) 5802.

[10]   IEEE Standard on Piezoelectricity, 1988.

[11]   C. Chang, V.H. Tran, J. Wang, Y.-K. Fuh, L. Lin, Direct-write piezoelectric polymeric nanogenerator with high energy conversion efficiency., Nano Letters. 10 (2010) 726-31.

[12]   H. Lee, G.-Y. Jung, Full wafer scale near zero residual nano-imprinting lithography using UV curable monomer solution, Microelectronic Engineering. 77 (2005) 42-47.

[13] K. Venkatakrishnan, B.K.A. Ngoi, P. Stanley, L.E.N. Lim, B. Tan, N.R. Sivakumar, Laser writing techniques for photomask fabrication using a femtosecond laser, Applied Physics A: Materials Science & Processing. 74 (2002) 493-496.

[14] Y. Matsubara, J. Taniguchi, I. Miyamoto, Fabrication of Three-Dimensional Hydrogen Silsesquioxane Resist Structure using Electron Beam Lithography, Japanese Journal of Applied Physics. 45 (2006) 5538-5541.

[15] Fabrication of high-Q chalcogenide photonic crystal resonators by e-beam lithography, Applied Physics Letters. 90 (2007) 071102-071102-3.

[16] L. Wang, S. Zhang, Q. Wang, J. Chen, W. Jiang, R. Chen, Fabrication of three-dimensional (3D) woodpile structure photonic crystal with layer by layer e-beam lithography, Applied Physics A: Materials Science & Processing. 95 (2009) 329-334.

[17] S.C. Minne, H.T. Soh, P. Flueckiger, C.F. Quate, Fabrication of 0.1 μm metal oxide semiconductor field effect transistors with the atomic force microscope, Applied Physics Letters. 66 (1995) 703-705.

[18] Z.J. Davis, G. Abadal, O. Hansen, X. Borisé, N. Barniol, F. Pérez-Murano, et al., AFM lithography of aluminum for fabrication of nanomechanical systems., Ultramicroscopy. 97 (n.d.) 467-72.

[19] K.-I. Park, S. Xu, Y. Liu, G.-T. Hwang, S.-J.L. Kang, Z.L. Wang, et al., Piezoelectric BaTiO(3) Thin Film Nanogenerator on Plastic Substrates., Nano Letters. 10 (2010) 4939-4943.

[20] F. Dotti, A. Varesano, A. Montarsolo, A. Aluigi, C. Tonin, G. Mazzuchetti, Electrospun Porous Mats for High Efficiency Filtration, Journal of Industrial Textiles. 37 (2007) 151-162.

[21] E. Boland, G. Wnek, D. Simpson, K. Pawlowski, G. Bowlin, Tailoring Tissue Engineering Scaffolds Using Electrostatic Processing Techniques: a Study of Poly(Glycolic Acid) Electrospinning, Journal of Macromolecular Science, Part A. 38 (2001) 1231-1243.

[22] J. Chen, G. Chang, Electrospun collagen/chitosan nanofibrous membrane as wound dressing, Colloids and Surfaces A: Physicochemical and Engineering Aspects. 313-314 (2008) 183-188.

[23] R. Gonzalez, N. Pinto, Electrospun poly(3-hexylthiophene-2,5-diyl) fiber field effect transistor, Synthetic Metals. 151 (2005) 275-278.

[24] B. Ding, M. Wang, X. Wang, J. Yu, G. Sun, Electrospun nanomaterials for ultrasensitive sensors, Materials Today. 13 (2010) 16-27.

[25] J.M. Corres, Y.R. Garcia, F.J. Arregui, I.R. Matias, S. Member, Optical Fiber Humidity Sensors Using PVdF Electrospun Nanowebs, Sensors Journal. 11 (2011) 2383-2387.

[26] A.L. Yarin, S. Koombhongse, D.H. Reneker, Taylor cone and jetting from liquid droplets in electrospinning of nanofibers, Journal of Applied Physics. 90 (2001) 4836.

[27] D.H. Reneker, A.L. Yarin, H. Fong, S. Koombhongse, Bending instability of electrically charged liquid jets of polymer solutions in electrospinning, Journal of Applied Physics. 87 (2000) 4531.

[28] E. Boland, G. Wnek, D. Simpson, K. Pawlowski, G. Bowlin, Tailoring Tissue Engineering Scaffolds Using Electrostatic Processing Techniques: a Study of Poly(Glycolic Acid) Electrospinning, Journal of Macromolecular Science, Part A. 38 (2001) 1231-1243.

[29] J.A. Matthews, G.E. Wnek, D.G. Simpson, G.L. Bowlin, Electrospinning of collagen nanofibers., Biomacromolecules. 3 (2002) 232-8.

[30] A. Theron, E. Zussman, A.L. Yarin, Electrostatic field-assisted alignment of electrospun nanofibres, Nanotechnology. 12 (2001) 384-390.

[31] P. Katta, M. Alessandro, R.D. Ramsier, G.G. Chase, Continuous Electrospinning of Aligned Polymer Nanofibers onto a Wire Drum Collector, Nano Letters. 4 (2004) 2215-2218.

[32] D. Li, Y. Wang, Y. Xia, Electrospinning of Polymeric and Ceramic Nanofibers as Uniaxially Aligned Arrays, Nano Letters. 3 (2003) 1167-1171.

[33] J. Deitzel, Controlled deposition of electrospun poly(ethylene oxide) fibers, Polymer. 42 (2001) 8163-8170.

[34] C. Chang, K. Limkrailassiri, L. Lin, Continuous near-field electrospinning for large area deposition of orderly nanofiber patterns, Applied Physics Letters. 93 (2008) 123111.

[35] R. Yang, Y. Qin, C. Li, L. Dai, Z.L. Wang, Characteristics of output voltage and current of integrated nanogenerators, Applied Physics Letters. 94 (2009) 022905.

[36] A. Baji, Y.-W. Mai, Q. Li, Y. Liu, Electrospinning induced ferroelectricity in poly(vinylidene fluoride) fibers., Nanoscale. 3 (2011) 3068-71.

[37] G. Zhang, S. Xu, Y. Shi, Electromechanical coupling of lead zirconate titanate nanofibres, Micro & Nano Letters. 6 (2011) 59-61.

[38] Z.L. Wang, J. Song, Piezoelectric nanogenerators based on zinc oxide nanowire arrays., Science. 312 (2006) 242-6.

[39] C. Sun, J. Shi, D.J. Bayerl, X. Wang, PVDF microbelts for harvesting energy from respiration, Energy & Environmental Science. 4 (2011) 4508-4512.

[40] B. Kumar, S.-W. Kim, Recent advances in power generation through piezoelectric nanogenerators, Journal of Materials Chemistry. 21 (2011) 18946-18958.

[41] Y. Qin, X. Wang, Z.L. Wang, Microfibre-nanowire hybrid structure for energy scavenging., Nature. 451 (2008) 809-813.

[42] S.N. Cha, J.-S. Seo, S.M. Kim, H.J. Kim, Y.J. Park, S.-W. Kim, et al., Sound-driven piezoelectric nanowire-based nanogenerators., Advanced Materials (Deerfield Beach, Fla.). 22 (2010) 4726-30.

[43] M.-Y. Lu, J. Song, M.-P. Lu, C.-Y. Lee, L.-J. Chen, Z.L. Wang, ZnO-ZnS heterojunction and ZnS nanowire arrays for electricity generation., ACS Nano. 3 (2009) 357-62.

[44] C.-T. Huang, J. Song, W.-F. Lee, Y. Ding, Z. Gao, Y. Hao, et al., GaN nanowire arrays for high-output nanogenerators., Journal of the American Chemical Society. 132 (2010) 4766-71.

[45] X. Wang, J. Song, F. Zhang, C. He, Z. Hu, Z. Wang, Electricity generation based on one-dimensional group-III nitride nanomaterials., Advanced Materials. 22 (2010) 2155-58.

[46] Y.-F. Lin, J. Song, Y. Ding, S.-Y. Lu, Z.L. Wang, Piezoelectric nanogenerator using CdS nanowires, Applied Physics Letters. 92 (2008) 022105.

[47] Y.-F. Lin, J. Song, Y. Ding, S.-Y. Lu, Z.L. Wang, Alternating the Output of a CdS Nanowire Nanogenerator by a White-Light-Stimulated Optoelectronic Effect, Advanced Materials. 20 (2008) 3127-3130.

[48] X. Wang, J. Song, J. Liu, Z.L. Wang, Direct-current nanogenerator driven by ultrasonic waves., Science (New York, N.Y.). 316 (2007) 102-5.

[49] H.-K. Park, K.Y. Lee, J.-S. Seo, J.-A. Jeong, H.-K. Kim, D. Choi, et al., Charge-Generating Mode Control in High-Performance Transparent Flexible Piezoelectric Nanogenerators, Advanced Functional Materials. 21 (2011) 1187-1193.

[50] X. Chen, S. Xu, N. Yao, Y. Shi, 1.6 V nanogenerator for mechanical energy harvesting using PZT nanofibers., Nano Letters. 10 (2010) 2133-7.

[51] X. Chen, S. Xu, N. Yao, W. Xu, Y. Shi, Potential measurement from a single lead zirconate titanate nanofiber using a nanomanipulator, Applied Physics Letters. 94 (2009) 253113.

[52] G. Zhang, S. Xu, Y. Shi, Electromechanical coupling of lead zirconate titanate nanofibres, Micro & Nano Letters. 6 (2011) 59-61.

[53] J. Fang, X. Wang, T. Lin, Electrical power generator from randomly oriented electrospun poly(vinylidene fluoride) nanofibre membranes, Journal of Materials Chemistry. 21 (2011) 11088-91.

[54] J. Chang, L. Lin, Large array electrospun PVDF nanogenerators on a flexible substrate, in: 2011 16th International Solid-State Sensors, Actuators and Microsystems Conference, IEEE, 2011: pp. 747-750.

[55] T.D. Nguyen, J.M. Nagarah, Y. Qi, S.S. Nonnenmann, A.V. Morozov, S. Li, et al., Wafer-scale nanopatterning and translation into high-performance piezoelectric nanowires., Nano Letters. 10 (2010) 4595-9.

[56] C. Chang, K. Limkrailassiri, L. Lin, Continuous near-field electrospinning for large area deposition of orderly nanofiber patterns, Applied Physics Letters. 93 (2008) 123111.

[57] Y. Hu, L. Lin, Y. Zhang, Z.L. Wang, Replacing a Battery by a Nanogenerator with 20 V Output, Advanced Materials. 24 (2011) 110-4.

[58] S. Xu, B.J. Hansen, Z.L. Wang, Piezoelectric-nanowire-enabled power source for driving wireless microelectronics., Nature Communications. 1 (2010) 93.

[59] D. Choi, K.Y. Lee, M.-J. Jin, S.-G. Ihn, S. Yun, X. Bulliard, et al., Control of naturally coupled piezoelectric and photovoltaic properties for multi-type energy scavengers, Energy & Environmental Science. 4 (2011) 4607-13.

[60] C.R. Bowen, R. Stevens, L.J. Nelson, A.C. Dent, G. Dolman, B. Su, et al., Manufacture and characterization of high activity piezoelectric fibres, Smart Materials and Structures. 15 (2006) 295-301.

[61] Y. Qi, N.T. Jafferis, K. Lyons, C.M. Lee, H. Ahmad, M.C. McAlpine, Piezoelectric ribbons printed onto rubber for flexible energy conversion., Nano Letters. 10 (2010) 524-8.

[62] Piezoceramic fibers – Fraunhofer Institute for Ceramic Technologies and Systems IKTS, (n.d.).

[63] Z. Huang, A review on polymer nanofibers by electrospinning and their applications in nanocomposites, Composites Science and Technology. 63 (2003) 2223-2253.

[64] F.P. Sun, Z. Chaudhry, C. Liang, C.A. Rogers, Truss Structure Integrity Identification Using PZT Sensor-Actuator, Journal of Intelligent Material Systems and Structures. 6 (1995) 134-139.

[65] S. JUNG, S. KIM, Improvement of scanning accuracy of PZT piezoelectric actuators by feed-forward model-reference control, Precision Engineering. 16 (1994) 49-55.

[66] B.J. Hansen, Y. Liu, R. Yang, Z.L. Wang, Hybrid nanogenerator for concurrently harvesting biomechanical and biochemical energy., ACS Nano. 4 (2010) 3647-52.

[67] D. Mandal, S. Yoon, K.J. Kim, Origin of Piezoelectricity in an Electrospun Poly(vinylidene fluoride-trifluoroethylene) Nanofiber Web-Based Nanogenerator and Nano-Pressure Sensor., Macromolecular Rapid Communications. 32 (2011) 831-7.

[68] D. Farrar, K. Ren, D. Cheng, S. Kim, W. Moon, W.L. Wilson, et al., Permanent Polarity and Piezoelectricity of Electrospun α-Helical Poly(α-Amino Acid) Fibers, Advanced Materials. 23 (2011) 3954-3958.

[69] Y.R. Wang, J.M. Zheng, G.Y. Ren, P.H. Zhang, C. Xu, A flexible piezoelectric force sensor based on PVDF fabrics, Smart Materials and Structures. 20 (2011) 045009.

[70] J. Zheng, A. He, J. Li, C.C. Han, Polymorphism Control of Poly(vinylidene fluoride) through Electrospinning, Macromolecular Rapid Communications. 28 (2007) 2159-2162.

[71] C. Ribeiro, V. Sencadas, J.L.G. Ribelles, S. Lanceros-Méndez, Influence of Processing Conditions on Polymorphism and Nanofiber Morphology of

Electroactive Poly(vinylidene fluoride) Electrospun Membranes, Soft Materials. 8 (2010) 274-287.

[72] J.S. Andrew, D.R. Clarke, Effect of electrospinning on the ferroelectric phase content of polyvinylidene difluoride fibers., Langmuir : the ACS Journal of Surfaces and Colloids. 24 (2008) 670-2.

[73] S. Huang, W.A. Yee, W.C. Tjiu, Y. Liu, M. Kotaki, Y.C.F. Boey, et al., Electrospinning of polyvinylidene difluoride with carbon nanotubes: synergistic effects of extensional force and interfacial interaction on crystalline structures., Langmuir : the ACS Journal of Surfaces and Colloids. 24 (2008) 13621-6.

[74] L.M.M. Costa, Effect of Solution Concentration on the Electrospray/Electrospinning Transition and on the Crystalline Phase of PVDF, Materials Sciences and Applications. 01 (2010) 246-251.

[75] D.V. Isakov, E. de Matos Gomes, L.G. Vieira, T. Dekola, M.S. Belsley, B.G. Almeida, Oriented single-crystal-like molecular arrangement of optically nonlinear 2-methyl-4-nitroaniline in electrospun nanofibers., ACS Nano. 5 (2011) 73-8.

[76] H. Kawai, The Piezoelectricity of Poly (vinylidene Fluoride), Japanese Journal of Applied Physics. 8 (1969) 975-976.

[77] A.G. Holmes-Siedle, P.D. Wilson, A.P. Verrall, PVdF: An electronically-active polymer for industry, Materials & Design. 4 (1983) 910-918.

[78] D. Isakov, E. de M. Gomes, I. Bdikin, B. Almeida, M. Belsley, M. Costa, et al., Production of Polar β-Glycine Nanofibers with Enhanced Nonlinear Optical and Piezoelectric Properties, Crystal Growth & Design. 11 (2011) 4288-4291.

[79] J. Mccann, J. Chen, D. Li, Z.-G. Ye, Y. Xia, Electrospinning of polycrystalline barium titanate nanofibers with controllable morphology and alignment, Chemical Physics Letters. 424 (2006) 162-166.

[80] J.J. Santiago-Aviles, Y. Wang, R. Furlan, I. Ramos, Synthesis and characterization of micro/nanoscopic Pb(Zr 0.52 Ti 0.48)O 3 fibers by electrospinning, Applied Physics A: Materials Science & Processing. 78 (2004) 1043-1047.

[81] S. Kalinin, D. Bonnell, Imaging mechanism of piezoresponse force microscopy of ferroelectric surfaces, Physical Review B. 65 (2002) 1-11.

[82] H. Wu, L. Hu, M.W. Rowell, D. Kong, J.J. Cha, J.R. Mcdonough, et al., Electrospun Metal Nanofiber Webs as High-Performance Transparent Electrode, Nano. (2010) 4242-4248.

[83] Y. Wang, J.J. Santiago-Avilés, Synthesis of lead zirconate titanate nanofibres and the Fourier-transform infrared characterization of their metallo-organic decomposition process, Nanotechnology. 15 (2004) 32-36.

[84] X. Li, W. Cai, J. An, S. Kim, J. Nah, D. Yang, et al., Large-area synthesis of high-quality and uniform graphene films on copper foils., Science (New York, N.Y.). 324 (2009) 1312-4.

[85] Y.K. Du, P. Yang, Z.G. Mou, N.P. Hua, L. Jiang, Thermal decomposition behaviors of PVP coated on platinum nanoparticles, Journal of Applied Polymer Science. 99 (2006) 23-26.

[86] L. Kundakovic, M. Flytzani-Stephanopoulos, Reduction characteristics of copper oxide in cerium and zirconium oxide systems, Applied Catalysis A: General. 171 (1998) 13-29.

[87] Y. Sawada, H. Tamaru, M. Kogoma, M. Kawase, K. Hashimoto, The reduction of copper oxide thin films with hydrogen plasma generated by an atmospheric-pressure glow discharge, Journal of Physics D: Applied Physics. 29 (1996) 2539-2544.

[88] M. Bognitzki, M. Becker, M. Graeser, W. Massa, J.H. Wendorff, A. Schaper, et al., Preparation of Sub-micrometer Copper Fibers via Electrospinning, Advanced Materials. 18 (2006) 2384-2386.

[89] H. Liu, Y. Liu, D. Zhu, Chemical doping of graphene, Journal of Materials Chemistry. 21 (2011) 3335.

[90] E. Häsler, L. Stein, G. Harbauer, Implantable physiological power supply with PVDF film, Ferroelectrics. 60 (1984) 277-282.

[91] R. Yang, Y. Qin, C. Li, G. Zhu, Z.L. Wang, Converting biomechanical energy into electricity by a muscle-movement-driven nanogenerator., Nano Letters. 9 (2009) 1201-5.

[92] A.H. Castro Neto, N.M.R. Peres, K.S. Novoselov, A.K. Geim, The electronic properties of graphene, Reviews of Modern Physics. 81 (2009) 109-162.

[93]   F. Güneş, H.-J. Shin, C. Biswas, G.H. Han, E.S. Kim, S.J. Chae, et al., Layer-by-layer doping of few-layer graphene film., ACS Nano. 4 (2010) 4595-600.

[94]   X. Wang, X. Li, L. Zhang, Y. Yoon, P.K. Weber, H. Wang, et al., N-doping of graphene through electrothermal reactions with ammonia., Science (New York, N.Y.). 324 (2009) 768-71.

[95]   J. Deval, P. Tabeling, Chaotic mixing in electrokinetically and pressure driven micro flows, in: Technical Digest. MEMS 2001. 14th IEEE International Conference on Micro Electro Mechanical Systems (Cat. No.01CH37090), IEEE, n.d. pp. 483-486.

[96]   H.-Y. Lee, J. Voldman, Optimizing micromixer design for enhancing dielectrophoretic microconcentrator performance., Analytical Chemistry. 79 (2007) 1833-9.

[97]   H. Nagasawa, N. Aoki, K. Mae, Design of a New Micromixer for Instant Mixing Based on the Collision of Micro Segments, Chemical Engineering & Technology. 28 (2005) 324-330.

[98]   P. Paik, V.K. Pamula, M.G. Pollack, R.B. Fair, Electrowetting-based droplet mixers for microfluidic systems., Lab on a Chip. 3 (2003) 28-33.

[99]   N.-T. Nguyen, Z. Wu, Micromixers—a review, Journal of Micromechanics and Microengineering. 15 (2005) R1-R16.

[100] A.A.S. Bhagat, E.T.K. Peterson, I. Papautsky, A passive planar micromixer with obstructions for mixing at low Reynolds numbers, Journal of Micromechanics and Microengineering. 17 (2007) 1017-1024.

[101] B. Davey, T. Halliday, M. Hirst, Human Biology and Health, Prentice hall, 2001.

[102] K. Limkrailassiri, Chip-to-chip fluidic connectors via near-field electrospinning, in: 2007 IEEE 20th International Conference on Micro Electro Mechanical Systems (MEMS), IEEE, 2007: pp. 61-64.

[103] J.T. de Campos, Festas juninas nas escolas: lições de preconceitos, Educação & Sociedade. 28 (2007) 589-606.